HIGHWAY RESEARCH RECORD

Number 302

Bridges, Foundations, and Retaining Walls

10 Reports

Subject Areas

22 Highway Design
27 Bridge Design
33 Construction
62 Foundations (Soils)
63 Mechanics (Earth Mass)

HIGHWAY RESEARCH BOARD
DIVISION OF ENGINEERING NATIONAL RESEARCH COUNCIL
NATIONAL ACADEMY OF SCIENCES—NATIONAL ACADEMY OF ENGINEERING

Washington, D.C. 1970

Standard Book Number 309-01796-3

Price: $3.00

Available from

Highway Research Board
National Academy of Sciences
2101 Constitution Avenue
Washington, D.C. 20418

Department of Design

W.B. Drake, Chairman
Kentucky Department of Highways, Lexington

L.F. Spaine
Highway Research Board Staff

GENERAL DESIGN DIVISION

M.D. Shelby, Chairman
Texas Transportation Institute, Texas A&M University, College Station

COMMITTEE ON GUARDRAIL, MEDIAN BARRIERS AND SIGN, SIGNAL AND LIGHTING SUPPORTS

(As of December 31, 1969)

Paul C. Skeels, Chairman
General Motors Proving Ground, Milford, Michigan

W.C. Anderson
John L. Beaton
Alan E. Brickman
Edward M. Conover
James J. Crowley
Albert L. Godfrey, Sr.
Malcolm D. Graham
Wayne Henneberger
Robert N. Hunter
John W. Hutchinson
Jack E. Leisch
J.E. McCracken
Eric F. Nordlin
Walter C. Oram
John M. Quigg
Edmund R. Ricker
Neilon J. Rowan
Frank G. Schlosser
J. Robert Stemler
Flory J. Tamanini
James A. Thompson
M.A. Warnes
Howard L. White
Earl C. Williams, Jr.
Robert Winans

BRIDGE DIVISION

J. N. Clary, Chairman
Virginia Department of Highways, Richmond

COMMITTEE ON BRIDGE DESIGN

(As of December 31, 1969)

Richard J. Posthauer, Chairman
New York Department of Transportation, Albany

W.C. Anderson
Louis M. Bjorn
Vernon J. Burns
Arthur L. Elliott
Frede Gloersen
George G. Goble
T.R. Higgins
John J. Hogan
Nelson C. Jones
Robert J. McDonagh
Adrian Pauw
Charles F. Scheffey
C.P. Siess
Robert F. Wellner

COMMITTEE ON CONCRETE SUPERSTRUCTURES

(As of December 31, 1969)

W.E. Baumann, Chairman
Illinois Division of Highways, Springfield

Harry N. Wenke, Secretary
Portland Cement Association, Skokie, Illinois

James W. Baldwin, Jr.
Henry W. Derthick
Carl E. Ekberg, Jr.
Phil M. Ferguson
C.L. Hulsbos
Daniel P. Jenny
Alan H. Mattock
Robert A. Norton
Paul F. Rice
W.T. Robertson
Earle E. Wilkinson

COMMITTEE ON SUBSTRUCTURES, RETAINING WALLS AND FOUNDATIONS

(As of December 31, 1969)

Wayne Henneberger, Chairman
Texas Highway Department, Austin

Raymond Archibald
Frank M. Fuller
H.D. Gibbons
Stanley Gordon
Bernard A. Grand
T.J. Hirsch
Wayne T. Hunzicker
Philip Keene
Joseph H. Moore
Joe S. Robinson
Charles B. Trueblood

COMMITTEE ON DYNAMICS AND FIELD TESTING OF BRIDGES

(As of December 31, 1969)

LeRoy T. Oehler, Chairman
Michigan Department of State Highways, Lansing

James W. Baldwin, Jr.
W.E. Baumann
Raymond E. Davis
Michael E. Fiore
Charles F. Galambos
Egbert R. Hardesty
J.M. Hayes
Conrad P. Heins, Jr.
C.L. Hulsbos
Henry L. Kinnier
John J. Kozak
K.H. Lenzen
Charles T.G. Looney
W.H. Munse
W.W. Sanders, Jr.
Charles F. Scheffey
C.P. Siess
John W. Trank
Robert F. Varney
A.S. Veletsos
Ivan M. Viest
W.H. Walker
R.K.L. Wen
Douglas T. Wright
George W. Zuurbier

Department of Soils, Geology and Foundations

Eldon J. Yoder, Chairman
Purdue University, Lafayette, Indiana

Chester McDowell, Vice Chairman
Texas Highway Department, Austin

J.W. Guinnee
Highway Research Board Staff

DIVISION B

Carl L. Monismith, Chairman
University of California, Berkeley

William P. Hofmann, Vice Chairman
New York Department of Transportation, Albany

COMMITTEE ON EMBANKMENTS AND EARTH SLOPES
(As of December 31, 1969)

William P. Hofmann, Chairman
New York Department of Transportation, Albany

Philip P. Brown
Wilbur M. Haas
C.W. Heckathorn
Raymond C. Herner
Henry W. Janes
Martin S. Kapp
Philip Keene
Richard E. Landau
Ivan C. MacFarlane
Harry E. Marshall
Glen L. Martin
Lyndon H. Moore
Melvin W. Morgan
Robert L. Schuster
Rockwell Smith
Robert T. Tierney
David J. Varnes
Walter C. Waidelich
William G. Weber Jr.

Department of Materials and Construction

R. L. Peyton, Chairman
State Highway Commission of Kansas, Topeka

R. E. Bollen and W. B. Gunderman
Highway Research Board Staff

CONSTRUCTION DIVISION

H. W. Humphres, Chairman
Washington Department of Highways, Olympia

COMMITTEE ON CONSTRUCTION PRACTICES—STRUCTURES

(As of December 31, 1969)

K. R. Scurr, Chairman
Pierre, South Dakota

Randle B. Alexander
H. B. Britton
W. E. Crum
Richard M. Dowalter
Dale F. Downing
Albert L. Grubb
John J. Hogan
Carl E. Klamm
H. G. Lux
John F. McGovern
James Calvin McGrew
Charles A. Pestotnik
William Smith Ritchie, Jr.
G. I. Sawyer
P. H. Schultz
Norman L. Scott
Clyde F. Silvus
Howard L. White

Foreword

The ten papers in this RECORD describe the results of bridge and foundation research and observations on a wide variety of projects ranging from dynamic testing of bridge barrier rails to the development of specifications for steel forms for bridge decks. Both design engineers and investigators will find the information to be of value.

The first three papers are addressed to the subject of developing more effective bridge barrier rails. The primary objective of the research by Nordlin, Hackett, and Folsom was to test the effectiveness of California's type 9 bridge barrier rail and type 8 bridge approach guardrail. With modifications to the latter, full-scale tests led to the conclusion that both systems will adequately retain and redirect a standard passenger vehicle impacting at an approach angle of 25 degrees and a speed of 60 mph. Woolam and Garza discuss the design theory for a new concept of energy-absorbing bridge rail utilizing a fragmenting tube as the primary energy-absorbing element. The procedures for fabricating and installing a prototype rail are also discussed. Stocker, Ivey, and Hirsch report the results of full-scale testing of the fragmenting-tube bridge rail. They conclude that, when the transverse vehicle energy level is sufficient to activate the fragmenting tubes, the vehicle will be redirected with a significant lowering in the expected g level.

The study by Kozlov and Desai is an attempt to indicate the thermal characteristics of bridge joint movements and the possible solution of the bridge end movements problem. The authors present up-to-date knowledge on the thermal characteristics of a mass, such as a concrete bridge deck, and on the principles of heat transfer as related to bridge end movements. Using an empirical approach, they have developed a method for prediction of reasonably accurate concrete temperatures.

The problem of dynamic response of single span, simply supported horizontally curved highway bridges subjected to moving loads is treated by Vashi, Schelling, and Heins. Analysis of an idealized bridge under single or double constant-force moving loads leads to the development of impact factors for both flexural and torsional response of the bridge. Impact factor design curves are presented for various span lengths and central angles.

Anchorage of large-diameter column bars into the top beam of single-column highway bridge pylons is complicated by varying stress conditions, making analysis uncertain. A paper by Rajagopalan and Ferguson presents the results of a full-size test of a specific anchorage detail currently being used in Texas. The authors conclude that the design was adequate, but that some conservatism in the anchorage length provided under ultimate strength design may be desirable.

The differential settlements between bridge decks and the adjoining highway approach pavements often present hazardous conditions and require costly maintenance. The abridgment of the paper by Hopkins and Deen summarizes the data obtained from a survey of existing bridge approaches in Kentucky. In addition to providing general information as to the prevalence of the problem, the data imply that there is a general relationship between development of the approach fault and such causative factors as abutment type, geological conditions, and soils conditions. The companion paper by Hopkins and Scott presents the results of an attempt to determine if the settlement at bridge abutments is primarily a result of volume changes in the embankment or foundation. Based on consolidation tests performed on undisturbed samples secured from the foundation soils prior to construction, predicted settlements were compared with measured settlements and found to show good agreement.

The purpose of the study by Stiles was to discuss the construction and application of a series of graphs used to show how changes in toe and heel length affect bearing pressures under footings of cantilever retaining walls. Several loading conditions are given and problems associated with each are discussed.

The final paper reports on the investigation of bridge deck slabs constructed with steel forms designed to remain in place. Causes of failures of the steel forms are discussed and suggested specifications are included.

Contents

Dynamic Tests of California Type 9 Bridge Barrier Rail and Type 8 Bridge Approach Guardrail

ERIC F. NORDLIN, RAYMOND P. HACKETT, and JOHN J. FOLSOM,
Materials and Research Department, California Division of Highways

The results of one full-scale vehicle impact test into the California type 9 bridge barrier rail and three tests into various modifications of the California type 8 bridge approach guardrail are reported. The results indicate that the type 9 bridge barrier rail and the final type 8 bridge approach guardrail designs will retain and redirect a 4,500-lb passenger vehicle, impacting at 60 mph and 25 deg, with tolerable deceleration rates, moderate vehicle damage, and minimal barrier damage. The bridge barrier rail and bridge approach guardrail, together, provide structural continuity and a pleasing appearance.

•HIGHWAY ENGINEERS are continually striving to improve their product. Efforts along this line are expended in a multitude of directions motivated by advances in technology, concern for safety and aesthetics, and a desire to give the public the greatest value for each tax dollar. In the area of highway barrier systems, significant improvements are being made as new concepts and designs are developed and tested.

The first series of vehicle impact tests on bridge rails by the California Division of Highways was conducted in the mid-1950s. These tests were initiated because of the serious operational deficiencies, primarily structural, that were showing up with the increased use of heavier, higher speed vehicles and higher speed highways. These and subsequent tests provided a better knowledge of the requirements for modern bridge rails and for the dynamic actions of impacting high-speed vehicles. From this early testing, for example, it was learned that vehicles impacting baluster-type bridge rails tended to snag on the openings, thereby causing severe vehicle decelerations and frequent rail failures.

As a result of these earlier tests, in 1962 the California Division of Highways settled on a design called the California type 1 bridge barrier rail (2). This design is composed of a single 5-in. diameter metal pipe railing mounted 15 in. above the top of a 21-in. high solid reinforced concrete parapet wall. The overall height of this barrier system is 36 in. This design has given good operational performance, both structurally and in the reduction of the severity of accidents. However, operational information indicated that the following aspects could be improved:

1. The type 1 bridge barrier rail is not self-cleaning. In certain areas, sand and other debris tend to pile up against the solid parapet wall.
2. Visibility through the railing is somewhat restricted, both for the motorist on the bridge wishing to view the surrounding scenery and from a safety standpoint for the motorist needing adequate sight distance from an approach ramp adjacent to the structure.

In 1965-1966, these considerations led to the design, testing, and subsequent use of the California type 8 bridge rail (1). The design is composed of two 2- by 6-in. steel

Paper sponsored by Committee on Guardrail, Median Barriers and Sign, Signal and Lighting Supports and Committee on Bridge Design and presented at the 49th Annual Meeting.

Figure 1.

rectangular tube rails mounted 15 and 27 in. high on welded, open-type steel posts spaced 10 ft on centers. From the standpoint of structural adequacy and appearance, this bridge rail also performs well. However, operational experience has indicated that on higher structures motorists tend to shy away from this low, open, fragile-appearing railing and thus crowd the inner lanes of traffic.

The inadequate appearance of the California type 8 bridge rail then led to the compromise design of the California type 9 bridge barrier rail. The type 9 bridge rail and the California type 8 bridge approach guardrail used with it are the subject of the tests covered by this report. The type 9 bridge rail consists of a single 2- by 6-in. steel rectangular tube rail attached to welded steel posts mounted on a 15-in. high concrete parapet for an overall barrier height of 27 in. The double-rail type 8 system was adapted as a bridge approach guardrail that maintains structural and aesthetic continuity while protecting the motorist from end-on collision into the bridge rail.

In this study, the new California type 9 bridge barrier rail and the new California type 8 bridge approach guardrail were subjected to controlled vehicle impact tests. Thus, the primary objectives of this research project were to (a) test the California type 9 bridge barrier rail, (b) test the California type 8 approach guardrail flare, and (c) develop and test subsequent design modifications to the barriers as determined from the results of the tests on the initial designs.

TEST PARAMETERS

The test vehicles used in this study were 1966 sedans weighing approximately 4,500 lb including a dummy and instrumentation. The test procedures taken to prepare, remotely control, and target the test vehicle are similar to those used in past test series and detailed in previous California reports (3, 4). These test parameters generally meet the guidelines established by the Highway Research Board Committee on Guardrails and Guide Posts (5).

INSTRUMENTATION

Photographic and mechanical instrumentation procedures and equipment employed in this test series are similar to those used in past test series and are detailed in previous California reports (3, 4).

Figure 2.

DESIGN AND PERFORMANCE

Test 172—California Type 9 Bridge Barrier Rail

The California type 9 bridge barrier rail (Fig. 1) consists of a single steel rail mounted 12 in. above the top of a 15-in. high reinforced concrete parapet wall. The total barrier rail height is 27 in. from the bridge deck to the top of the steel rail.

The rail is fabricated from 6-in. by 2-in. by 12.02-lb structural steel rectangular tubing

conforming to ASTM Specification A 500, Grade B. An interior sleeve-type rail splice, proven effective in a previous test series (1), is used. The minimum length of a steel rail segment is 20 ft except at the end of the barrier downstream to traffic where a shorter length is bent down at a 36-in. radius to butt against the top of the parapet. At the end of the barrier upstream to traffic, the single steel rail extends beyond the end of the parapet for transition connection with the bridge approach guardrail.

The rail is supported on welded steel posts spaced at 10-ft centers and fabricated from ASTM Specification A 36 structural steel. Two ¾-in. steel bolts, stud-welded to the rail, are used to connect the rail to each post. The posts are secured to the parapet by two high-strength bolts, one ¾-in. diameter by 8 in. and the other 1-in. diameter by 10 in., cast in the concrete (Fig. 2).

For this test installation, the concrete parapet was 65 ft long and was constructed on a reinforced concrete simulated cantilevered bridge deck. The deck and parapet reinforcing, as well as other details of the type 9 bridge barrier rail constructed for test 172, are shown in Figure A1 of the Appendix. This barrier rail system was designed in accordance with the requirements of the 1965 AASHO Standard Specifications for Highway Bridges.

The vehicle in test 172 impacted the barrier midspan between posts 3 and 4 at 57 mph and 26 deg. Because of the relatively low parapet height (15 in.) in relation to the vehicle bumper (Fig. 3), the bumper and leading frame members projected over the concrete parapet on impact.

As the vehicle progressed through impact, the front bumper and chassis snagged on the vertical flanges of post 4, causing the fillet welds connecting the post flange to the horizontal mounting bar to fail. This severe loading was also transmitted to the anchor bolts, causing some spalling of the concrete parapet (Fig. 4). The failure at post 4 increased lateral and longitudinal loadings to posts 3 and 5. Post 5, located 15 ft downstream of initial impact, sustained only minor flange deformation. However, post 3, located 5 ft upstream, was apparently subjected to higher loading, as evidenced by spalling of the concrete around the anchor bolts in addition to slight flange deformation (Fig. 5). Even though the rail was released at post 4, the maximum permanent rail deflection was only 0.42 ft laterally and 0.45 ft vertically. All deflection occurred between posts 3 and 5 (Fig. 6).

Figure 3.

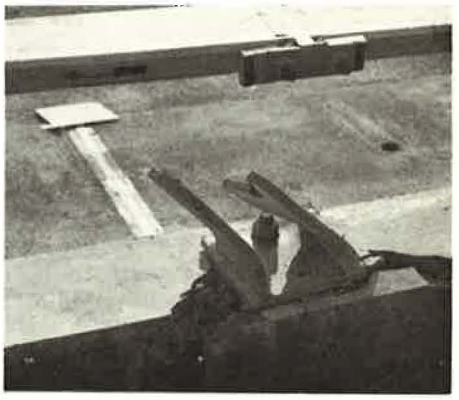

Figure 4.

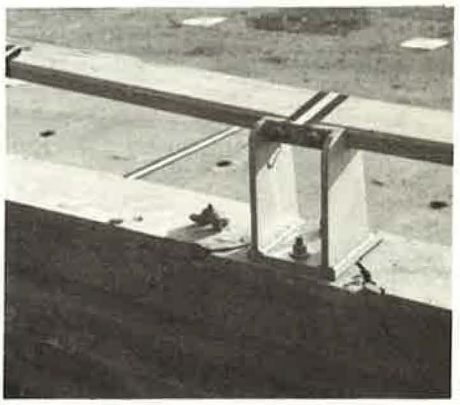

Figure 5.

Figure 6.

Figure 7.

Figure 8.

Barrier damage was considered moderate under the severe impact conditions of this test. Rail damage would require replacement of one post and two rail sections. The concrete parapet could have been repaired by straightening the anchor bolts at post 3, chipping out the spalled concrete at posts 3 and 4, and patching with an epoxy-cement grout.

Vehicle dynamics were considered satisfactory with minimal jump and no tendency to roll. Vehicle-barrier contact was approximately 15 ft and the exit angle was about 6 deg. Pertinent data on this test are shown in Figure A2 of the Appendix. The vehicle damage, although relatively severe, is characteristic of high-speed impact at relatively high angles into nonyielding barriers (Fig. 7).

Test 171—California Type 8 Bridge Approach Guardrail, Initial Design

The initial bridge approach guardrail design (Fig. 8) was adapted from the California type 8 bridge rail design developed and tested in 1965-1966 (1). This design uses two 6-in. by 2-in by 12.02-lb structural steel rectangular tube rails mounted 15 and 27 in. to the top above the ground. However, the welded steel posts, spaced at 10 ft on centers from the earlier bridge rail, are altered to permit attachment over 8- by 8-in. Douglas fir posts embedded 36 in. in drilled holes in original ground with tamped backfill.

The rail segments are fastened together with an interior sleeve-type rail splice using two $\frac{3}{4}$-in. diameter by $3\frac{1}{4}$-in. long through bolts to transmit tensile forces. The

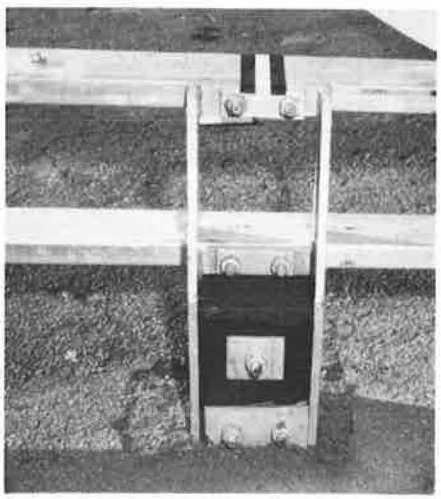

Figure 9.

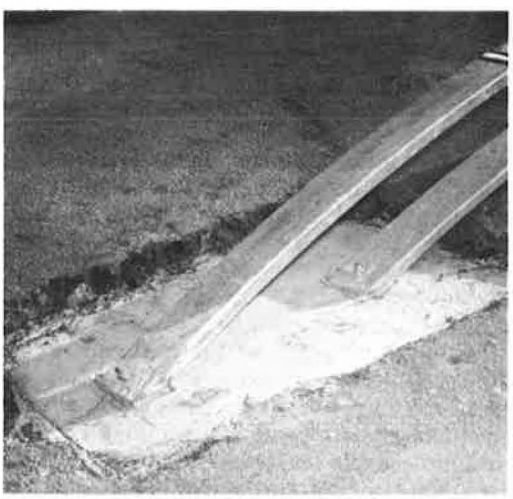

Figure 10.

rails are secured to each steel post with two ¾-in. diameter welded stud bolts (Fig. 9) in the same manner employed on the California type 8 and 9 bridge rails.

The upper and lower rails in the leading 10 ft of approach guardrail at the end upstream of traffic are bent down on 20-ft and 19-ft radii respectively. The end of each rail is anchored with one ¾-in. diameter by 12-in. long high-strength steel bolt cast in the 24- by 54- by 24-in. deep reinforced concrete anchor block (Fig. 10). In plan view, the upstream end of the approach guardrail is offset 3 ft from the projected straight line of the bridge rail (Fig. 11). This offset is achieved by curving all but the end 10 ft of the approach guardrail on a 230-ft radius.

At the downstream end, the upper approach rail was spliced to the single rail of the type 9 bridge barrier rail. The lower approach rail was secured to the bridge barrier rail concrete parapet with two ¾-in. diameter by 12-in. long high-strength bolts cast in the parapet (Fig. 12). The length of the type 8 bridge approach guardrail was 38.5 ft and the length of the type 9 bridge rail to which it was attached was 65 ft, providing a total installation length for test 171 of 103.5 ft. Details of the type 8 bridge approach rail design used in this test are shown in Figure A3 of the Appendix.

In order to determine the redirecting characteristics of this system, a 60-mph, 25-deg impact was planned to contact the approach guardrail approximately 20 ft from the upstream end. However, because of an inaccuracy in vehicle steering control, the test vehicle in test 171 impacted the approach guardrail within the upstream sloping section approximately 4 ft from the leading end at 60 mph and 27 deg.

At the point of initial contact, the upper approach rail was approximately 15 in. above the pavement. This low height permitted the bumper and leading frame members of the vehicle to pass over the rail upon impact. The sloping rails imparted both a vertical force and a rolling moment to the vehicle as it vaulted the barrier. The vehicle rolled in a counterclockwise direction while it was airborne before landing on its left side. It then rolled over onto its top as it skidded an additional 140 ft before coming to rest. Pertinent data on this test are shown in Figure A4 of the Appendix.

The rails deflected laterally and high tensile forces caused the upstream rail end anchor bolts to strip (Fig. 13). The loss of upstream end anchorage transmitted additional impact loading downstream to the barrier posts. The timber portion of post 1 was sheared at ground level and post 2 was severely fractured (Fig. 14). Damage

Figure 11.

Figure 12.

Figure 13.

Figure 14.

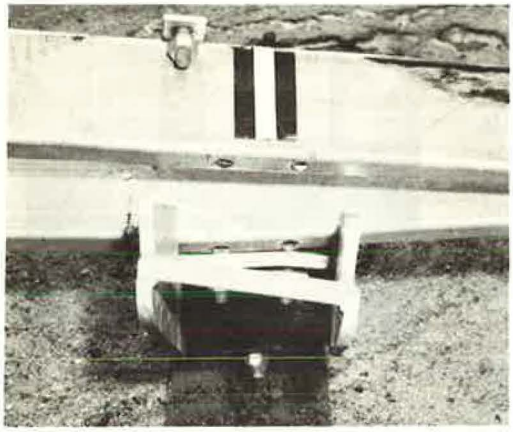

Figure 15.

Figure 16.

to the steel portion occurred at post 1 only. This damage consisted of moderate deformation of the side flanges and the rail mounting bars.

All tubular steel rail sections were damaged. Stud-weld failures occurred on the upper rail at all three approach guardrail posts and on the lower rail at post 1 only (Figs. 15 and 16). However, there were no rail splice failures and the downstream rail-to-parapet connection was not damaged.

Vehicle damage consisted of moderate sheet metal deformation of the left side and top. Deformation of the front bumper occurred when it impacted post 1 and snagged under the upper rail (Fig. 17).

Test 173—Type 8 Bridge Approach Guardrail, Modified

For this second approach guardrail test, several modifications were made to the post and end anchorage details to correct deficiencies noted in the design used in test 171. At the end upstream to traffic, the rail end anchorage was substantially strengthened by welding a steel plate to both the upper and lower rails and securing each with two 1-in. diameter by 15-in. long high-strength bolts cast in separate 2-ft diameter by 4-ft deep cylindrical reinforced concrete anchors (Fig. 18). The downstream rail ends were attached to the type 9 bridge barrier rail as in test 171 except that the cast-in anchor bolts were increased in size from a $^{3}/_{4}$-in. to a 1-in. diameter and the bolt edge distance from the face of the parapet was increased to 4 in. from 3 in.

The composite fabricated steel and timber guardrail post used in test 171 was replaced with fabricated steel posts at 10-ft centers anchored with three 1-in. diameter by 15-in. long high-strength bolts cast in 2-ft diameter by 4-ft deep cylindrical reinforced concrete cast in drilled hole footings (Fig. 19).

As an additional measure, the interior sleeve rail splice used in test 171 was strengthened by the use of a $1^{3}/_{8}$-in. solid

Figure 17.

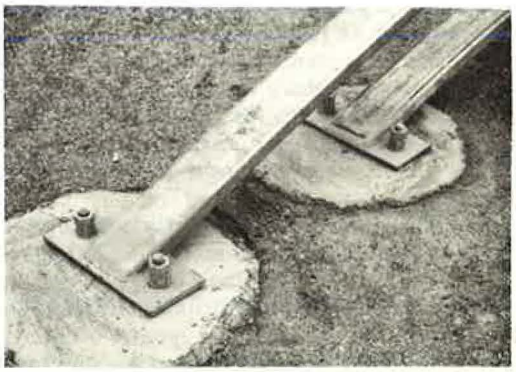

Figure 18.

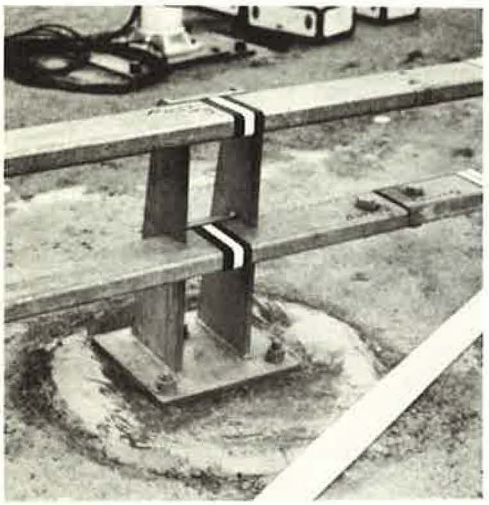

Figure 19.

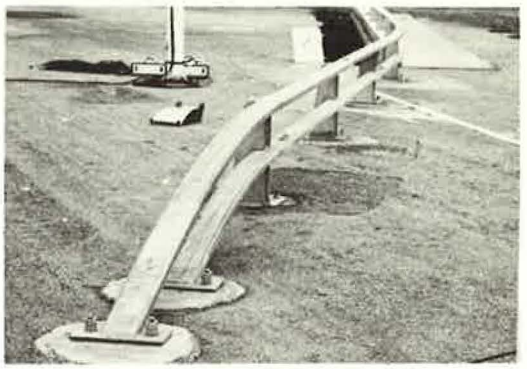

Figure 20.

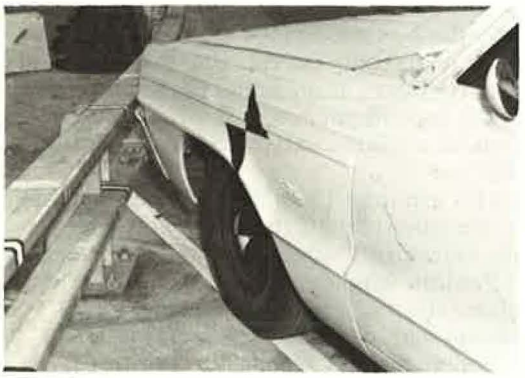

Figure 21.

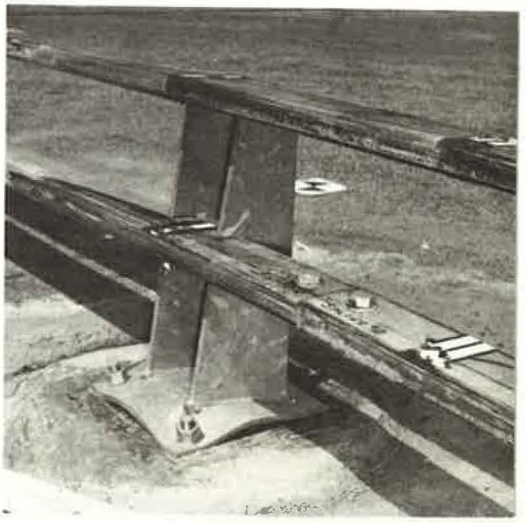

Figure 22.

steel splice plate and the splice bolts were increased from $\frac{3}{4}$ in. to 1 in. in diameter. Details on the bridge approach guardrail design employed in test 173 are shown in Figure A5 of the Appendix.

For this test installation, the 3-ft upstream end offset was obtained by curving the 17 ft of rail adjacent to the bridge rail at a 170-ft radius with the remaining 31.5 ft of rail being constructed on a tangent. The total approach guardrail length was 48.5 ft and bridge rail length was 65 ft, providing a total installation length for test 173 of 113.5 ft (Fig. 20). The initial impact point for this second approach guardrail test was near the center of the installation 2.5 ft upstream of post 3 at 61 mph and 24 deg.

The height of the lower rail (15 in.) in relation to the vehicle bumper (Fig. 21) permitted the bumper and chassis to project over the lower rail upon impact as the upper rail "knifed" into the vehicle body just below the headlamp.

This penetration of the vehicle into the guardrail permitted metal components to snag on the steel posts. The weld ruptures and base plate deformation at post 3 are indicative of this high loading (Fig. 22). There were no anchor-bolt, rail-splice, or stud-bolt failures. However, the guardrail was under considerable lateral stress, as indicated by the displacement between the concrete footings under the fabricated steel

Figure 23.

Figure 24.

posts and the surrounding soil. There was also a slight weld rupture and base plate deformation at post 4, which was 12.5 ft downstream of impact (Fig. 23).

Considering the severity of the impact, overall guardrail damage was relatively minor, with only one post sustaining deformation extensive enough to require replacement. Three approach rail sections were also deformed with maximum permanent deflection of 0.5 ft laterally and 0.15 ft vertically. Even after this severe impact, all components were intact and the approach guardrail was still functional (Figs. 24 and 25).

There was no damage to any of the concrete portions of the bridge approach guardrail or the bridge barrier rail, and repairs would consist only of replacing the deformed post and rail sections in the approach guardrail. However, if deemed necessary, interim repairs could be effected by straightening the bent members. Based on the results of test 173, it appears that this guardrail would perform satisfactorily for fairly severe impacts with little maintenance being required.

Vehicle dynamics were considered tolerable with minimal jump and only a moderate tendency to roll. Vehicle-barrier contact was approximately 10 ft and the exit angle was about 19 deg. Pertinent data on this test are shown in Figure A6 of the Appendix.

Vehicle damage consisted of moderate deformation of the left front wheel and chassis and extensive sheet metal deformation at the left front end. The left front fender was deeply indented where the upper rail knifed into it (Fig. 26). Damage to the left side, rear fender, and rear bumper occurred during the secondary impact as

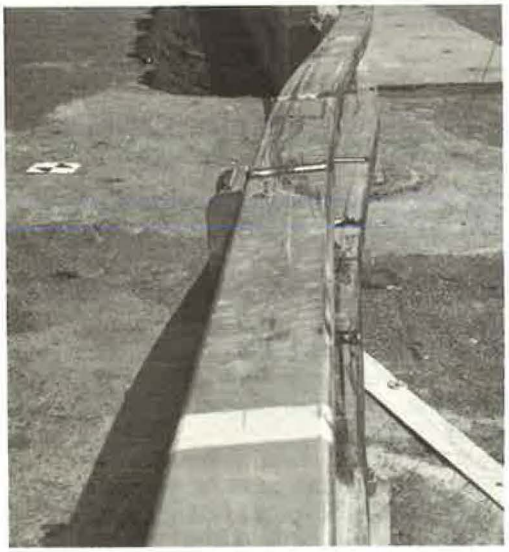

Figure 25.

Figure 26.

the vehicle was redirected parallel to the barrier (Fig. 27).

Figure 27.

Test 174—Type 8 Bridge Approach Guardrail

Results of the previous two bridge approach guardrail tests (tests 171 and 173) suggested further design refinements for this third and final bridge approach guardrail test installation (test 174). The first test (test 171) had indicated that the upstream end anchorage system and the barrier post design were inadequate. In the second test (test 173), an attempt was made to correct these deficiencies by using a strengthened tubular rail end anchorage attachment and a modified post design. The strengthened end anchorage attachment was considered adequate and was not changed for test 174. However, the two separate cylindrical concrete footings used to anchor the rails were replaced by a single, 36- by 42- by 24-in. deep rectangular reinforced concrete footing.

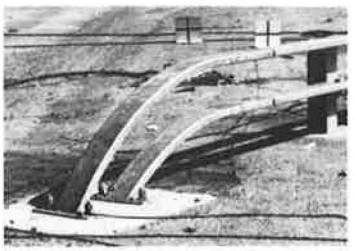

Figure 28.

Based on the previous two tests, it was also felt that the 10-ft long sloping upstream rail end section presented an excessive area of vulnerability to an errant vehicle. Therefore, this sloping section was reduced in length to 4 ft 7 in., with the lower rails curved down at 6-ft and 5-ft radii respectively (Fig. 28).

The modified welded steel post design used in test 173, although structurally adequate, was expensive and difficult to construct, repair, and/or replace. Therefore, for test 174 a more economical and practicable design was used consisting of steel wide-flange beam (6WF25) posts on 10-ft centers embedded in 36-in. deep by 18-in. diameter concrete footings (Fig. 29).

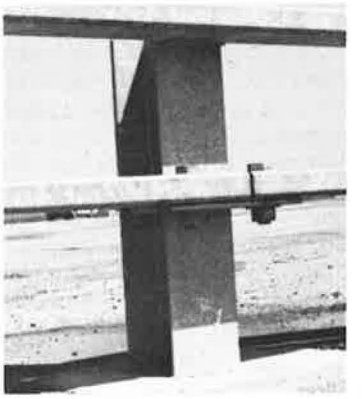

Figure 29.

In lieu of the interior sleeve splice design used in the previous tests, rail splicing was accomplished by bolting the rail section ends to a 5- by $2\frac{1}{2}$- by $\frac{1}{2}$-in. steel angle with 1-in. diameter by 4-in. long high-strength bolts. The steel angle was secured, along with the rails, to the steel posts by $\frac{3}{4}$-in. stud bolts welded on the tubular rail (Figs. 30 and 31). The steel angle was used only at tubular rail splices. All other rail-to-post attachment was accomplished utilizing the welded stud bolt with a $\frac{1}{2}$-in. thick backup spacer.

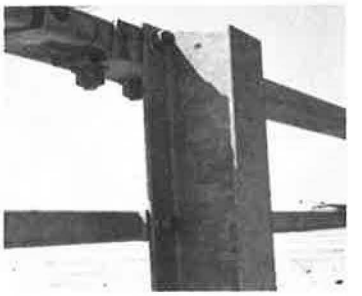

Figure 30.

The same rail-to-parapet connection was used at the downstream end as in the preceding test. Details on the final type 8 bridge approach guardrail design used in test 174 are shown in Figure A7 of the Appendix. The guardrail was flared to a 3-ft offset at the upstream end by curving the 18.5 ft of approach rail adjacent to the bridge rail to a 240-ft radius. The remaining 30 ft of rail was constructed on a straight tangent. The total approach guardrail length was 48.5 ft and the bridge barrier rail length

Figure 31.

Figure 32.

Figure 33.

was 65 ft, thus providing a total installation length for test 174 of 113.5 ft (Fig. 32).

The initial impact point for this third and final approach guardrail test was approximately midspan between posts 3 and 4 at 60 mph and 26 deg. As in the previous tests, the front bumper and left front chassis members projected over the 15-in. high lower rail as the upper rail indented a deep groove into the vehicle body.

Vehicle dynamics through impact were considered to be good with no tendency to jump and only a minimal roll toward the barrier. Vehicle-barrier contact was approximately 10 ft and the exit angle about 19 deg. Pertinent data on this test are shown in Figure A8 of the Appendix.

Vehicle damage was moderate, with substantial sheet metal deformation at the left front end (Fig. 33). Deformation of the left side body panels and the left front wheel were less severe than in test 173. The secondary impact from the rear of the vehicle striking the barrier was also less severe, as indicated by the minimal damage to the left rear body panels and rear bumper.

The guardrail damage from this severe impact was relatively minor. Although a butt-welded splice in the upper rail at post 3 did fracture, as shown in Figures 34 and 35, this failure was attributed to poor welding practice. An internal welding backup plate was not used, resulting in poor weld penetration. Future specifications will require that a backup plate be used on all butt-welded rail elements to ensure full weld penetration. As shown in Figure 34, the rail elements downstream of post 3 were twisted up at the rail splices. This is indicative of the torsional force applied

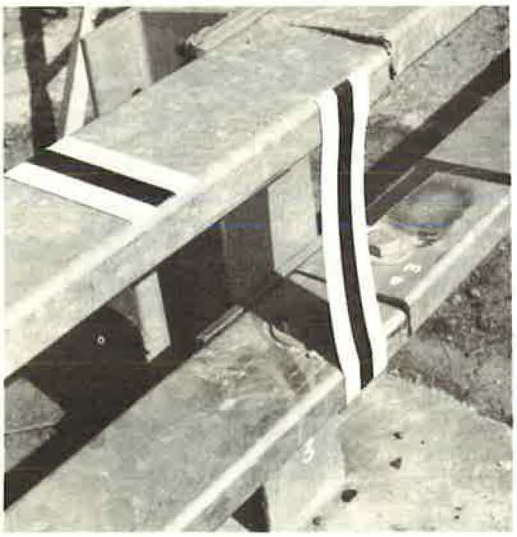

Figure 34.

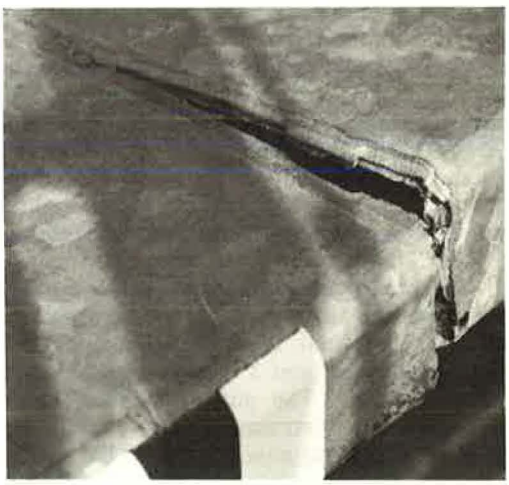

Figure 35.

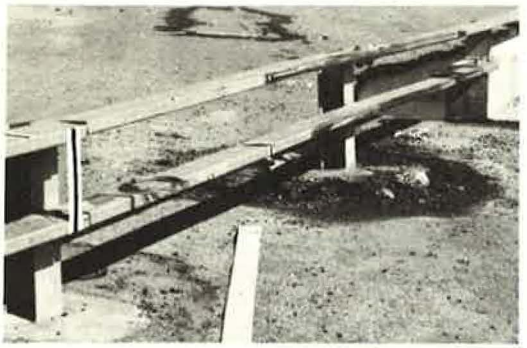

Figure 36.

Figure 37.

to the rails. Post 3, although rotated back approximately 10 deg, was not deformed. Three rail sections were only slightly deformed, with maximum residual deflections of 0.23 ft laterally and 0.03 ft vertically. After impact all barrier components were intact and the barrier was still considered to be functional (Fig. 36). The concrete parapet at the downstream lower rail connection was cracked. However, the anchor bolts were not deformed and would not require replacement (Fig. 37).

It was concluded that the final California type 8 bridge approach guardrail design in test 174 fulfills the current requirements for an approach guardrail leading up to a rigid-type bridge barrier rail. This approach guardrail design is relatively economical to construct and the reduced vehicle damage and more tolerable vehicle damage observed show it to be an improvement over the two previous preliminary designs.

CONCLUSIONS

The following conclusions are based on an analysis of the results of the full-scale vehicle impact tests conducted during this test series:

1. The type 9 bridge barrier rail design impacted in test 172 will retain and redirect a 4,500-lb sedan impacting at a 25-deg approach angle and a speed of 60 mph. Barrier damage from such an impact can be expected to be moderate but repairable and the barrier will remain effective with all critical components intact.
2. The initial type 8 bridge approach guardrail design impacted in test 171 will not retain nor redirect a 4,500-lb sedan impacting at a wide angle and high speed when impact is within the upstream sloping rail section. Barrier damage also indicated that the upstream bolted rail anchorage and the composite fabricated steel and timber post design were structurally inadequate. It was further concluded that any impact into the sloped rail section at the upstream end of the bridge approach guardrail could cause the vehicle to overturn, and therefore this section should be as short as possible to reduce the area of vulnerability.
3. The modified type 8 bridge approach guardrail design impacted in test 173 will retain and redirect a 4,500-lb sedan impacting at a 25-deg approach angle and a speed of 60 mph. However, this barrier design with its fabricated steel posts and reinforced concrete post anchors is expensive to fabricate and difficult to construct.
4. The final type 8 bridge approach guardrail design impacted in test 174 will retain and redirect a 4,500-lb sedan impacting at a 25-deg approach angle and a speed of 60 mph. In addition to performing satisfactorily under a severe impact, this final design utilizing a shorter, stronger upstream rail anchorage and steel wide-flange (6WF25) post is considered relatively easy and economical to fabricate and construct.

ACKNOWLEDGMENT

This work was accomplished in cooperation with the U.S. Department of Transportation, Federal Highway Administration, Bureau of Public Roads. The opinions, findings,

and conclusions expressed in this paper are those of the authors and not necessarily those of the Bureau of Public Roads.

REFERENCES

1. Nordlin, E. F., Field, R. N., and Stoker, J. R. Dynamic Full-Scale Tests of Steel Bridge Rails. Series 11, California Division of Highways, June 1967.
2. Beaton, J. L. Full-Scale Tests of Concrete Bridge Rails Subjected to Automobile Impacts. HRB Proc., Vol. 35, 1956, pp. 251-267.
3. Field, R. N., and Prysock, R. H. Dynamic Full-Scale Impact Tests of Double Blocked-Out Metal Beam Barriers and Metal Beam Guard Railing. Series 10, California Division of Highways, Feb. 1965.
4. Nordlin, E. F., Field, R. N., and Hackett, R. P. Dynamic Full-Scale Impact Tests of Bridge Barrier Rails. Series 8, presented at the 43rd Annual Meeting of the Highway Research Board, Jan. 1964.
5. Proposed Full-Scale Testing Procedures for Guardrails. Highway Research Circular 482, Sept. 1962.

Appendix

The following figures contain pertinent data and photographs of the impact tests discussed in this report.

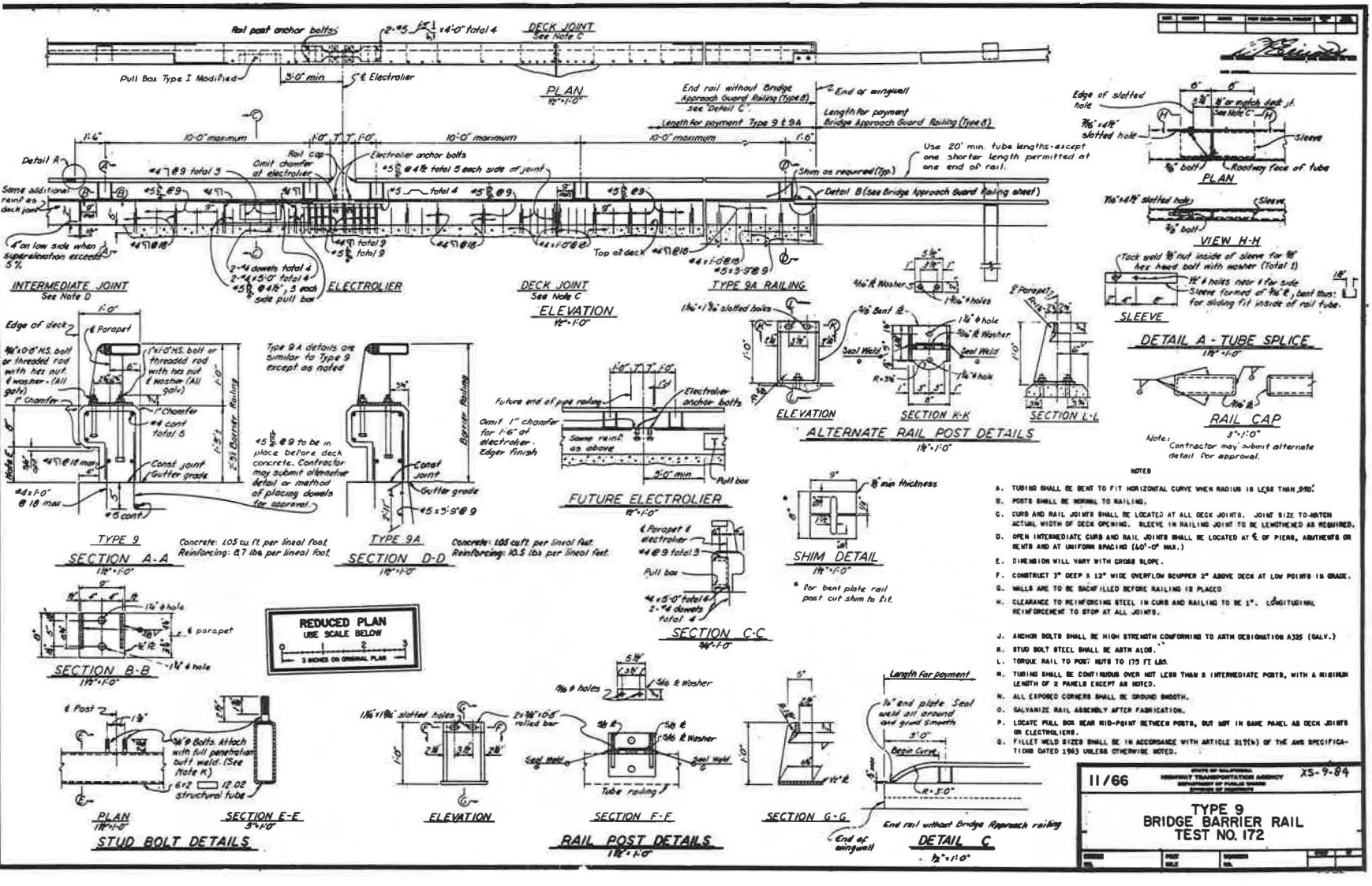
PLAN
ELEVATION
INTERMEDIATE JOINT
See Note D
ELECTROLIER
DECK JOINT
See Note C
TYPE 9A RAILING
ALTERNATE RAIL POST DETAILS
SECTION K-K
SECTION L-L
DETAIL A - TUBE SPLICE
RAIL CAP
SLEEVE
VIEW H-H
TYPE 9
SECTION A-A
TYPE 9A
SECTION D-D
FUTURE ELECTROLIER
SECTION C-C
SHIM DETAIL
SECTION B-B
REDUCED PLAN
USE SCALE BELOW
STUD BOLT DETAILS
SECTION E-E
RAIL POST DETAILS
SECTION F-F
SECTION G-G
DETAIL C
NOTES
A. TUBING SHALL BE BENT TO FIT HORIZONTAL CURVE WHEN RADIUS IS LESS THAN 950'.
B. POSTS SHALL BE NORMAL TO RAILING.
C. CURB AND RAIL JOINTS SHALL BE LOCATED AT ALL DECK JOINTS. JOINT SIZE TO MATCH ACTUAL WIDTH OF DECK OPENING. SLEEVE IN RAILING JOINT TO BE LENGTHENED AS REQUIRED.
D. OPEN INTERMEDIATE CURB AND RAIL JOINTS SHALL BE LOCATED AT ℄ OF PIERS, ABUTMENTS OR BENTS AND AT UNIFORM SPACING (40'-0" MAX.)
E. DIMENSION WILL VARY WITH CROSS SLOPE.
F. CONSTRUCT 3" DEEP X 12" WIDE OVERFLOW SCUPPER 2" ABOVE DECK AT LOW POINTS IN GRADE.
G. WALLS ARE TO BE BACKFILLED BEFORE RAILING IS PLACED
H. CLEARANCE TO REINFORCING STEEL IN CURB AND RAILING TO BE 1". LONGITUDINAL REINFORCEMENT TO STOP AT ALL JOINTS.
J. ANCHOR BOLTS SHALL BE HIGH STRENGTH CONFORMING TO ASTM DESIGNATION A325 (GALV.)
K. STUD BOLT STEEL SHALL BE ASTM A108.
L. TORQUE RAIL TO POST NUTS TO 175 FT LBS.
M. TUBING SHALL BE CONTINUOUS OVER NOT LESS THAN 2 INTERMEDIATE POSTS, WITH A MINIMUM LENGTH OF 2 PANELS EXCEPT AS NOTED.
N. ALL EXPOSED CORNERS SHALL BE GROUND SMOOTH.
O. GALVANIZE RAIL ASSEMBLY AFTER FABRICATION.
P. LOCATE PULL BOX NEAR MID-POINT BETWEEN POSTS, BUT NOT IN SAME PANEL AS DECK JOINTS OR ELECTROLIERS.
Q. FILLET WELD SIZES SHALL BE IN ACCORDANCE WITH ARTICLE 217(h) OF THE AWS SPECIFICATIONS DATED 1963 UNLESS OTHERWISE NOTED.
11/66
X5-9-84
TYPE 9
BRIDGE BARRIER RAIL
TEST NO. 172

Figure A1.

IMPACT + 0.01 Sec.

I + 0.06 Sec.

I + 0.16 Sec.

I + 0.26 Sec.

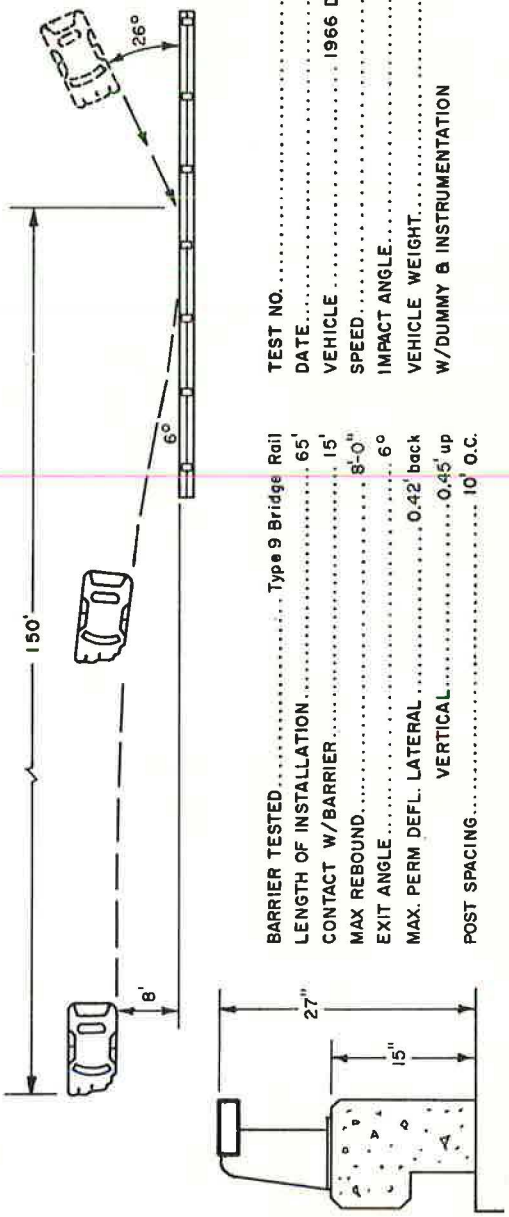

Figure A2.

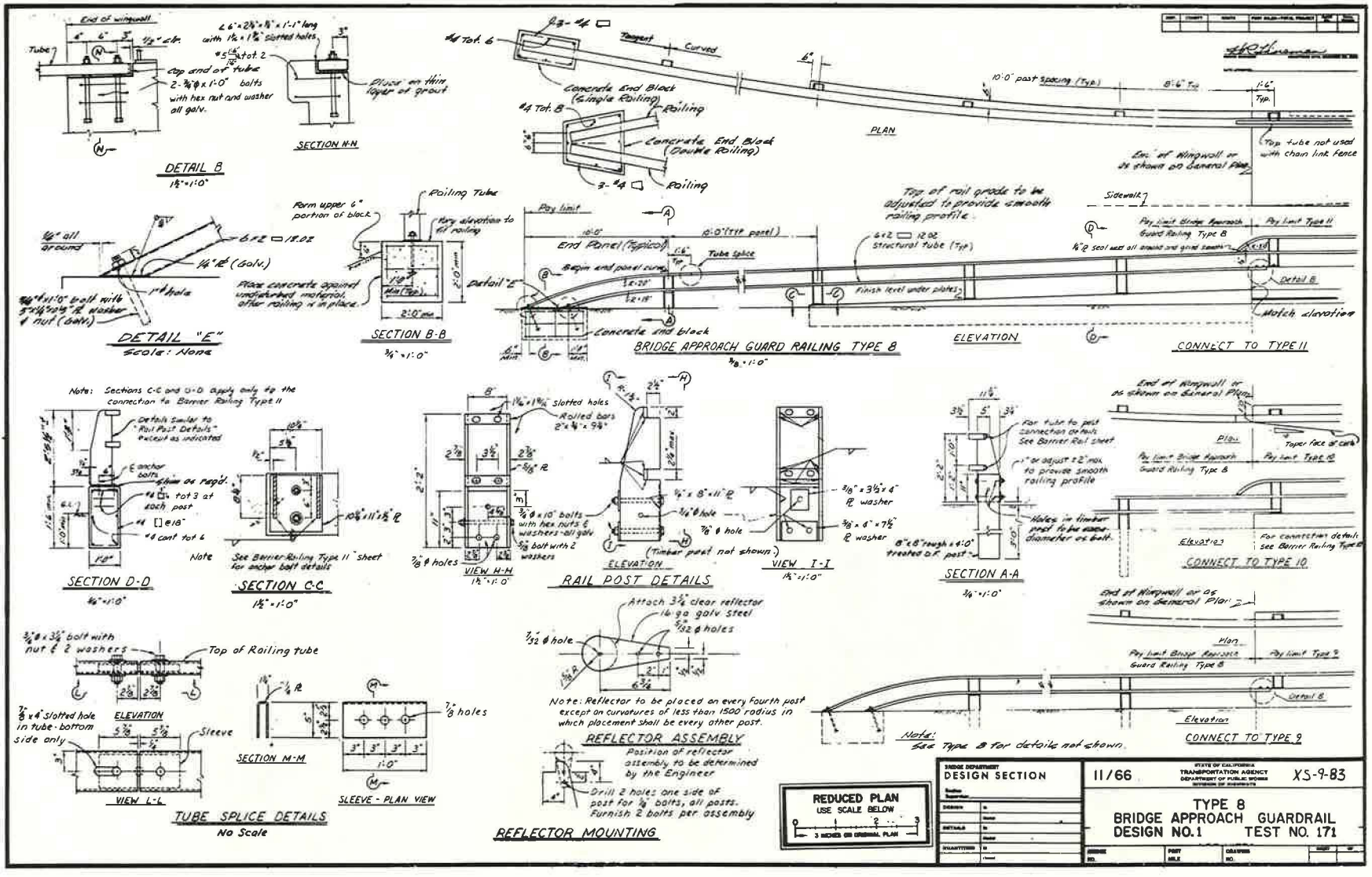
DETAIL B
SECTION N-N
PLAN
Concrete End Block (Single Railing)
Concrete End Block (Double Railing)
Railing
Tangent
Curved
10'-0" post spacing (Typ.)
Top tube not used with chain link fence
DETAIL "E"
Scale: None
SECTION B-B
Railing Tube
Detail "E"
Concrete end block
BRIDGE APPROACH GUARD RAILING TYPE 8
ELEVATION
Top of rail grade to be adjusted to provide smooth railing profile.
Sidewalk
Pay limit
End Panel (Typical)
Tube splice
Finish level under plates
Match elevation
CONNECT TO TYPE 11
Note: Sections C-C and D-D apply only to the connection to Barrier Railing Type 11
SECTION D-D
SECTION C-C
See Barrier Railing Type 11 sheet for anchor bolt details
Slotted holes
Rolled bars
VIEW H-H
RAIL POST DETAILS
(Timber post not shown)
VIEW I-I
SECTION A-A
For tube to post connection details see Barrier Rail sheet
Holes in timber post to be same diameter as bolt.
Taper face of curb
Elevation
For connection details see Barrier Railing Type 8
CONNECT TO TYPE 10
Attach 3/4" clear reflector to 10 ga galv steel
Note: Reflector to be placed on every fourth post except on curvatures of less than 1500 radius in which placement shall be every other post.
REFLECTOR ASSEMBLY
Position of reflector assembly to be determined by the Engineer
Drill 2 holes one side of post for 1/2" bolts, all posts. Furnish 2 bolts per assembly
REFLECTOR MOUNTING
Top of Railing tube
ELEVATION
VIEW L-L
SECTION M-M
SLEEVE - PLAN VIEW
TUBE SPLICE DETAILS
No Scale
Note: See Type B for details not shown.
CONNECT TO TYPE 9
REDUCED PLAN
USE SCALE BELOW
3 INCHES ON ORIGINAL PLAN
DESIGN SECTION
11/66
XS-9-83
TYPE 8
BRIDGE APPROACH GUARDRAIL
DESIGN NO. 1
TEST NO. 171

Figure A3.

IMPACT

I + 0.15 Sec.

I + 0.30 Sec.

I + 0.60 Sec.

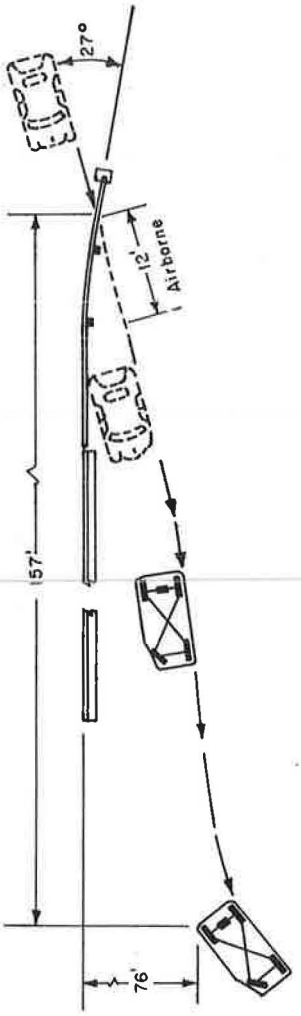

TEST NO.	171
DATE	10-19-68
VEHICLE	1966 Dodge Sedan
SPEED	60 mph
IMPACT ANGLE	27°
VEHICLE WEIGHT	4540 #
W/DUMMY & INSTRUMENTATION	
BARRIER TESTED	Type 8 B.A.G.
LENGTH OF INSTALLATION	103.5'
CONTACT W/BARRIER	Penetration
MAX REBOUND	Penetration
EXIT ANGLE	Penetration
MAX. PERM DEFL. LATERAL	0.5' back
VERTICAL	0.15' dn
POST SPACING	10' O.C.

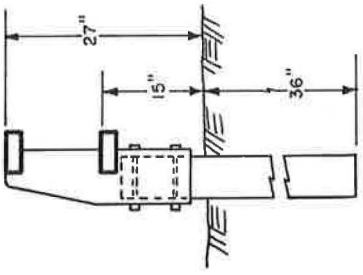

Figure A4.

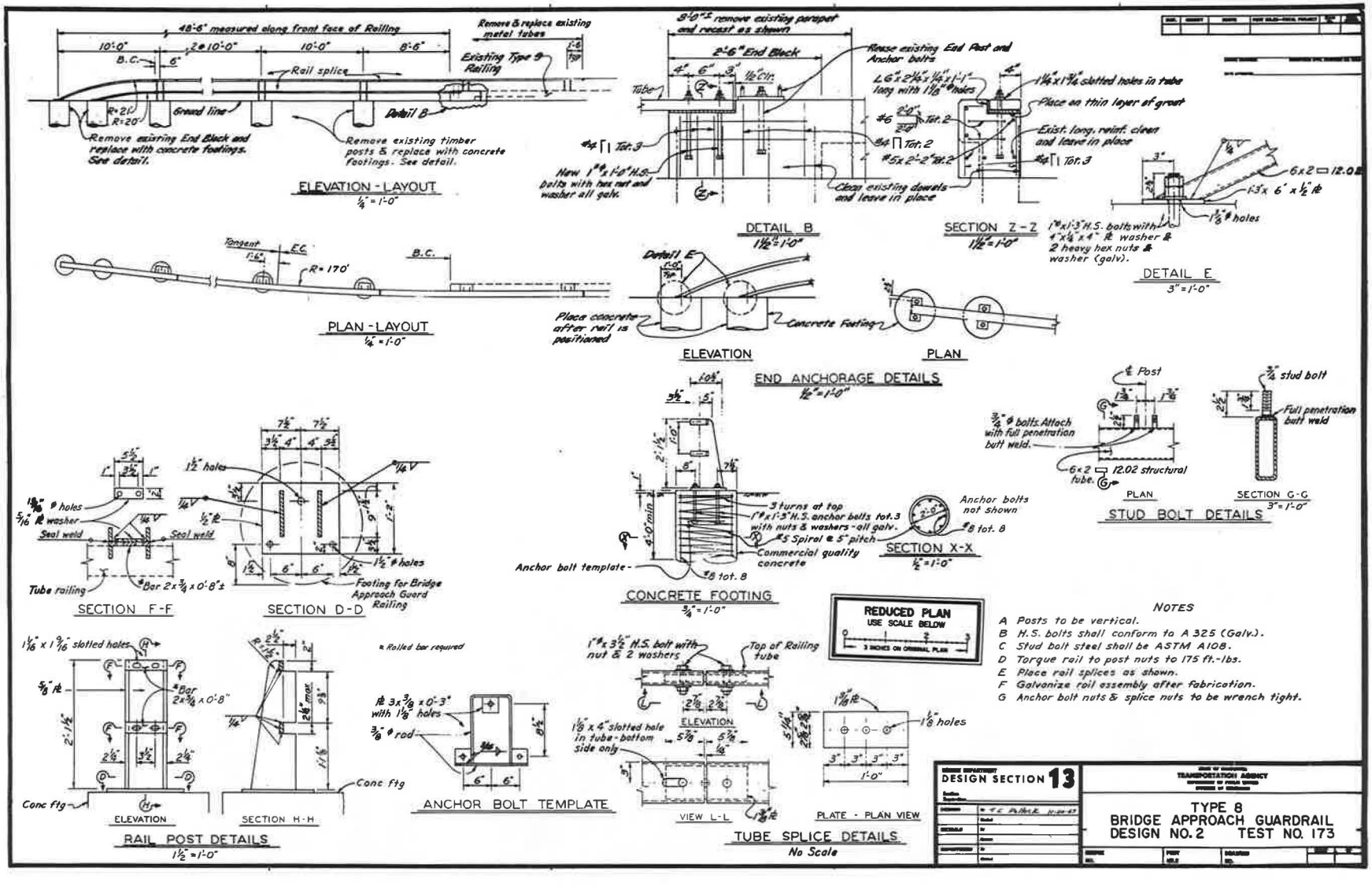
ELEVATION - LAYOUT
PLAN - LAYOUT
DETAIL B
SECTION Z - Z
DETAIL E
ELEVATION
PLAN
END ANCHORAGE DETAILS
CONCRETE FOOTING
STUD BOLT DETAILS
SECTION F-F
SECTION D-D
SECTION X-X
RAIL POST DETAILS
ANCHOR BOLT TEMPLATE
TUBE SPLICE DETAILS
No Scale
PLATE - PLAN VIEW
REDUCED PLAN
USE SCALE BELOW
NOTES
A Posts to be vertical.
B H.S. bolts shall conform to A 325 (Galv.).
C Stud bolt steel shall be ASTM A108.
D Torque rail to post nuts to 175 ft.-lbs.
E Place rail splices as shown.
F Galvanize rail assembly after fabrication.
G Anchor bolt nuts & splice nuts to be wrench tight.
DESIGN SECTION 13
TYPE 8
BRIDGE APPROACH GUARDRAIL
DESIGN NO. 2 TEST NO. 173

Figure A5.

IMPACT + 0.03 Sec.

I + 0.13 Sec.

I + 0.23 Sec.

I + 0.33 Sec.

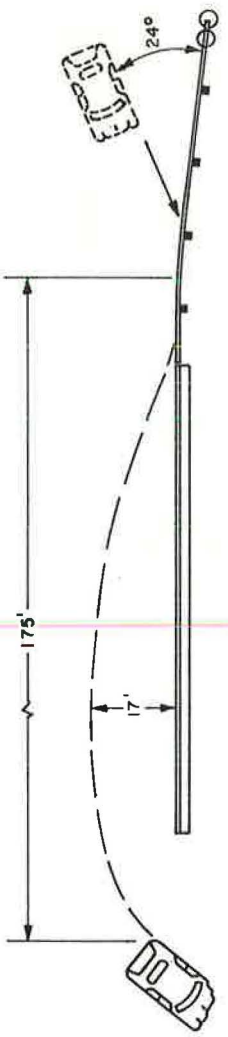

TEST NO.	173
DATE	4-16-68
VEHICLE	1966 Dodge Sedan
SPEED	61 mph
IMPACT ANGLE	24°
VEHICLE WEIGHT	4540 #
W/DUMMY & INSTRUMENTATION	

BARRIER TESTED	Type B B.A.G.
LENGTH OF INSTALLATION	113.5'
CONTACT W/BARRIER	10'
MAX REBOUND	17'
EXIT ANGLE	19°
MAX. PERM DEFL. LATERAL	0.5' back
VERTICAL	0.15' up
POST SPACING	10' O.C.

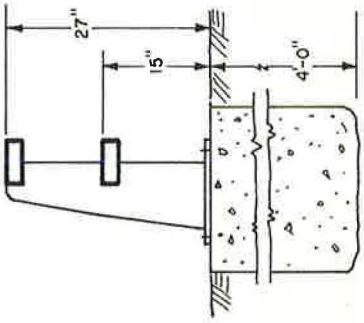

Figure A6.

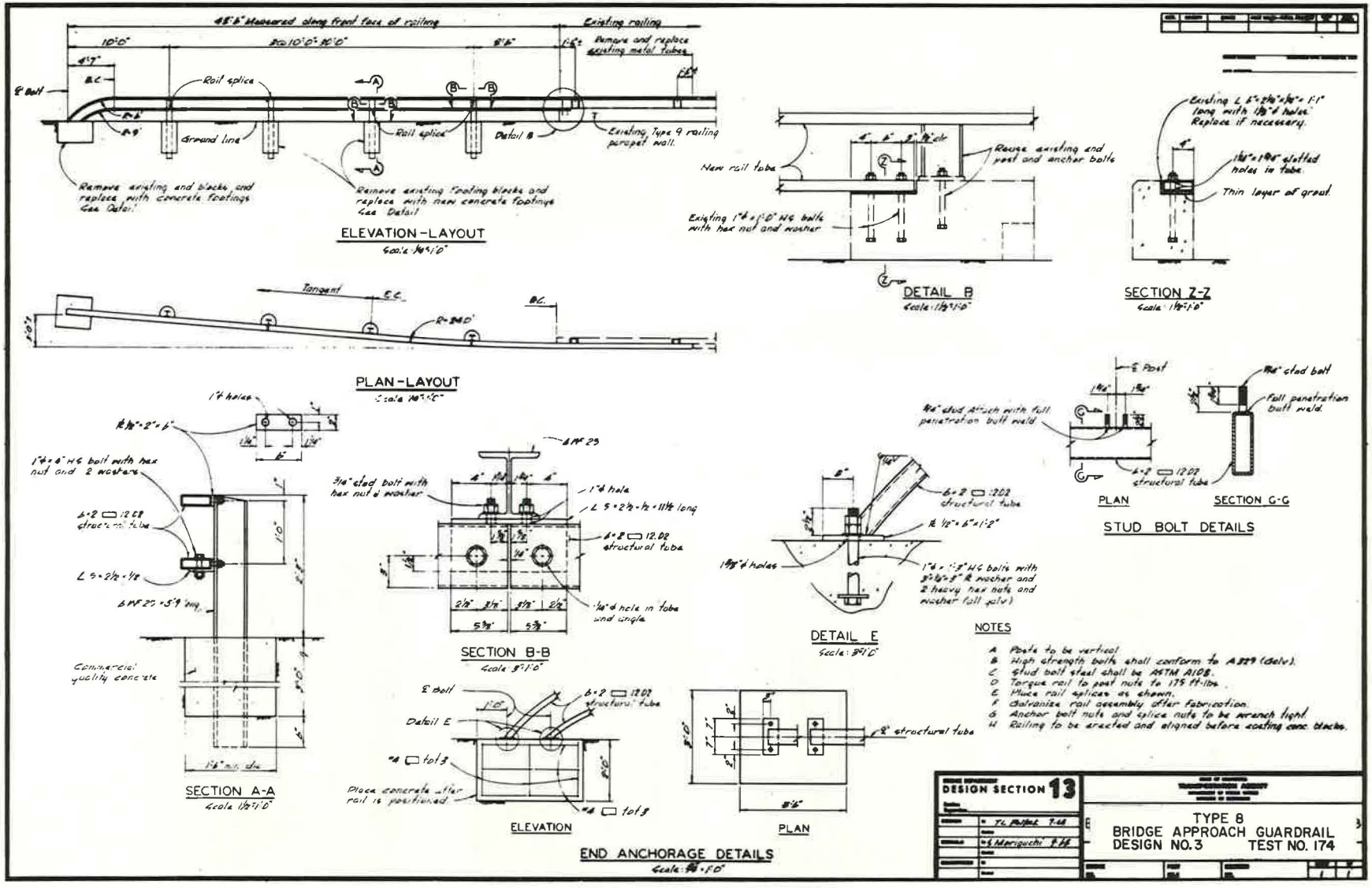
ELEVATION - LAYOUT
PLAN - LAYOUT
DETAIL B
SECTION Z-Z
STUD BOLT DETAILS
PLAN
SECTION G-G
DETAIL E
NOTES
A Posts to be vertical.
B High strength bolts shall conform to A325 (Type).
C Stud bolt steel shall be ASTM A108.
D Torque rail to post nuts to 175 ft-lbs.
E Make rail splices as shown.
F Galvanize rail assembly after fabrication.
G Anchor bolt nuts and splice nuts to be wrench tight.
H Railing to be erected and aligned before casting conc. blocks.
SECTION A-A
SECTION B-B
ELEVATION
PLAN
END ANCHORAGE DETAILS
DESIGN SECTION 13
TYPE 8
BRIDGE APPROACH GUARDRAIL
DESIGN NO. 3 TEST NO. 174

Figure A7.

IMPACT + 0.05 Sec.

I + 0.15 Sec.

I + 0.20 Sec.

I + 0.35 Sec.

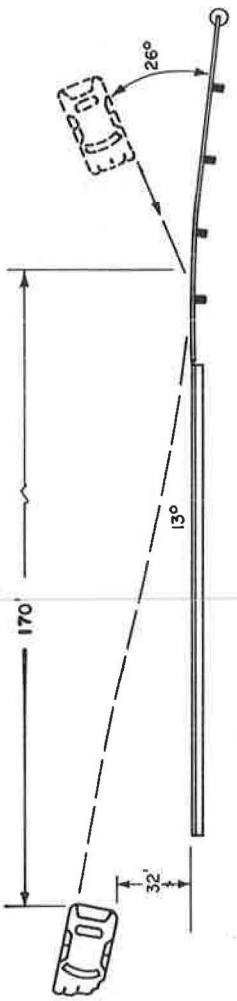

TEST NO.	174
DATE	3-11-69
VEHICLE	1966 Dodge Sedan
SPEED	60 mph
IMPACT ANGLE	26°
VEHICLE WEIGHT	4540 #
W/DUMMY & INSTRUMENTATION	

BARRIER TESTED	TYPE 8 B.A.G.
LENGTH OF INSTALLATION	113.5'
CONTACT W/BARRIER	10'
MAX REBOUND	32'
EXIT ANGLE	13°
MAX. PERM DEFL. LATERAL	0.23' back
VERTICAL	0.03' up
POST SPACING	10' O.C.

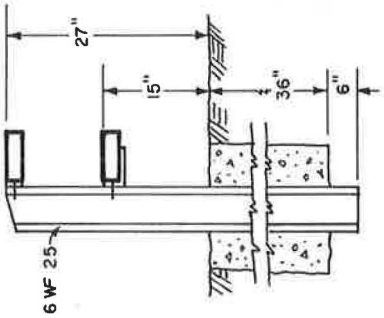

Figure A8.

Design, Fabrication, and Installation of a Fragmenting-Tube-Type Energy Absorber in Conjunction With a Bridge Rail

WILLIAM E. WOOLAM and LUIS R. GARZA,
Department of Mechanical Sciences, Southwest Research Institute,
San Antonio, Texas

Conventional modern bridge rails are rigid installations that redirect the vehicle without providing any energy absorption. This report discusses the design theory that provides a new concept of an energy-absorbing bridge rail, utilizing a fragmenting tube as the primary energy-absorbing element. The paper discusses the separate functions of the bridge rail as both an energy-absorbing system for small vehicles and a redirecting rail for large vehicles. Also presented is a new concept in guardrail design—the cantilevered rail concept. The procedures for fabrication and installation of this prototype energy-absorbing rail are discussed in detail.

•THE TECHNICAL DETAILS involved in the design, fabrication, and installation of an aerospace-developed energy absorber in conjunction with a bridge rail system are discussed in this paper. The primary objective of this research and development program was to demonstrate the feasibility of using a fragmenting-tube-type energy absorber in order to improve the energy-absorbing capability of conventional rigid bridge rail systems. The energy absorber not only effectively diminished the damage potential of the rigid bridge rail systems but also provided the following fringe benefits:

1. It introduced a cantilevered guardrail attachment that eliminated wheel-snagging.
2. It provided the possibility of a dual-purpose guardrail—a primary soft rail system for automobiles (light vehicles), and a secondary stiff rail system for trucks and buses (heavy vehicles).
3. It provided a mechanical-type load relief valve that prevents dynamic loads of over 10,000 lb per post, thus reducing bridge deck damage as a result of the light vehicle impacts.
4. It provided an extremely promising approach to the problem of transition of the bridge rail systems from an off-deck to an on-deck condition.

The design philosophy that resulted in this unique energy-absorbing bridge rail is outlined and described in the present paper. In addition, photographs are used to illustrate the energy absorber and its installation into the bridge rail system.

The full-scale crash tests and the subsequent evaluation of the energy-absorbing bridge rail system are presented in a separate paper by the evaluator, the Texas Transportation Institute (TTI). At the conclusion of the two papers, recommendations for improvements of the overall bridge rail system are presented. These recommendations contain inputs from both the designers and the evaluators.

Paper sponsored by Committee on Guardrail, Median Barriers and Sign, Signal and Lighting Supports and Committee on Bridge Design and presented at the 49th Annual Meeting.

DESIGN

The following design philosophy was utilized in formulating the energy-absorbing bridge rail:

1. Provide a primary energy-absorbing system with a stroke limited to less than 2 ft and simultaneously provide a tolerable environment for a properly restrained occupant of a light vehicle;
2. Provide a secondary backup guardrail system that would provide sufficient strength to prevent penetration of a heavy vehicle;
3. Prevent damage to the vehicle as a result of wheels snagging on the backup posts; and
4. Provide a transition section from the softer off-deck guardrail system to the stiffer on-deck bridge rail.

Although the secondary backup guardrail system was not recognized initially as a portion of the beneficial design philosophy, the backup system was designed to retain large vehicles and for that reason is mentioned here. This benefit was later pointed out by the Bureau of Public Roads.

It was deemed absolutely necessary that the preceding overall philosophy be considered when designing an energy-absorbing bridge rail. Even though these were foremost in the minds of the designers, the primary objective was to demonstrate that the fragmenting tube would fragment and that the energy absorbers would function mechanically as well as conceptual designs indicated they would.

In addition to the major design philosophy outlined, there were other secondary design features incorporated into the system in order to provide a complete guardrail installation. Because of the limited scope of the present research, the following features were assigned secondary importance: end treatments, backup post for heavy vehicles, rub rails, steel-reinforced concrete decks, and a backup rail installed at a suitable height for larger vehicles having a higher center of gravity. This does not imply that because these features were assigned secondary importance they are sufficiently well developed.

Primary Energy-Absorbing Rail

The three major contributors to the overall energy-absorbing process are the vehicle, the guardrail, and the fragmenting-tube energy absorber. In the case at hand, only the guardrail and the fragmenting tubes are design variables in the energy-absorbing system. After consideration of the various types of conventional guardrail systems, the New York-type 6- by 6- by $^{3}/_{16}$-in steel tubing was selected for inclusion in the system. The guardrail provided suitable stiffness and simplified the attachment of the energy-absorbing device to the backup posts. Next, it was necessary to select the guardrail height and backup post spacing. The guardrail height was selected to be 27 in. as measured from the concrete deck to the top of the beam. This selection was based on results of previous successful crash tests with this particular rail height.

The backup post spacing was selected simultaneously with the energy absorber. Prototype tests at Southwest Research Institute indicated that by using a nominal 3-in. OD 2024 T-3 aluminum tubing and a 0.120-in. wall thickness, each fragmenting tube could be expected to provide a 10,000-lb constant load. Considering an 8 ft 4-in. post spacing combined with the fragmenting-tube absorbers and the New York box beam, we anticipated the approximate peak g deceleration values for three weight ranges of automobiles. These g values would be predicted only near bottoming out. The average would be considerably lower because first one tube is initiated, then two, and so forth, as indicated in the following:

1. 1,600-lb Class—Only a single tube, at the most, would fragment, providing 10,000 lb or 6.2 peak g laterally.
2. 3,200-lb Class—Three tubes would finally fragment, providing a peak force of 30,000 lb or 9.35 peak g laterally.
3. 4,500-lb Class—Five tubes would fragment finally, providing a peak force of 50,000 lb or 11 peak g laterally.

These dynamic conditions were estimated based on an assumed beam deformation curve derived from full-scale crash tests. It was anticipated at this stage that the design could be verified by the Barrier III computer program developed by the University of California at Berkeley. Unfortunately, the computer program was in its developmental stages and could not be used to predict the average g values to be expected from the energy-absorbing system prior to the final design. During the full-scale crash tests, the computer program was debugged and checked out with the energy absorbers represented by a Coulomb damper that would provide a retarding force in only one direction. Future developments can presently be evaluated on the Barrier III computer program using the first four crash tests as test cases.

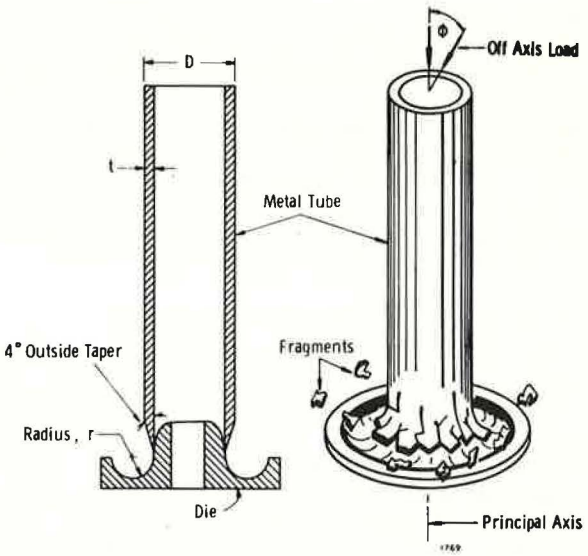

Figure 1. Fragmenting-tube concept.

Because the computer program would require several more months of debugging, the energy-absorbing guardrail designs were frozen at that point and the tubes, post spacing, height, and box beam size were selected. Fortunately, the intuitive design was extremely well optimized, considering that it was predominately designed from engineering judgment.

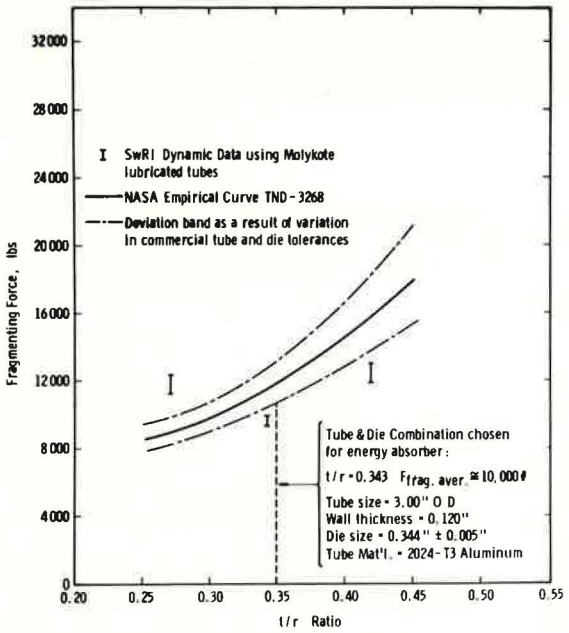

Figure 2. Data on fragmenting tubes.

For those unfamiliar with the fragmenting-tube-type energy absorber concept, it is worthwhile to discuss the mechanics of the energy absorber, the variables that control the fragmenting loads, and designers' problems in using the absorber. The fragmenting tube concept, which was developed at NASA-Langley by J. R. McGehee (filed as Patent 3,143,321, August 4, 1964, and discussed in NASA TN D-3268, February 1966), is shown schematically in Figure 1. The energy absorber consists of a thick-walled aluminum tube and a heat-treated steel flaring die. In the process of forcing the thick-walled aluminum tube over the die, the walls of the tube fail and fragments are shed, thus providing energy absorption. The loads provided by each fragmenting tube can be controlled primarily by a variation of the ratio of the tube-wall thickness to the die radius, referred to as the t/r ratio (Fig. 2). The two most attractive features of the energy absorber are that 100 percent of the tube

can be utilized for energy absorption and the fragmenting forces can be controlled by a simple variation of the tube-wall thickness.

The major design problem encountered in including the fragmenting-tube energy absorbers into a guardrail system was control of the fragmentation. Even in the short distance of 2 ft it was considered desirable to control the fragmenting and to cause the box beam and tubes to be driven straight into the fragmenting dies. In order to accomplish this controlled fragmenting, a steel tubular guide system, similar to the one shown in Figure 3, was designed. The tubular guide system also acted as a cantilever-type support for the box beam and led to an interesting design concept that provided a solution to another problem to be discussed later.

The Secondary Backup Guardrail System

The backup guardrail system should serve two important functions in the overall design concept. First, the backup posts should provide a rigid attachment for the fragmenting die, because otherwise it is doubtful that the energy absorber would function properly. Second, the combination of the backup posts and the concrete deck should survive the dynamic loads that would occur as a result of a large vehicle (truck or bus) impact and at the same time redirect the vehicle.

The backup post system was chosen from a conventional Texas T-1 bridge rail design. This design calls for a 6-in. wide-flange (WF) post welded to a 1-in. steel plate on the base and an 8-in., 11.5-lb channel on the top of the wide flange. In addition, a steel bearing plate is used below the concrete deck, a steel support plate is used internally in the bridge deck, and high-strength steel bolts are used to secure the WF posts to the concrete deck.

The backup post design was stress-analyzed for dynamic loads that would be experienced as a result of a 10,000-lb constant load applied at 27 in. above the bridge deck. The post was considered to be adequate. Therefore, the 6-in. WF post was the post design selected for proving the feasibility of the energy absorbers. As a caution it should be emphasized here that the 6-in. WF has not yet been proven crashworthy for the case of large vehicle impacts (buses and trucks). Before the system is acceptable for redirecting large vehicles, the backup posts should be initially stress-analyzed and finally full-scale crash-tested. The initial stress analysis might lead to a redesign of the backup posts and the base plate, and might require the addition of a second rail mounted higher than the 27-in.-high box beam in order to sufficiently redirect a large vehicle. Because the primary objective, at least initially, was to evaluate the fragmenting tube energy absorbers only for small vehicle impacts, we accepted the 6-in. WF posts for the prototype system.

Elimination of Wheel-Snagging

As a result of the need for a guide tube to control the fragmenting process, the wheel-snagging problems were eliminated. The guide tube, in addition to providing guidance, supported the 6- by 6- by $^3/_{16}$-in. box beam. As a result, the box beam was supported by the guide assembly in an unusual cantilever fashion a distance of approximately 20 in. from the 6-in. WF posts.

It was anticipated that there would be instances when the fragmenting tubes would "bottom out" and the box beam would be forced flush against the backup posts. As a result, a $2^1/_2$-in. pipe rub rail was attached to the 6-in. WF posts at an arbitrary height of 12 in. Results of the full-scale crash tests indicated that this was a wise selection. The full-scale crash tests illustrated that a rub rail is a necessary feature of the bridge rail installation.

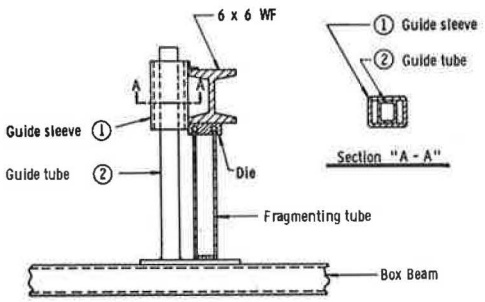

Figure 3. Guide for fragmenting tube.

Transition from Guardrail to Bridge Rail

One of the most difficult tasks of the design program was to provide an adequate transition from guardrail to bridge rail. It appeared that the off-bridge deck system, which consisted of the box beam mounted on a 3I5.7 post with a 6-ft interval spacing, would allow a maximum deflection of 4 ft for the design test conditions, while the on-deck system would allow a maximum deflection of 2 ft for the same test conditions. It appeared then that a reasonable transition could be provided by installing two 4-ft post spacings just prior to entering the energy-absorbing bridge deck installation.

As a result of the final crash test in the TTI evaluation, the transition appeared promising. It is conceivable, however, that the transition can be optimized by either closer spacing of the 3I posts near the transition or a weakening of the first fragmenting tube. The proposed modification should be evaluated first on the Barrier III computer program.

FABRICATION

Only those facets of energy-absorbing bridge rail fabrication that are unconventional with respect to a guardrail system are discussed. Thus, most of the comments in this section apply to the energy absorber per se.

In a sense, the prototype energy absorbers were custom-fabricated because they were the only portion of the system that was not subcontracted but, instead, constructed entirely at Southwest Research Institute. The majority of the energy absorbers, with the exception of the fragmenting tube and die, required simply cutting and welding of construction steel components. The fragmenting tube was cut to length and tapered a prescribed amount on one end, thus allowing a more consistent fragmentation. This tapering also initiates the fragmenting process. Fabricating of the die required a machining process and was, therefore, a more crucial step in fabrication of the energy absorber. It is important to avoid excessive machining error when turning the radius of the die. This problem would be eliminated in the final design because a thin-shell die-casting process would be used to fabricate the finished product.

If a system were chosen for large-scale production of the energy absorber, a manufacturer would thin-shell die-cast the die and would fabricate the guide assembly from structural steel tubing. The 2024 T-3 aluminum tubes could be purchased in large quantities, precut to length, and tapered on one end.

The total estimated cost of the fragmenting-tube energy absorber would be approximately 50 percent above a conventional installation. As an example, the system installed at TTI cost the following: (a) standard bridge rail installation, similar to the Texas T-1 installation but with the New York-type (6- by 6- by $^{3}/_{16}$ in.) box beam used in place of the "Flex Beam Rail," energy absorber not included, $11.58/ft; and (b) additional cost of the aluminum fragmenting tubes, die, and guide assembly, i.e., the energy absorber, $6.25/ft. These costs do not include labor costs for installation. Prices may differ slightly from bids finally given to highway departments; however, if anything, they are on the conservative side.

A question often asked is, Can you taper the tubes to get a variable force? Yes, the tubes can be tapered; however, it would increase the cost of the tube. The tubes can be tapered or can have step increases in the wall thickness that would give many possibilities for variation of the force-deformation curves. The possibility of tapering or step changes in tube sizes was considered for the small car (1,600-lb) test but was later rejected in favor of the constant-thickness tubing. A more important application of tube tapering might be considered for the transition section. Consideration could be given to tapering the first tube in the series, thus softening the initial portion of the energy-absorbing system.

INSTALLATION

In the same fashion as the section on fabrication, the installation details allude primarily to the energy-absorber portion of the total bridge rail system. The remaining portion of the system is a conventional guardrail installation.

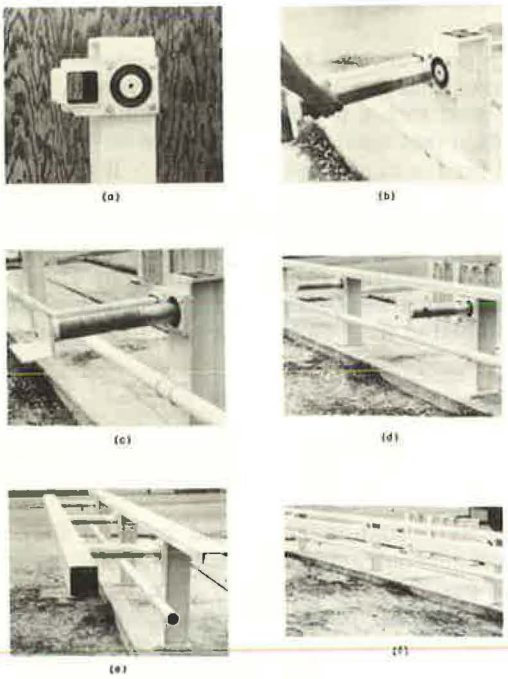

Figure 4. Prototype installation of energy-absorbing guardrail with breakdown of parts: (a) die and guide assembly; (b) assembling energy-absorbing fragmenting tube and guide; (c) assembled energy absorber; (d) spacing between absorbers and wide-flange posts; (e) end view of overall prototype assembly; and (f) front view of overall prototype assembly.

Figure 4 shows the sequential steps of installing the fragmenting-tube energy absorber, the guide assembly, and, finally, the box beam rail section. The steps, quite simply, are as follows:

1. The 6-in. WF posts are leveled, lined up with one another, and securely bolted to the bridge deck.
2. The die and guide assembly is bolted to the 6-in. WF post with the die facing the traffic lane as shown in Figure 4(a).
3. The inside of the 2024 T-3 aluminum tube and the face of the fragmenting die are lubricated with Molykote, a high-pressure lubricant that works its way into the metal pores much like graphite.
4. The fragmenting tube (tapered end facing the die) and the guide are then mounted on the die and guide assembly. The attachment plate is placed on the back side of the guide. This plate is later used to draw the guide and tube assembly into the wide-flange backup posts.
5. The $2\frac{1}{2}$-in. pipe rub rail is attached.
6. The 8-in., 11.5-lb channel is placed on top of the WF post and bolted down.
7. The 6- by 6- by $\frac{3}{16}$-in. box beam is placed on the fragmenting tube and guide assembly, and the box beam is drilled and bolted to the steel angle plate.
8. The backup plate is tightened and the fragmenting tube and tube guide assembly are drawn snug up to the WF posts.

Estimated installation time per section is 4 man-hours. The installation photographs shown were taken at Southwest Research Institute during a mock-up installation.

After the mock-up installation, the system was shipped to TTI and installed on a simulated bridge rail installation. The steel-reinforced concrete simulated bridge deck was a 62- by 8-ft concrete slab with a $2\frac{1}{2}$-ft cantilever overhang that was to simulate the dynamic loads experienced by a full-scale bridge deck. The simulated bridge deck was of conventional design with an added 4-ft long anchorage plate cast in the center of the concrete deck to transmit bending loads to a larger portion of the bridge deck. The bridge deck was built to a uniform 8-in. thickness.

The bridge deck sustained all crash tests with only minor surface cracks that appeared to be compression shear cracks. It is questionable, however, if the existing bridge deck design would be sufficient for either large vehicle crashes or even for a small vehicle crash where the energy absorbers are not used. It must be pointed out that at no time did the dynamic load to any single post exceed 10,000 lb. In a sense, the fragmenting tubes act not only as an energy absorber but also as a load limiter that prevents extensive damage to the concrete deck. It will be interesting to follow closely the results of tests that are presently under way at TTI utilizing the Texas T-1 type bridge rail system. The same simulated bridge deck will be used and the same basic backup post system, but with a Flex Beam type rail and no energy absorber. These tests should illustrate the effectiveness of the fragmenting tube as a load limiter as well as an energy absorber.

CONCLUSIONS AND SUMMARY

Evaluation of the energy-absorbing bridge rail system has been the assigned responsibility of Texas Transportation Institute and therefore the data and evaluation of the full-scale crash tests are presented in a separate paper by TTI. Design engineers at Southwest Research Institute are satisfied that the fragmenting-tube energy absorber can be feasibly combined with a bridge rail system. In addition, a new cantilevered design was introduced that eliminated wheel-snagging, possibilities of a dual-purpose bridge rail were demonstrated, a load limiter for the backup posts was a resulting fringe benefit, and an extremely promising bridge rail to guardrail transition was crash-tested.

RECOMMENDATIONS

Based on a detailed analysis of the high-speed movies, the deceleration data, and the post-crash scenes, the following recommendations are submitted for consideration:

1. Further design studies and full-scale crash tests should be conducted to improve the following specific areas of the integrated bridge rail-guardrail system: (a) Height of the box beam might be raised to 30 or 32 in., as compared to the 27-in. height that was crash-tested, in order to eliminate excessive damage to the steering mechanism on the side of the vehicle that strikes the rail; (b) an improved box beam splice should be considered in order to reduce vehicle snagging; (c) an improved rub rail should be considered in order to prevent wheel-snagging on the backup wide-flange posts and provide additional energy absorption; (d) the transition design between the guardrail and bridge rail should be improved in order to provide a more gradual stiffness transition, thus reducing the pocketing and snagging at the bridge rail; and (e) increasing the height of the backup post should be considered.
2. Analytical parametric studies using the Barrier III program from the University of California at Berkeley should be conducted. These parametric studies could be used to optimize the overall bridge rail and guardrail design.
3. A full-scale field installation of the fragmenting-tube energy-absorbing bridge rail should be considered. The location should be chosen where it could be observed frequently by engineers familiar with the design concept of the fragmenting-tube energy absorber.

ACKNOWLEDGMENTS

This research and development effort was undertaken by Southwest Research Institute under contract with the U. S. Bureau of Public Roads as a part of the Structural Systems in Support of Safety (4S) Program. Credit should be given to John Viner of the Bureau for providing valuable assistance in specific areas of the design of the energy-absorbing bridge rail. In particular, he made contributions to the overall design philosophy, proposed the cantilevered-type guide tube concept, suggested a transition rail treatment, requested the use of a rub rail, and recognized the additional possibility of the bridge rail serving a dual purpose for both large and small vehicles.

The authors acknowledge the contributions of P. A. Cox of Southwest Research Institute to the dynamic analysis of the energy-absorbing bridge rail and the efforts of Guido Ransleben, who assisted in the design feasibility study. The authors also acknowledge the contributions and assistance of Graham H. Powell, Assistant Professor of Civil Engineering at the University of California, Berkeley. Powell provided Southwest Research Institute with the Barrier III computer program and frequently assisted Cox with the dynamic analysis.

The opinions, findings, and conclusions expressed in this publication are those of the authors and not necessarily those of the Bureau of Public Roads.

EDITOR'S NOTE

This paper as originally submitted included an Appendix containing complete installation drawings of the energy-absorbing bridge rail along with detailed drawings of the fragmenting-tube energy absorber. When these drawings are reduced to publication size, much of the detail becomes illegible, and therefore the Appendix material is not included here.

Full-Scale Crash Tests of the Fragmenting-Tube-Type Energy-Absorbing Bridge Rail

ARTHUR J. STOCKER, DON L. IVEY, and T. J. HIRSCH,
Texas Transportation Institute, Texas A&M University

Four full-scale crash tests of a fragmenting-tube-type energy-absorbing bridge rail were conducted to determine the capabilities of the system. Vehicle weights varied from 1,560 to 4,720 lb. Desired test conditions were 60 mph with an angle of attack of 25 deg. Three tests were conducted on the bridge rail and a fourth test was run on the transition zone between the guardrail and the bridge rail. When the transverse vehicle energy level was sufficient to activate the energy-absorbing fragmenting tubes, the vehicle was redirected with a significant lowering in the expected g levels because of the deformation characteristics of the system.

•THE EXTREME RIGIDITY of most types of bridge rails creates high deceleration forces on passengers in impacting vehicles as well as heavy damage to these vehicles. In an effort to produce a bridge rail design that would have sufficient strength to retain heavy vehicles and also be sufficiently flexible to lower deceleration forces on vehicle passengers, the U.S. Bureau of Public Roads entered into a contract with the Southwest Research Institute as part of the Structural Systems in Support of Highway Safety (4S) Program. The bridge rail system tested by the Texas Transportation Institute was designed as a joint effort by engineers of the Bureau of Public Roads and of the Southwest Research Institute. The fragmenting tubes incorporated in this system were designed by the Southwest Research Institute (1).

The energy-absorbing system is a blocked-out 6- by 6-in. box beam guardrail, attached to 6-in. wide flange (WF) support posts as shown in Figure 1. The blocking out of the box beam is accomplished at each WF support point by a guide tube and an energy-absorbing fragmenting tube. The thin aluminum fragmenting tube is rigidly connected to the 6- by 6-in. box beam. It is not rigidly connected to the WF post, but fits into a die that is attached to the post. Under lateral load, the fragmenting tube is forced onto the die and breaks progressively into small segments at a predictable load level. The bridge guide tube prevents movement of the box beam in a longitudinal and vertical direction, but slips through its support on the WF post to allow lateral movement of the box beam. The box beam is then capable of lateral deformation (up to a distance of approximately 18 in.) under the loads imposed by an impacting vehicle. After 18 in. of lateral movement, the box beam comes into contact with the rigid WF support posts that develop a high level of lateral restraint.

TEST PROGRAM

General Description

Four tests were conducted to determine the capabilities of this bridge rail and guardrail system. Three of the tests were against the box beam rail at a post point or

Paper sponsored by Committee on Guardrail, Median Barriers and Sign, Signal and Lighting Supports and Committee on Bridge Design and presented at the 49th Annual Meeting.

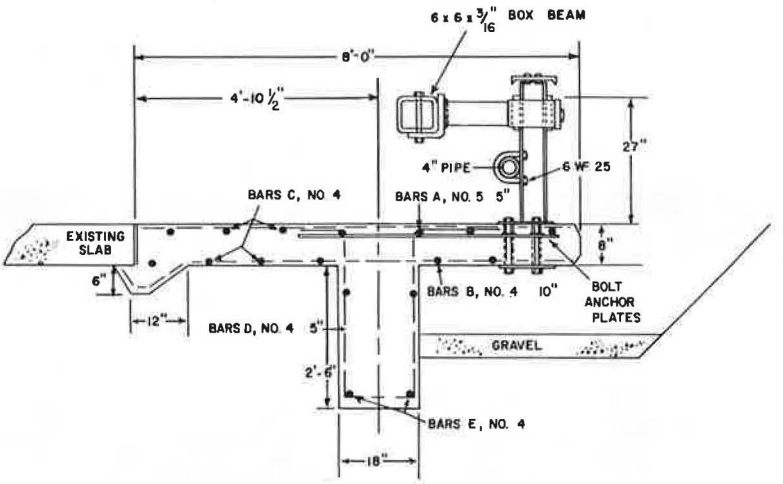

Figure 1. Cross section of bridge deck and bridge rail.

between posts with vehicles varying in weight from 1,560 to 4,720 lb. A fourth crash was made at a point in the guardrail section to test the transition area between the guardrail and bridge rail. Vehicle weight for the fourth test was 3,270 lb. A plan view of the test installation and a summary of the four tests are shown in Figure 2.

Seven cameras were used for documentation and data reduction. One Hycam motion picture camera, operating at 500 frames per second, photographed the impact point perpendicular to the vehicle line of approach while a second similar camera was focused on the impact point perpendicular to the bridge rail. A Fastax camera, operating at 500 frames per second, was positioned in line with the rail at one end to record rail deformation and vehicle deflection parallel to the rail. An overhead high-speed Photosonics camera gave a good view of the vehicle movement at impact. Documentary cameras operating at from 32 to 128 frames per second provided documentary coverage of each test.

Impact velocities were determined electronically as well as photographically. A pair of tape switches was placed so that they would be crossed by the right front wheel

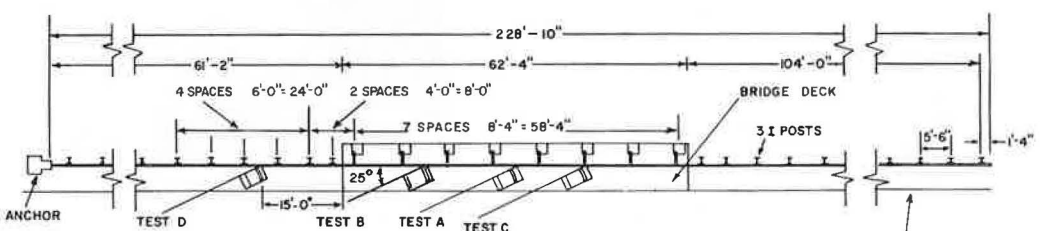

TEST NUMBER	A	B	C	D
ANGLE OF ATTACK	25°	25°	25°	25°
VEHICLE WEIGHT	3200 LBS	4720 LBS	1560 LBS	3270 LBS
IMPACT SPEED	58.3 mph	54.8 mph	46.1 mph	61.8 mph
INITIAL KINETIC ENERGY (KIP-FT)	363.	474.	111.	416.

Figure 2. Location of vehicle impacts.

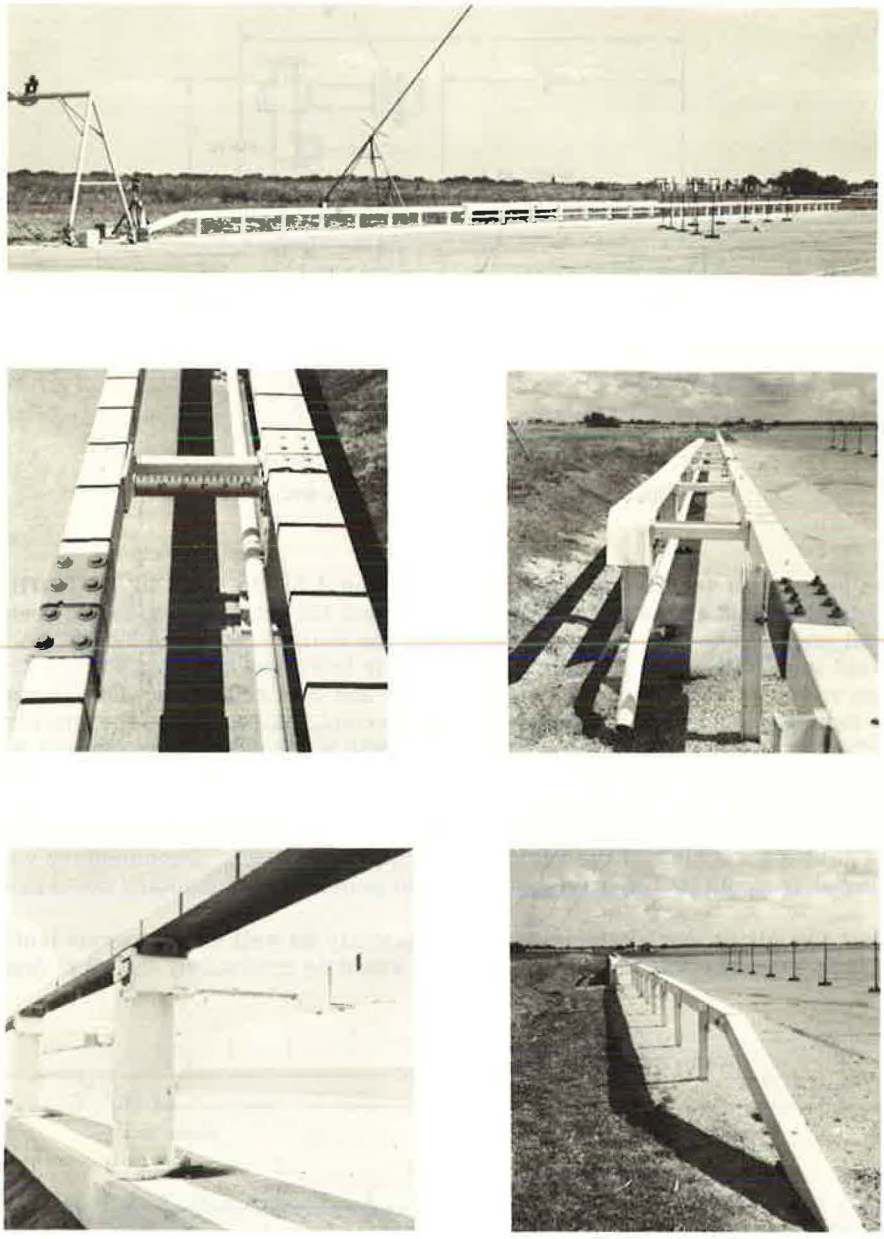

Figure 3. Bridge rail and guardrail installation and details.

of the vehicle just before impact with the bridge rail. The time between actuation of the first and second switch was measured electromechanically, permitting the speed to be calculated.

Figure 3 shows detailed views of the bridge rail and guardrail. A parts listing of the hardware in the system, with basic dimensions of each, is given in the Appendix.

Test A

The first test in the series of four was conducted June 5, 1969, with a 3,200-lb, 1963 4-door Plymouth. The angle of attack was 25 deg and impact velocity was 58.3 mph.

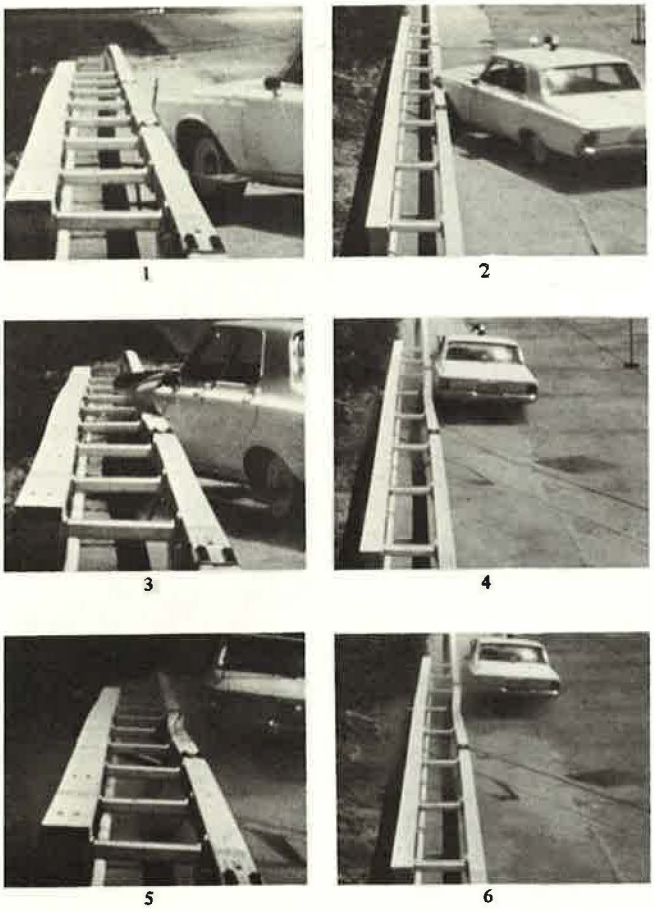

Figure 4. Sequential photographs of test A.

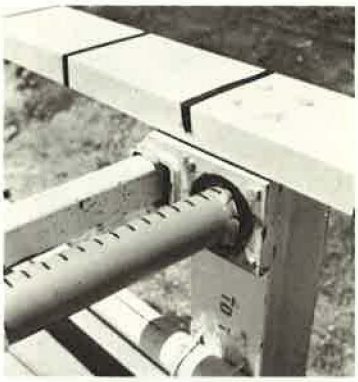

Figure 5. Installation after test A.

Figure 6. Vehicle after test A.

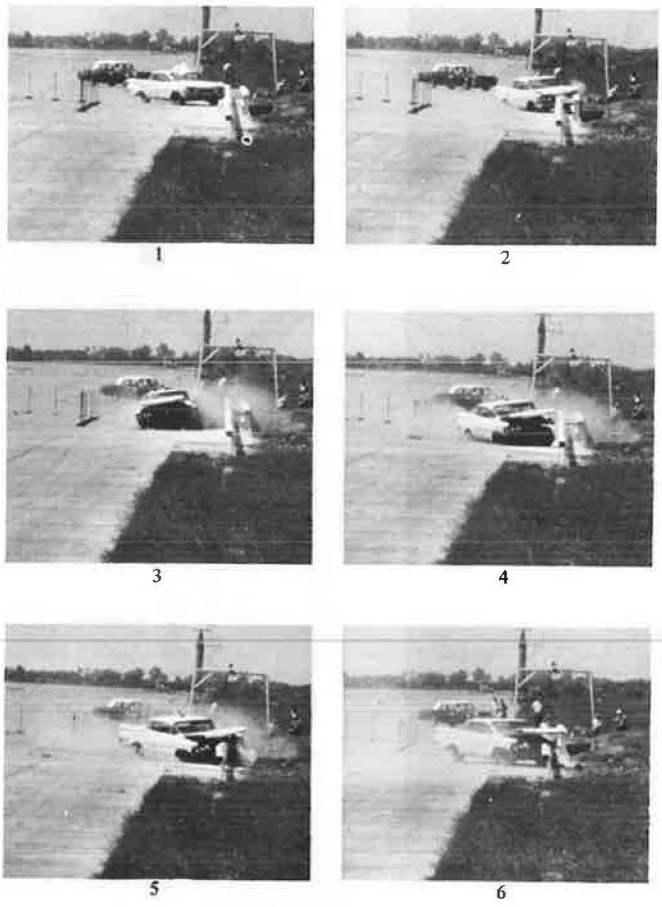

Figure 7. Sequential photographs of test B.

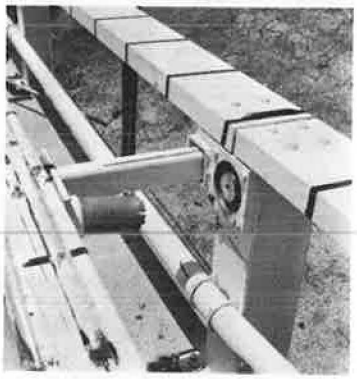

Figure 8. Installation after test B.

Figure 9. Vehicle after test B.

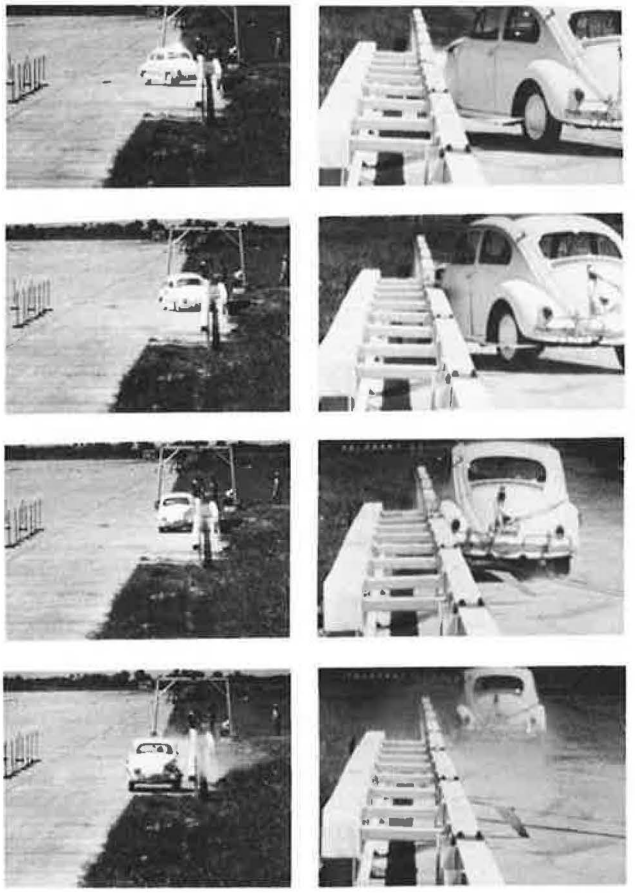

Figure 10. Sequential photographs of test C.

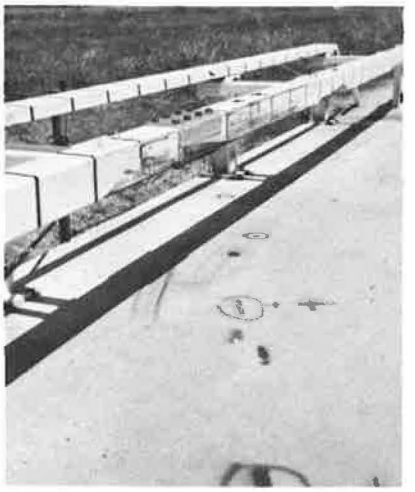

Figure 11. Installation after test C.

Figure 12. Vehicle after test C.

Figure 13. Sequential photographs of test D from rear.

The impact point for the left front bumper was chosen between two posts in an effort to test the weakest point of the box beam and to exert maximum force on the first fragmenting tube downstream from the point of impact.

Figure 4 shows sequential photographs of the test. The vehicle was redirected by the rail and followed the box beam closely for approximately 75 ft before recontact occurred. This return to the guardrail was caused by drag of the damaged left front wheel. Four guardrail posts were knocked down and the vehicle wedged in the guardrail turndown (Fig. 5). Vehicle passenger compartment encroachment was negligible (Fig. 6).

Prior to tests B, C, and D, the end anchorage was eliminated on the downstream end and an additional length of guardrail was installed so that vehicle damage would not be increased by contact with the guardrail anchorage area.

Test B

A heavy vehicle was selected for the second test in the program—a 1959 4-door Oldsmobile weighing 4,720 lb. Impact velocity was 54.8 mph at an angle of 25 deg. The point of impact was again chosen at a point on the rail halfway between two posts. After impact, the vehicle left the rail at an angle of approximately 30 deg, moved to a position some 5 ft from the original rail position, followed the rail, and then turned back into the guardrail because of the left front drag caused by wheel damage (Fig. 7). After tearing down four guardrail line posts, the vehicle came to rest at an angle of approximately 45 deg to the guardrail, some 100 ft from the point of impact (Fig. 8). No visible vehicle compartment encroachment was noted (Fig. 9).

Test C

Because the first two tests involved medium- and heavy-weight vehicles, a 1,560-lb, 1961 Volkswagen was chosen for the third test. The impact angle was 25 deg and the impact velocity was 46.1 mph. Although 60 mph was desired, the vehicle did not have sufficient power to achieve this in the available acceleration distance. After impact,

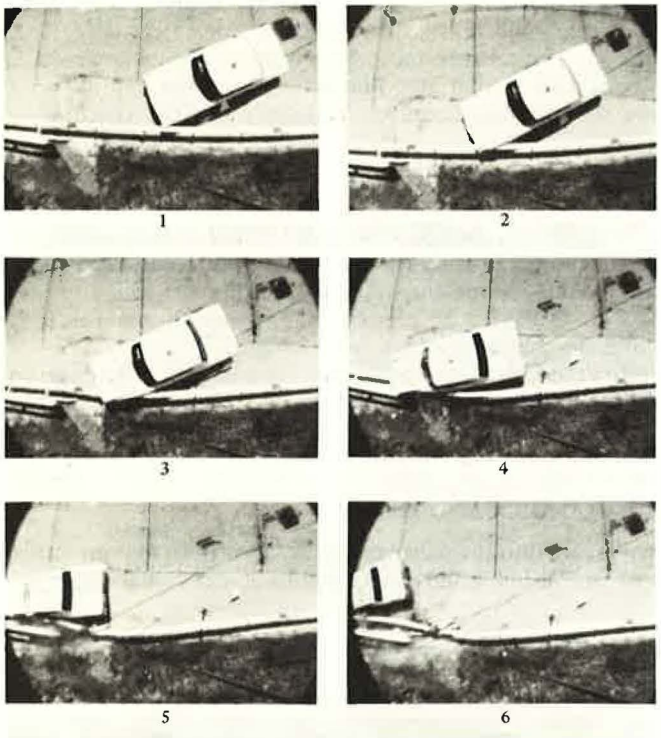

Figure 14. Sequential photographs of test D from above.

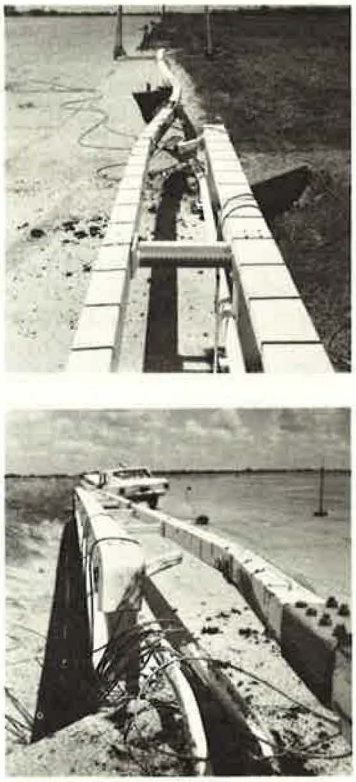

Figure 15. Installation after test D.

Figure 16. Vehicle after test D.

the vehicle followed the rail at a distance of from 1 to 2 ft some 120 ft from point of impact, brushing the end in a long left turn and coming to rest in an open field (Fig. 10). As indicated in Figure 11, there was no measurable tube deformation resulting from the impact, although one tube was partially activated. The left side of the vehicle was dented from front to rear, but there was no significant encroachment of the vehicle compartment (Fig. 12).

Test D

The fourth and final test in this project was designed to test the transition area between the bridge rail and guardrail. A point 15 ft upstream from the bridge deck (17 ft from the first bridge rail post) was chosen for the impact point. The test was run on July 8, 1969, with a 3,270-lb, 1963 4-door Plymouth similar to the vehicle used in test A. Impact velocity was 61.8 mph and the angle of attack was 25 deg.

The vehicle was successfully redirected although there was considerable damage to the installation and the vehicle. After traveling approximately 80 ft from the point of impact, the vehicle came to rest in the guardrail system just downstream from the bridge (Figs. 13, 14, 15). The left front door was torn off at the point of impact (Fig. 16).

SUMMARY AND CONCLUSIONS

Results of the full-scale tests to determine the interaction of a vehicle and an energy-absorbing-type bridge rail are given in Tables 1 and 2. In Table 1, the figures given indicate how much of each fragmenting tube was used in absorbing the energy at a particular bridge post. In tests A, B, and C the largest of these deflections is a rough approximation of the maximum deflection of the box beam rail. Approximately 10,000 lb is required to activate each fragmenting aluminum tube.

TABLE 1

DEFORMATION OF FRAGMENTING TUBES, INCHES

Bridge Post No.	Bridge Tube No.[a]	Test A	Test B	Test C	Test D
10	1	0	1/8	0	1 1/4
11	2	0	6	0	0
12	3	0	14	0	0
13	4	2 1/2	10	0	0
14	5	5 1/2	1/8	0	0
15	6	0	0	0	0
16	7	0	0	0	0
17	8	0	0	0	0

[a]Tubes are numbered from south to north end of bridge (vehicle travels from south to north).

TABLE 2

AVERAGE VEHICLE DECELERATIONS

Test	$\bar{a}_t$, Note 1	$\bar{a}_t$, Note 2	$\bar{a}_l$, Note 3
A	4.5	5.3	2.1
B	3.7	3.7	2.0
C	3.7	4.7	2.0
D	4.5	4.3	3.3

1. Average deceleration (g) perpendicular to bridge rail up to maximum penetration, calculated from photographic measurement of initial velocity and transverse distance the vehicle's center of gravity travels from initial contact to maximum penetration.
2. Average deceleration (g) perpendicular to bridge rail up to maximum penetration, calculated from photographic measurement of initial velocity and bridge rail deflection (2).
3. Average deceleration (g) along vehicle's longitudinal axis during contact with bridge rail, calculated from photographic measurement of initial and final velocities and distance in contact.

Table 2 gives decelerations in g's. All deceleration levels are within the survivable range given by Olson, Post, and McFarland (2). In all of the tests, there was no significant vehicle compartment encroachment, but in test D the left door was torn off. In all tests in this series, the vehicles were redirected and came to rest without rolling over. A passenger who had his seatbelt and shoulder harness properly attached would probably have sustained only minor injuries in each test.

REFERENCES

1. Woolam, William E., and Garza, Luis R. Design, Fabrication, and Installation of a Fragmenting-Tube-Type Energy Absorber in Conjunction With a Bridge Rail. Paper presented at 49th Annual Meeting and included in this Record.
2. Olson, R. M., Post, E. R., and McFarland, W. F. Tentative Service Requirements for Bridge Rail Systems. NCHRP Rept. 86, 1970.

Appendix

SYSTEM COMPONENTS AND DIMENSIONS

Bridge Rail

Box beam rail	$^{3}/_{16}$ by 6 by 6 in.
Fragmenting tube (2024T-3 aluminum)	3 in. OD by 0.120-in. wall
Guide tube	$^{1}/_{4}$ by 2 by 3 in.
Post	6 WF 25
Post base plate	1 by $9^{1}/_{2}$ by 10 in.
Post to slab bolts	$^{7}/_{8}$ in.
Plate under slab	$^{1}/_{4}$ by 8 by 9 in.
Top of post channel	8 in., 11.5 lb
Rub rail	4 in. SCHD 40 pipe
Bridge deck to top of box beam	27 in.
Bridge deck to top of channel on post	$29^{9}/_{16}$ in.
Front of post to front of box beam	26 in.
Fragmenting tube length	19 in.

Guardrail

Box beam rail	$^{3}/_{16}$ by 6 by 6 in.
Line post	3 in. I 5.7 lb
Line post stabilizing plate	$^{1}/_{4}$ by 8 by 24 in.
Ground to top of box beam	27 in.

Preformed Elastomeric Bridge Joint Sealers: Thermal Characteristics of Bridge End Movements

GEORGE S. KOZLOV and DINKAR DESAI, Division of Research and Evaluation, New Jersey Department of Transportation

This paper, the third in a series, presents current knowledge on the thermal characteristics of a mass, such as a concrete deck, and on the principles of heat transfer. Using an empirical approach, a method for predicting reasonably accurate concrete temperatures is given. Information is included on the subjects of actual time difference and phase shifts between peaks of solar radiation and air temperatures.

•IN EARLIER PAPERS covering the design and construction of bridge joints sealed by elastomeric material (1, 2), consideration was given to the thermal characteristics of bridge deck end movements. In the meantime, the need for increased knowledge about these thermal characteristics has become apparent, leading to this portion of the subject study.

As a by-product of the research phase dealing with the relationship between deck and air temperatures and joint movements, the knowledge of heat transfer through a concrete slab has been expanded. Using field data made available by the Louisiana Department of Highways, we were able to develop an empirical approach to the problem of calculating concrete temperatures. This work should advance the knowledge of the temperature effects on bridge joint movements.

THEORETICAL BACKGROUND

It has been recognized that the temperature of a mass, in this case a concrete bridge deck, is influenced by a number of rather complex factors, such as solar radiation, ambient air temperature, wind velocity, insolation, re-radiation, evaporation, conductivity, diffusivity, surface conditions, specific heat, and density. By making assumptions of average values of the secondary parameters and a sinusoidal effective daily temperature cycle, a solution is obtained. Figure 1 shows the sinusoidal cycle assumption.

A reasonably accurate solution would necessitate the gathering and evaluation of a substantial amount of secondary parameter data for each specific location. Because such expanded research is not within the scope of this study, further development of this problem will have to be the object of separate analysis. Thus, assumptions made and data used for this particular discussion are mainly informative in nature.

In a paper by Barber (3), an equation was developed for the temperature of a semi-infinite mass in contact with air that can be expressed as follows:

$$T = (T_A + R) + \eta_o (0.5T_R + 3R) \exp\left(-X\sqrt{\frac{\pi}{t_o a}}\right) \sin\left(2\pi \frac{t}{t_o} - X\sqrt{\frac{\pi}{t_o a}} - \epsilon_o\right) \quad (1)$$

Paper sponsored by Committee on Bridge Design.

where

$$R = 0.103\frac{b}{\alpha}L;$$

$$\eta_o = \sqrt{\frac{1}{1 + 2\sqrt{\frac{\pi}{H^2 t_o a}} + 2\frac{\pi}{H^2 t_o a}}};$$

$$a = \frac{k}{sw};$$

$$H = \frac{\alpha}{k};$$

$$\alpha = 1.3 + 0.62\, v^{0.75};$$

$$\epsilon_o = \arctan\frac{1}{1 + \sqrt{\frac{H^2 t_o a}{\pi}}}; \text{ and}$$

X = distance as measured from the top of mass (Fig. 2).

It is obvious that for the top surface of this mass X = 0. Thus, the equation for the temperature of the top surface can be written in the following form:

$$T = (T_A + R) + \eta_o\,(0.5T_R + 3R)\sin\left(2\pi\frac{t}{t_o} - \epsilon_o\right) \qquad (2)$$

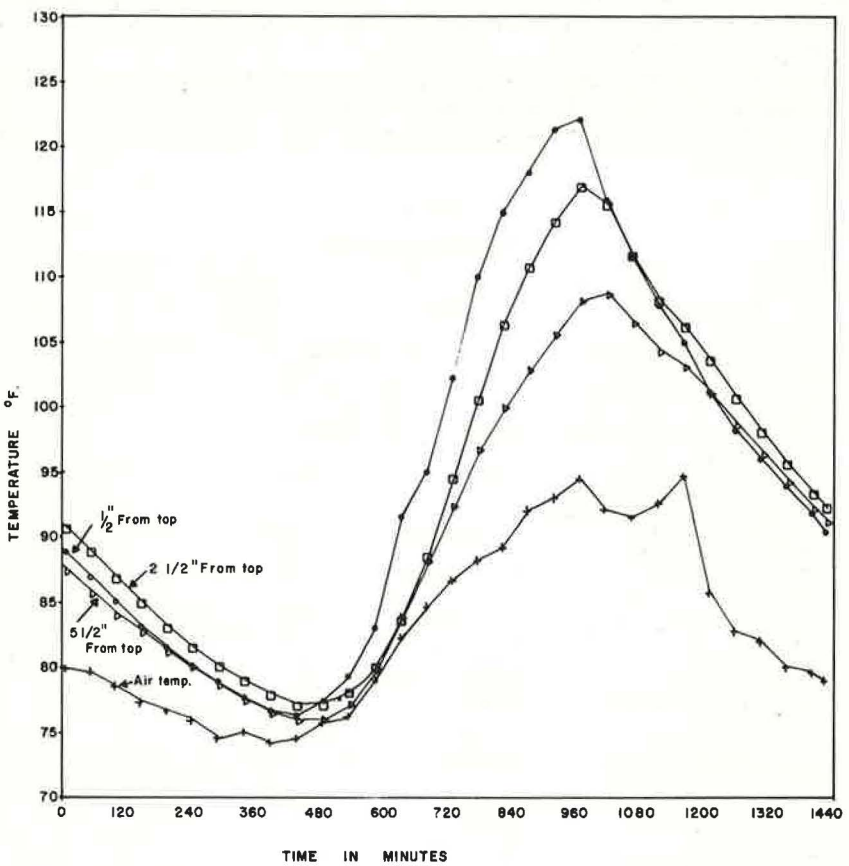

Figure 1. Sinusoidal variation of temperature (Aug. 5, 1967).

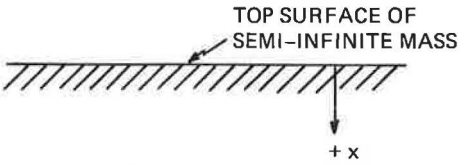

Figure 2. Top surface in contact with air temperature.

For T to become maximum, $\sin\left(2\pi\frac{t}{t_o} - \epsilon_o\right)$ = 1.0 and X = 0; therefore

$$T_{max} = (T_A + R) + \eta_o (0.5T_R + 3R) \quad (2a)$$

On the basis of previously made assumptions, as given in Table 1, the above equations can be transformed as

$$T = T_A + 0.0135L + 0.687(0.5T_R + 0.0405L) \quad (2b)$$

where

L = solar radiation received on a horizontal surface in Langleys (cal/cm^2/day);
α = 4.95 for V = 10.7 mph (for New Jersey);
a = 0.0334 for k = 1.00 Btu/ft^2/hour, deg F/ft;
s = 0.20 Btu/lb, deg F and w = 150 lb/ft^3;
η_o = 0.687 for H = 4.95 and t_o = 24 hours; and
R = 0.0135L for b = 0.65.

The discussion here pertains to the temperature of a semi-infinite mass—that is, a very thick mass exposed on the top only, such as a pavement slab, with soil below.

Groeber (4, p. 86), defines the harmonic surface temperature oscillations in semi-infinite mass as being of the same period as the temperature of the surrounding air but lagging in time by an amount determined by ϵ_o. It is an analytical expression for semi-infinite mass; in the case of finite dimensions, the thickness and other properties will have to enter into the calculations of the time lag.

In the case of a slab such as a bridge deck exposed on the top and bottom and having a relatively thin mass, the problem becomes different, obviously because of physical limitations exposed to the same influences as previously indicated. By superimposing

TABLE 1
PARAMETER VALUES

Definition	Value	Assumed Average Value	Source
T_A = average daily air temperature (deg F)		Varies	U.S. Weather Bureau
T_R = daily range in air temperature (deg F)		Varies	U.S. Weather Bureau
R = average contribution to effective air temperature (deg F)	Varies	Varies	
L = solar radiation received on a horizontal surface in Langleys (cal/cm^2/day = 3.69 Btu/ft^2/day)	Varies	Varies	Heating and Ventilating, July and Jan. 1949, pp. 62 and 72
k = conductivity of concrete (Btu/ft^2/hour, deg F/ft)	k = 7 to 16 per in.	k = $\frac{12.0}{12}$ = 1.0	Ref. (9), p. 5-14; Ref. (10), p. 178
s = specific heat of concrete (Btu/lb, deg F)	s = 0.19 to 0.27	s = 0.20	Ref. (9), p. 5-4; Ref. (10), p. 1175
w = density of concrete (lb/ft^3)		w = 150	
b = absorptivity of surface to solar radiation	b = 0.65 to 0.80	b = 0.65 (for concrete)	Ref. (10), p. 95
v = wind velocity (mph)	Varies	v = 10.7	Ref. (10), p. 253
a = diffusivity (ft^2/hour)	Varies		
α = surface coefficient (Btu/ft^2/hour, deg F)	Varies		
t_o = length of period (hours)	t_o = 24		
t = time from beginning of cycle (hours)	Varies		
h = thickness of slab (ft)	Varies		
x = distance as measured from top of mass (ft)	Varies		
y = distance as measured from bottom of slab (ft)	Varies		

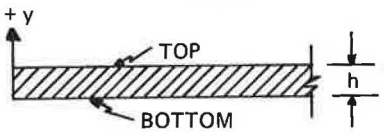

Figure 3. Exposure of bridge deck slab.

the steady-state heat transfer solutions developed by Carslaw and Jaeger (6) for periodic temperature states on an infinite plate, Zuk (5) has evolved the following equation for the time-temperature-depth relation:

$$T = \left(T_A + \frac{y}{h} R\right) + \eta_o \left[(0.5T_R + 3R) Y \sin\left(2\pi \frac{t}{t_o} - \phi + \ell n Y\right) + (0.5T_R) Y^1 \sin\left(2\pi \frac{t}{t_o}\right) \right] \quad (3)$$

where

$$Y = \left(\frac{\cosh 2my - \cos 2my}{\cosh 2mh - \cos 2mh}\right)^{1/2},$$

$$Y^1 = \left[\frac{\cosh 2m\,(h - y) - \cos 2m\,(h - y)}{\cosh 2mh - \cos 2mh}\right]^{1/2},$$

$$m = \left(\frac{\pi}{t_o a}\right)^{1/2}, \text{ and}$$

y = distance as measured from the bottom of the slab (Fig. 3).

According to Zuk (5), ϕ is to represent the phase angle difference in the sine curves of surface temperatures between the bottom and the top of the slab; for the time being there is no analytical expression for its value, because it must come basically from field observations.

Also, Zuk's opinion was that, although Eq. 1 seems to predict the magnitude of surface temperatures fairly well, it does not adequately take into account the phase shift between peaks of solar radiation and air temperatures, the phenomenon vital to the analytical determination of ϕ. However, his tests indicate the time difference to be of the order of 3 hours. The function of ϕ in Eq. 3 is in no way intended to relate to the ϕ of Carslaw and Jaeger.

Zuk suggests an empirical approach to this problem. In this way the established values will be suitable for use only in specific locations, unless enough data are collected to establish average values of this parameter. It seems, though, that an effort should be made to develop theoretically correct analytical expressions, correlated to the actual field observations. Perhaps it might be possible after such values are secured empirically.

By further developing Eq. 3, the temperature of the top surface of the slab, when y = h, is

$$T_{top} = (T_A + R) + \eta_o (0.5T_R + 3R) \sin\left(2\pi \frac{t}{t_o} - \phi\right) \quad (3a)$$

Again, for T_{top} to become maximum, $\sin\left(2\pi \frac{t}{t_o} - \phi\right) = 1.0$ and y = h; therefore

$$T_{top\ max} = (T_A + R) + \eta_o (0.5T_R + 3R) \quad (3b)$$

Equations 2a and 3b are obviously identical. Thus, the temperature of the bottom surface of the slab, when y = o, is

$$T_{bot} = T_A + \eta_o (0.5T_R) \sin\left(2\pi \frac{t}{t_o}\right) \quad (3c)$$

T_{bot} is maximum when $\sin\left(2\pi \frac{t}{t_o}\right) = 1.0$ and y = o; therefore

$$T_{bot\ max} = T_A + \eta_o (0.5T_R) \quad (3d)$$

Again utilizing previous assumptions, this equation can be expressed as follows:

$$T_{bot\ max} = T_A + 0.687(0.5T_R) = T_A + 0.3435T_R \qquad (3e)$$

And finally the temperature T of the slab can be determined from Eq. 3 for the length of the period t_o = 24 hours and various values of time t from the beginning of the cycle and the depth of slab y. Again, assumed average values of secondary parameters are given in Table 1.

In a bridge deck, the slab is often rigidly connected to the supporting beams forming a composite section. Within the scope of this report, only the case of steel beams is mentioned because it is not too unreasonable to assume that, considering the high heat conductivity of steel, the temperature of the beams will be the same as that of the ambient air. This was confirmed by Naruoka, Hirai, and Yamaguti (7).

Also significant is the configuration of the temperature distribution curve through a slab (Fig. 4). Being nonlinear, it follows an oscillatory wave of decreasing amplitude, as indicated in the mathematical argumentation of heat transfer analysis by Groeber (4) and confirmed also by the tests outlined by Zuk, and by Naruoka, Hirai, and Yamaguti. Zuk explains, "Generally speaking, in normal bridge structures, a temperature extreme (either hot or cold) at the top of the slab rapidly decays with depth, so that at approximately mid-depth the temperature is virtually the same as at the bottom of the slab" (5). The difference of the top and bottom temperatures can be about 20 F.

Inasmuch as the subject study is bridge end movements reflected in the sealing of joints, not the thermal stresses, the basic problem is to determine the average effective temperature for a bridge deck. Forgetting the monolithic character of a slab of, say, L = 100 ft, with an average coefficient of expansion C = 0.000066 in./ft/deg F, the differential movement between top and bottom (if they were free to move separately) would be $\Delta = c\Delta tL = 0.132$ in. This example is given only to accentuate the problem. The problem is even more pronounced in a composite section where, in the case of steel beams, the difference in coefficients of expansion would also have to be considered.

It is obvious that, because of the monolithic nature of a slab, all that can be expected is a small amount of rotation of the joint sides. For the purposes shown earlier, this differential movement can be neglected and only overall average joint side movements should be considered. In other words, the stabilizing effect of the structural characteristics of a bridge deck will produce, for these purposes, effective average movements. These average effective movements can be expected to result from so-called average effective deck temperatures.

Only continuous data, obtained by field observations for a period of at least 1 year, would give a lead to such a temperature in the spectrum of the temperature variations discussed in preceding paragraphs. Consequently, the preceding synthesis is an attempt to make understandable the complexity of the problems and the difficulty encountered in determining the actual effective temperatures that govern the thermal behavior of the specific bridge elements.

CALCULATION OF MAXIMUM TOP AND BOTTOM TEMPERATURES

A numerical example of a bridge deck slab temperature calculation is given here to illustrate the preceding synopsis.

A bridge in northern New Jersey was arbitrarily selected on July 26, 1966. Maximum daily temperature recorded was 90 F and minimum daily temperature recorded was 68 F. Solar radiation received on a horizontal surface was assumed to be L = 500 Langleys (see average solar radiation charts for month of July in New Jersey area). Thickness of the slab was assumed to be h = $^{8}/_{12}$ ft. From these data T_A = 79 F and T_R = 22 F. Maximum slab top temperature, using Eq. 2b, is

$$T = T_A + 0.0135L + 0.687\ (0.5T_R + 0.0405L)$$

$$= 79.0 + 6.75 + 0.687\ (11.0 + 20.25)$$

$$= 107.2\ F$$

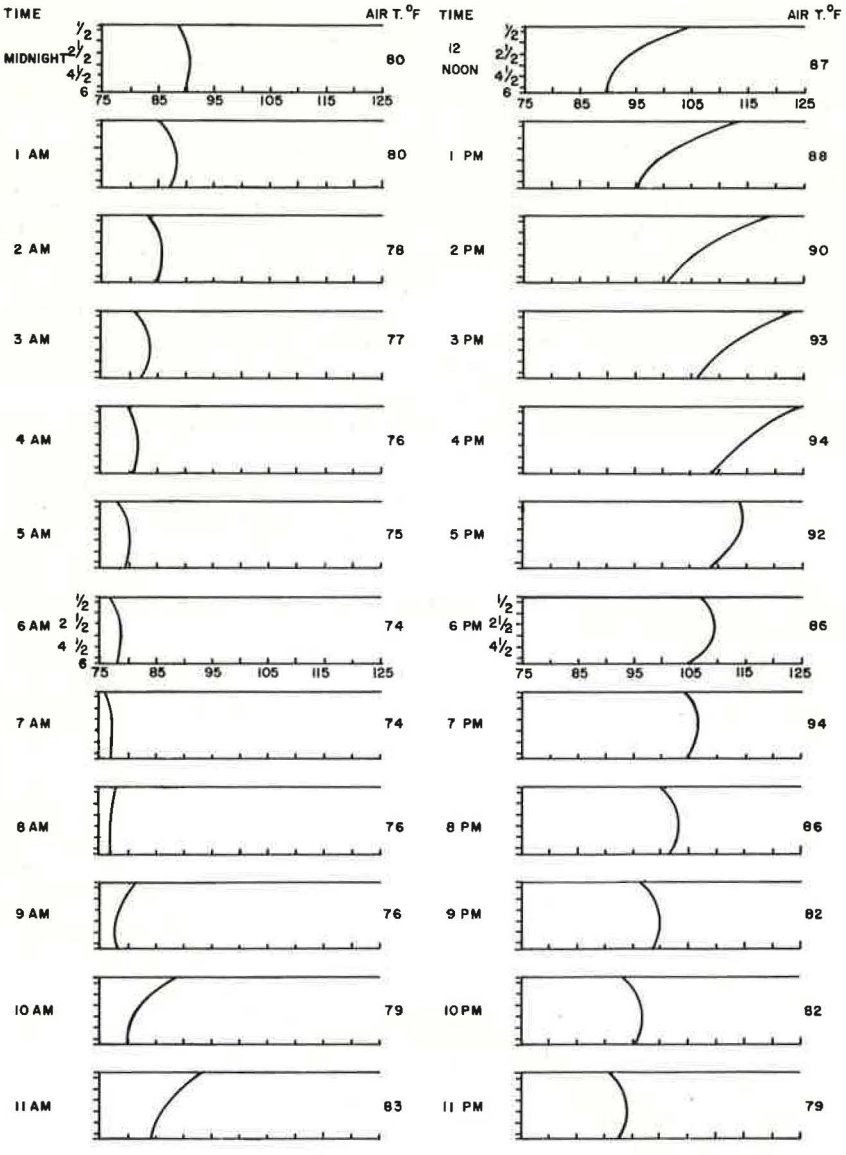

Figure 4. Temperature log at Ruston, Louisiana (Aug. 5, 1967).

Maximum slab bottom temperature, using Eq. 3e, is

$$T = T_A + 0.3435\ T_R$$

$$= 79.0 + 0.3435 \times 22.0$$

$$= 86.55\ F$$

EMPIRICAL APPROACH

The numerical analysis of temperature distribution through a slab is carried out here by an empirical approach as suggested by Zuk. The phase lag, ϕ, is computed

from field observations of air and bridge deck concrete temperatures measured at various depths for 24 hourly time periods. These observations were taken from a study conducted by the Louisiana Department of Highways research and development section. The bridge is located where Louisiana 408 crosses over Interstate 20 near Ruston.

The temperature gradient was determined throughout the depth of a 6-in. concrete bridge deck. As stated by Rushing (8), the thermocouples were placed in the concrete at 1-in. intervals starting ½ in. from the top with the last point being ½ in. from the bottom of the slab. Two thermocouples were also used to record air temperatures. Continuous recording was performed for one yearly cycle. In this paper the data for only the two hottest days, August 4 and 5, 1967, are utilized.

Although the temperatures have been measured, the average values of the secondary parameters must be assumed as indicated previously and shown in Tables 1 and 2. Table 2 is a supplement to Table 1 and provides the specific parameter values suitable for use during August 1967 at Ruston, Louisiana.

The variable ϕ is established by rearranging Eq. 3 and solving it for ϕ:

$$\phi = 2\pi \frac{t}{t_o} + \ell n\, Y - \text{arc sin}\left[\frac{T - T_A - \frac{Y}{h} R - 0.5\eta_o T_R Y^1 \sin 2\pi \frac{t}{t_o}}{\eta_o (0.5T_R + 3R)Y}\right] \qquad (4)$$

As can be seen from Eq. 4, values of ϕ depend on the time, depth of bridge deck, and air and concrete temperatures.

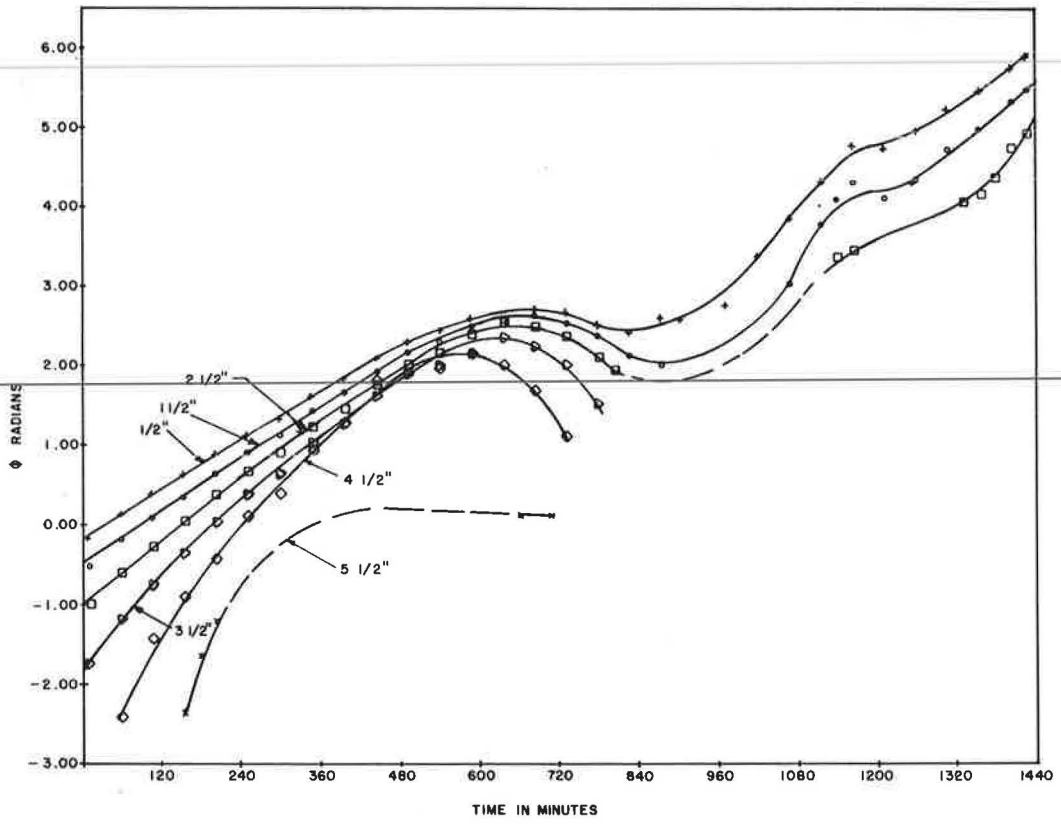

Figure 5. Phase lag between surface and bottom temperatures (Aug. 5, 1967).

TABLE 2

PARAMETER VALUES FOR USE DURING AUGUST 1967 AT RUSTON, LOUISIANA

Definition	Value	Assumed Average Value	Source
T_A = average daily air temperature (deg F)		Varies	Ref. (6)
T_R = daily range in air temperature (deg F)		26.1 for Aug. 5	Ref. (6)
L = solar radiation received on a horizontal surface in Langleys (cal/cm^2/day = 3.69 Btu/ft^2/day)	Varies	531	Ref. (11)
b = absorptivity of surface to solar radiation (dimensionless fraction)	b = 0.6 to 0.9	b = 0.65	Ref. (12)
v = wind velocity (mph)	Varies	V = 10.0 for Louisiana	Ref. (13)

DISCUSSION OF CURVES

For the purpose of the curve discussion of ϕ, as expressed in Eq. 4, the computed values are plotted as follows:

1. ϕ in radians, against time in minutes, for given depths in inches, as shown in Figure 5; and
2. ϕ against depth for given time in hours, as shown in Figure 6.

The computational work was facilitated by a FORTRAN program that was written for use on the IBM 360 computer while plotting was performed with the help of an on-line incremental plotter.

Before proceeding with the discussion of these curves, it should be remembered that ϕ represents the phase angle difference in the sine curves of surface temperatures between the bottom and the top of the slab. As such, it apparently should not vary with depth, but certainly it can vary with time. It is the term $\ell n\, Y$ in the expression

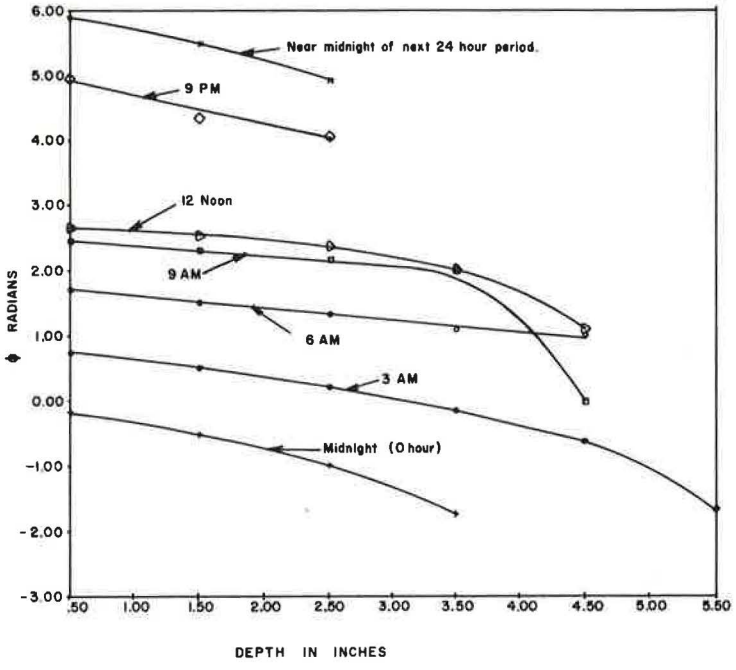

Figure 6. Phase lag variation with increase of depth measured from the top of the slab (Aug. 5, 1967).

$\sin\left(2\pi\frac{t}{t_o} - \phi + \ell n\, Y\right)$ in Eq. 3 that is apparently intended to take care of phase lag variation with depth.

Thus the analysis of these curves reveals that when the variable ϕ is plotted against time the phase lag ϕ seems to decrease with the increase of depth of a slab. This phenomenon indicates the inadequacy of the depth-related factor, possibly of the term $\ell n\, Y$. There should be only one ϕ curve for all depths. The resulting curves are approximately straight lines drooping in the middle, which possibly is caused by the sinusoidal component in Eq. 4. These curves also show that the value of ϕ is increasing with time, thus indicating that ϕ is a time-dependent variable.

In the case of ϕ plotted against depth, the variable ϕ increases with time as already explained. The curves are also approximately straight lines slightly drooping, which again indicates fallibility of depth-related factors. The components Y and Y^1 contain hyperbolic cosines and are depth-related variables. Specifically, as y decreases, so does the term Y, causing the denominator of arc sin also to diminish. As a result, $\ell n\, Y$ becomes smaller as the value of arc sin grows, obviously decreasing the variable ϕ.

The negative values of ϕ indicate a phase lead of the bottom temperature that occurs during the 24-hour time cycle sometime between midnight and morning. Air convection, absence of solar radiation, and nightly heat emission are possible causes of that.

Thus, on August 5, 1967, as can be seen in Figure 5, ϕ becomes positive soon after midnight at the depth of $\frac{1}{2}$ in. from the top, and at $5\frac{1}{2}$ in. down, ϕ is positive several hours after midnight, possibly as late as about 10 a.m. At this time the lag is equal to zero. This obviously occurs because radiation or re-radiation affects the top of a deck sooner than the lower concrete strata.

In going from top to bottom of the slab, the values of Y become relatively small at approximately mid-depth, causing the arc sin to become larger than unity. In such cases, obviously, no ϕ curves can be plotted for such depths. The reason for this phenomenon is the limits of Eq. 3 apparently established by Zuk, as indicated in his correspondence to Kozlov as follows: "...in proposing my temperature equation, I had assumed that the phase lag term would be a constant over a given daily period.... As your computations indicate, it appears to vary with both depth and time of day. Even if it varied only with time my theoretical equation would no longer be valid. This may in part explain the difficulty encountered." Zuk concludes with this remark: "Nevertheless, your paper has brought to light new information which will eventually help resolve the problem of predicting end movements of bridges."

From the preceding analysis, it appears that the validity of Eq. 3 could be measured in degrees, but it is obvious that further studies are needed. Furthermore, the effect that this phenomenon would have on the calculation of the slab temperatures in the region below mid-depth is indicated in the following observations.

If the expression $\left(2\pi\frac{t}{t_o} - \phi + \ell n\, Y\right) = \theta$, then in Eq. 3, the term $\eta_o\left[(0.5T_R + 3R)Y \sin\left(2\pi\frac{t}{t_o} - \phi + \ell n\, Y\right)\right] = \eta_o\,(0.5T_R + 3R)\,Y \sin\theta$ ("the term" is of consequence because ϕ cannot be evaluated in this region). For the values in Table 2, T = 26.1 F, $\eta_o = 0.6787$, R = 7.45 F, h = $\frac{6}{12}$ ft, a = 0.0334, and m = 1.98.

The maximum error in calculating the temperature at these depths, if Y will be assumed equal to zero, can be estimated as follows:

y in inches	Y	"The Term" in deg F	Maximum sin θ
$2\frac{1}{2}$	0.4120	9.85 sin θ	Near Unity
$1\frac{1}{2}$	0.2455	5.86 sin θ	
$\frac{1}{2}$	0.0208	0.50 sin θ	

The approximate maximum value of sin θ will occur at the time when variable ϕ is a minimum.

The maximum error, which is in reference to the slab temperatures actually observed, is shown here only in order to illustrate more completely the suspected limitations of Eq. 3, and is actually a would-be error, if Eq. 3 is used outside the limits indicated in this paper.

SIGNIFICANCE OF FINDINGS

The data evaluated are for a period of one day and in one location only, and therefore it is obvious that no generalization is advisable. But it seems to be true that ϕ is a time-related variable and that there is a slight error in a depth-related variable, possibly in the term $\ln Y$.

The cause for these seemingly small deviations of depth-related factors could be the apparent variations from actual conditions, which are mostly in the sinusoidal 24-hour cycle assumption, and also in all other secondary parameters that are assumed to be constant and average values. Nevertheless, it appears that, if the preceding statement is taken into account, Eq. 3 could be made applicable for predicting acceptably accurate temperatures.

The principal idea of this study was to find practical applications and to show ways for predicting temperatures. It was hoped that a nomogram, such as Figure 5, could be developed, giving values of ϕ for any time and thus enabling the engineer to predict reasonably accurate concrete temperatures, their changes, and, therefore, expected bridge deck movements. Perhaps if enough data were collected, for example on a zonal basis, this idea could become a distinct reality. Although it would be only as accurate as all the other parameters, it would nevertheless be much more than what an engineer has to work with at this time.

Thus the information presented in this paper should enlighten an engineer on the subjects of actual time difference and phase shift between air and concrete temperatures and on the effect of solar radiation. The increased comprehension of the problems has enhanced the feasibility of development of an equation for phase angle difference ϕ. The significance of this work is in showing the engineer the complexity of the subject problem.

CONCLUSIONS

In this paper, an attempt is made to summarize the reliable theoretical background of the thermal characteristics of a mass, such as a concrete bridge deck, and the fundamentals of heat transfer principles. Using the empirical approach suggested by Zuk, an attempt to determine the phase angle difference ϕ has been made on a limited basis, which clearly indicates the feasibility of such an approach. Within the limits available, one can draw the conclusion that phase lag ϕ increases with time in a roughly linear manner.

A recommendation, therefore, can now be made to implement Eq. 3 for the conditions established here so that a generalization of the approach shown in this paper could be attempted and a nomogram similar to Figure 5 could be made available.

The correlation between temperature and bridge end movements, in addition to some further information on the subject, will be investigated in future work, but only after the data from the experimental New Jersey sites are available.

ACKNOWLEDGMENT

The authors are grateful to Verdi Adam, Research and Development Engineer, and Hollis B. Rushing, Concrete Research Engineer, of the Louisiana Department of Highways for making their original data available to us. Our thanks also go to the personnel of the New Jersey Department of Transportation for giving assistance in evaluation of the data.

REFERENCES

1. Kozlov, George. Preformed Elastomeric Bridge Joint Sealers: Evaluation of the Material. Highway Research Record 287, 1969, pp. 59-75.

2. Kozlov, George. Preformed Elastomeric Bridge Joint Sealers. Highway Research Record 200, 1967, pp. 36-52.
3. Barber, E. S. Calculation of Maximum Pavement Temperatures From Weather Reports. HRB Bull. 168, 1957, pp. 1-8.
4. Groeber, H., and Erk, S. Fundamentals of Heat Transfer. McGraw-Hill, New York, 1961.
5. Zuk, William. Thermal Behavior of Composite Bridges—Insulated and Uninsulated. Highway Research Record 76, 1965, pp. 231-253.
6. Carslaw, H. S., and Jaeger, J. C. Conduction of Heat in Solids. Oxford Univ. Press, London, 1960.
7. Naruoka, M., Hirai, I., and Yamaguti, T. The Measurement of the Temperature of the Interior of the Reinforced Concrete Slab of the Shigita Bridge and Presumption of the Thermal Stress. Proceedings of the Symposium on the Stress Measurements for Bridges and Structures. Japan Society for the Promotion of Science, Tokyo, 1956.
8. Rushing, H. B. Durability of Lightweight Concrete: Phase 1—Concrete Temperature Study. Louisiana Highway Research Report, Louisiana Department of Highways, Baton Rouge.
9. Heating and Ventilating. Engineering Databook. The Industrial Press, New York, 1948, pp. 5-4, 5-14.
10. Heating Ventilating Air Conditioning Guide 1956. American Society of Heating and Air-Conditioning Engineers, Inc., New York, Vol. 34, pp. 95, 178, 253, 1175.
11. Bennet, I. Monthly Maps of Mean Daily Isolation for the United States. Solar Energy, Vol. 9, No. 3, July-Sept. 1965, pp. 145-158.
12. Yellott, J. How Materials React to Solar Energy. Architectural Record, May 1966, p. 196.
13. Fisher, V. Climatic Atlas of the United States. 1954, p. 157.

Impact Factors for Curved Highway Bridges

KIRAN M. VASHI, Teledyne Materials Research, Waltham, Massachusetts;
DAVID R. SCHELLING, Greiner Inc., Baltimore; and
CONRAD P. HEINS, JR., Department of Civil Engineering, University of Maryland, College Park

A method is presented to solve the problem of dynamic response of single-span, simply supported, horizontally curved highway bridges subjected to moving loads. The problem is analyzed by idealizing the bridge to be a single curved beam of equivalent rigidity and mass and the moving loads to be either a single constant force or two constant forces. The results of this analysis are utilized to develop impact factors for both flexural and torsional response of the bridge. The impact factor design curves are presented for various span lengths and central angles. These curves represent the response of the Bureau of Public Roads standard bridges of the I-beam noncomposite and welded girder composite types with four girders supporting the concrete slab.

•A TREND in recent years has been to construct bridges so that they accommodate highway alignment predetermined by considerations of tight geometric restrictions, simplicity of construction, aesthetics, and economics of cost. The increasingly frequent occurrence of structures on curved alignment therefore requires, for design purposes, an estimate of the general level of dynamic response when subjected to moving loads.

The response of horizontally curved highway bridges is analyzed by idealizing the bridge to be a simply supported, uniform, curved beam of equivalent mass and rigidity as shown in Figure 1. In general, moving loads on highway bridges possess sprung and unsprung components of mass and can be idealized as a single-axle or a two-axle load unit with sprung and unsprung mass as shown in Figure 2. The response analysis of curved bridges, based on such an elaborate analytical representation of the vehicle, was performed by Vashi (1). The results of this analysis were presented in the form of spectrum curves for the bridge response as a function of various parameters. This study showed that the constant-force solution was, in general, adequate for estimating the curved bridge response. For certain combinations of the parameters, the constant-force solution was found to form an upper bound to the data. The analysis presented herein, therefore, considers the loads to be either a single constant force or two constant forces moving with constant speed. The Appendix contains a notation of symbols used in this paper.

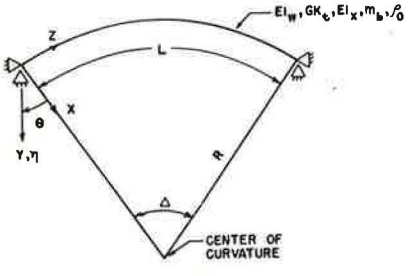

Figure 1. Idealization of simply supported horizontally curved bridge.

Paper sponsored by Committee on Dynamics and Field Testing of Bridges and presented at the 49th Annual Meeting.

THEORETICAL ANALYSIS

Differential Equations

The differential equations for the horizontally curved beam developed by Vlasov (2) may be modified to include the inertia forces of translation and rotation and may be written as

$$\left(\frac{EI_w}{R^2} + EI_x\right)\eta'''' - \frac{GK_t}{R^2}\eta'' + \frac{EI_w}{R}\theta''' - \frac{EI_x + GK_t}{R}\theta'' + m_b\ddot{\eta} = f(z, t) \tag{1a}$$

$$\frac{EI_w}{R}\eta''' - \frac{EI_x + GK_t}{R}\eta'' + EI_w\theta'''' - GK_t\theta'' + \frac{EI_x}{R^2}\theta + m_b\rho_o^2\ddot{\theta} = m(z, t) \tag{1b}$$

where

EI_x = flexural rigidity,
EI_w = warping rigidity,
GK_t = torsional rigidity,
R = radius of horizontal curvature,
η = vertical displacement of the shear center in the y-direction,
θ = angle of twist of the beam cross section,
m_b = beam mass per unit length,
ρ_o = polar radius of gyration of the beam cross section about its shear center,
$f(z, t)$ = external load in the y-direction per unit length, and
$m(z, t)$ = externally applied torsional moment per unit length.

Number of primes and number of dots above η and θ indicate the order of differentiation with respect to the coordinate z and the time t respectively.

For the simple-support boundary conditions, it is assumed that the normal stresses resulting from bending and warping torsion, the displacement η, and the rotation θ vanish at the support. These conditions can be written in their simplest mathematical form as

$$\eta(0, t) = \eta(L, t) = 0 \tag{2a}$$

$$\theta(0, t) = \theta(L, t) = 0 \tag{2b}$$

$$\eta''(0, t) = \eta''(L, t) = 0 \tag{2c}$$

$$\theta''(0, t) = \theta''(L, t) = 0 \tag{2d}$$

where L denotes the length of the curved beam between the supports along the z-axis.

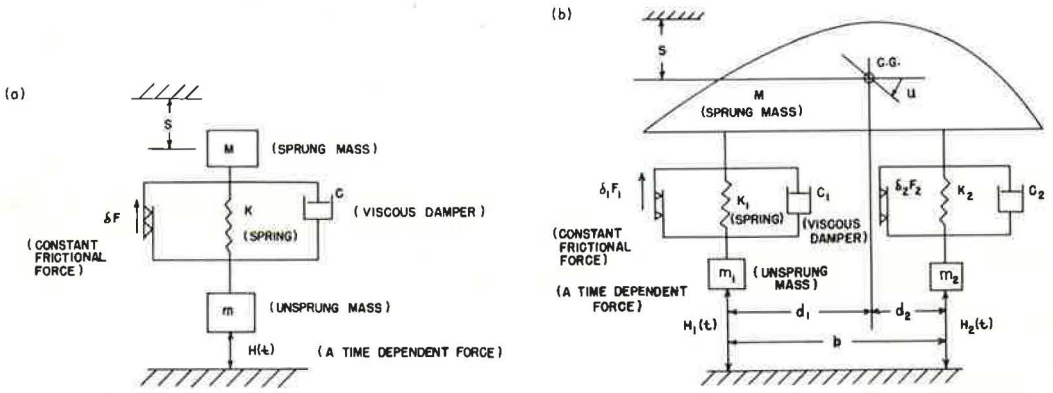

Figure 2. Idealization of vehicle: (a) single-axle load unit and (b) two-axle load unit.

Solution for a Single Constant Force

The problem of forced vibrations of a simply supported curved beam caused by a constant force P moving with constant speed V is governed by Eqs. 1 and 2. Assuming the curved beam to be initially at rest, the general solution for $\eta(z, t)$ and $\theta(z, t)$ was obtained previously (1) by use of the normal mode theory. Application of this theory results in the following equations:

$$\eta(z, t) = \frac{PL^3}{\pi^4 EI_x} \sum_{n=1}^{\infty} \sum_{s=1}^{2} \frac{\sin \frac{n\pi z}{L}}{RM_{ns}} G_{ns}(t) \tag{3a}$$

$$\theta(z, t) = \frac{PL^3}{\pi^4 EI_x R} \sum_{n=1}^{\infty} \sum_{s=1}^{2} \frac{K_{ns} \sin \frac{n\pi z}{L}}{RM_{ns}} G_{ns}(t) \tag{3b}$$

where

$$G_{ns}(t) = \frac{\sin 2\pi n\alpha \frac{t}{T_B}}{n^2(n^2\rho_{ns} - \alpha^2)} - \frac{\alpha \sin 2\pi n^2\sqrt{\rho_{ns}} \frac{t}{T_B}}{n^3\sqrt{\rho_{ns}}\,(n^2\rho_{ns} - \alpha^2)},$$

$$RM_{ns} = \frac{1}{2}\left[1 + \left(\frac{AK_{ns}}{D}\right)^2\right],$$

$$K_{ns} = -\frac{1 + \left(\frac{D}{A}\right)^2 \left(\frac{\omega_V}{\omega_\phi}\right)^2 \left[1 - \left(\frac{\omega_{ns}}{\omega_V}\right)^2\right]}{1 + \left(\frac{D}{n}\right)^2 \left(\frac{\omega_V}{\omega_\phi}\right)^2},$$

$$\alpha = \frac{VT_B}{2L} = \text{speed parameter},$$

$$T_B = \frac{2L^2}{\pi}\sqrt{\frac{m_b}{EI_x}},$$

$$\omega_{ns} = \frac{2\pi}{T_B} n^2 \sqrt{\rho_{ns}},$$

$$\left.\begin{matrix}\rho_{n1} \\ \rho_{n2}\end{matrix}\right\} = \frac{1}{2}\left\{C \mp \sqrt{C^2 - 4\left(\frac{\omega_\phi}{\omega_V}\right)^2 \left[1 - \left(\frac{A}{n}\right)^2\right]^2}\right\},$$

$$C = 1 + \left(\frac{AD}{n^2}\right)^2 + \left(1 + \frac{A^2}{D^2}\right)\left(\frac{\omega_\phi}{\omega_V}\right)^2,$$

$$\omega_\phi = \frac{n\pi}{L^2}\sqrt{\frac{n^2\pi^2 EI_w + GK_t L^2}{m_b \rho_o^2}},$$

$$\omega_V = n^2 \frac{2\pi}{T_B},$$

$$A = \frac{L}{\pi R} = \frac{\Delta}{180}, \text{ and}$$

$$D = \frac{L}{\pi \rho_o}.$$

It is to be noted that ω_ϕ, ω_v, and T_B, as defined here, represent respectively the nth uncoupled torsional natural frequency, the nth uncoupled flexural natural frequency, and the fundamental flexural natural period of a straight beam of the same length, mass, and rigidities as the curved beam. The symbol ω_{ns} denotes the two (s = 1 and 2) natural frequencies of the curved beam for each n = 1, 2, 3, ..., ∞. The natural frequencies of the curved beam depend on the three nondimensional parameters A, D, and $\frac{\omega_\phi}{\omega_v}$. Coefficients K_{ns} (s = 1 and 2 for each n = 1, 2, 3, ..., ∞) represent the amplitude ratios of the torsional rotation to the vertical displacement of a cross section for vibration with the nth natural frequency ω_{ns}. It should be noted that corresponding to s = 1, $\omega_{n1} < \omega_v$ and $K_{n1} < 0$, and when s = 2, $\omega_{n2} > \omega_v$ and $K_{n2} > 0$.

Dynamic Increments for Stress Resultants

Stress resultants relevant to the problem of a curved beam are the bending moment M, the St. Venant's torque S, the warping torque W, and the bimoment B. These stress resultants, as described by Vlasov (2), can be expressed in terms of η and θ as follows:

$$M = - EI_x\left(\eta'' - \frac{\theta}{R}\right) \tag{4a}$$

$$S = GK_t\left(\frac{\eta'}{R} + \theta'\right) \tag{4b}$$

$$W = - EI_w\left(\frac{\eta'''}{R} + \theta'''\right) \tag{4c}$$

$$B = - EI_w\left(\frac{\eta''}{R} + \theta''\right) \tag{4d}$$

For highway bridges, the parameter $\alpha < 1$ and the contribution of terms in Eqs. 3a and 3b for n > may be neglected in comparison with those for n = 1. Considering only the term n = 1, therefore, reduces Eqs. 3a and 3b to the following:

$$\eta(z, t) = \frac{PL^3 \sin\frac{\pi z}{L}}{\pi^4 EI_x} \sum_{s=1}^{2} \frac{G_{1s}(t)}{RM_{1s}} \tag{5a}$$

$$\theta(z, t) = \frac{PL^3 \sin\frac{\pi z}{L}}{\pi^4 EI_x R} \sum_{s=1}^{2} \frac{K_{1s}G_{1s}(t)}{RM_{1s}} \tag{5b}$$

Substituting Eqs. 5a and 5b into Eq. 4a yields

$$M = \frac{PL \sin\frac{\pi z}{L}}{\pi^2} \sum_{s=1}^{2} \frac{1 + A^2K_{1s}}{RM_{1s}} G_{1s}(t) \tag{6a}$$

The static bending moment M_{st} is obtained from Eq. 6a by setting $\alpha = 0$, but retaining the term $\sin 2\pi\alpha \frac{t}{T_B}$. This yields

$$M_{st} = \frac{PL \sin \frac{\pi z}{L} \sin 2\pi\alpha \frac{t}{T_B}}{\pi^2} \sum_{s=1}^{2} \frac{1 + A^2 K_{1s}}{\rho_{1s} RM_{1s}} \tag{6b}$$

The maximum static bending moment $M_{st,max}$ can be obtained by setting $\sin 2\pi\alpha \frac{t}{T_B} = 1$ in Eq. 6b. The instantaneous value of the dynamic increment for bending moment can be obtained by subtracting Eq. 6b from Eq. 6a. This value, when nondimensionalized with respect to the maximum static bending moment $M_{st,max}$, represents the dynamic increment for the bending moment $DI_{flexural}$, which can be written as

$$DI_{flexural} = \frac{\sum_{s=1}^{2} \frac{1 + A^2 K_{1s}}{RM_{1s}} H_{1s}(t)}{\sum_{s=1}^{2} \frac{1 + A^2 K_{1s}}{\rho_{1s} RM_{1s}}} \tag{7}$$

where

$$H_{1s}(t) = \frac{\alpha^2 \sin 2\pi\alpha \frac{t}{T_B}}{\rho_{1s}(\rho_{1s} - \alpha^2)} - \frac{\alpha \sin 2\pi \sqrt{\rho_{1s}} \frac{t}{T_B}}{\sqrt{\rho_{1s}}\,(\rho_{1s} - \alpha^2)}.$$

The dynamic increments associated with the St. Venant's torque, warping torque, and bimoment can be obtained by a similar procedure. It can be shown that these are all equal to $DI_{torsional}$, which is given by

$$DI_{torsional} = \frac{\sum_{s=1}^{2} \frac{1 + K_{1s}}{RM_{1s}} H_{1s}(t)}{\sum_{s=1}^{2} \frac{1 + K_{1s}}{\rho_{1s} RM_{1s}}} \tag{8}$$

The dynamic increments as given by Eqs. 7 and 8 are dimensionless and are independent of the magnitude of the moving force P. From Eqs. 7 and 8, an upper bound to the maximum value of $DI_{flexural}$ and $DI_{torsional}$ can be obtained by taking the sum of the absolute values of the individual terms. This approach yields

$$DI_{flexural,max} = \frac{\sum_{s=1}^{2} \frac{1 + A^2 K_{1s}}{\rho_{1s} RM_{1s}} \frac{\alpha}{(\sqrt{\rho_{1s}} - \alpha)}}{\sum_{s=1}^{2} \frac{1 + A^2 K_{1s}}{\rho_{1s} RM_{1s}}} \tag{9a}$$

$$DI_{torsional,max} = \frac{\sum_{s=1}^{2} \frac{(-1)^{s+1}(1 + K_{1s})}{\rho_{1s} RM_{1s}} \frac{\alpha}{\left[\sqrt{\rho_{1s}} - (-1)^{s+1}\alpha\right]}}{\sum_{s=1}^{2} \frac{1 + K_{1s}}{\rho_{1s} RM_{1s}}} \tag{9b}$$

These equations are useful in estimating the general level of response caused by moving vehicles and will form a basis for the impact factors to be developed in the next section.

IMPACT FACTORS

General Factors

Various investigations have studied the response of horizontally curved girders. The works of Tan and Shore (3, 4, 5) and Christiano and Culver (6, 7, 8) are the most current and important contributions. These works differ in some respects from that of Vashi (1). All of the works cited include the response due to a moving constant force. Tan and Shore assumed a doubly symmetric cross section to be the girder and extended their analysis to the case of a single-axle, single-wheel vehicle with sprung and unsprung mass. Assuming a singly symmetric, thin-walled, open cross section to be the girder, Christiano and Culver also investigated the response due to a single-axle, two-wheel vehicle with sprung and unsprung mass. Such an idealization for the vehicle permits the study of vehicle rolling effects on the response. The analysis by Vashi considered, in addition to the single-axle sprung vehicle, the case of a two-axle vehicle that is useful in studying the effects of vehicle-pitching and the axle spacing on the response. Christiano and Culver verified their analysis by tests on a laboratory model and Tan and Shore performed a parametric study of the bridge response using bridge parameters evaluated by an arbitrary method. However, no attempt was made to incorporate in their analyses the characteristics of actual highway bridges and provide information suitable for design purposes. The work of Vashi differs from other works because the analysis is applied to evaluate impact factors for Bureau of Public Roads standard bridges. The reduction of results to useful design information is based on certain important observations summarized elsewhere (1). The observations are as follows:

1. For a combination of a small value of frequency ratio σ_v and a large value of mass ratio RS, or, conversely, the peak values of the dynamic increments for the displacement and the stress resultants can be approximated by the constant force solution. This approximation is valid for the entire range of values of the axle spacing parameter $0 \leq \frac{b}{L} \leq 0.5$.
2. For a combination of arbitrary values of the mass ratio and the frequency ratio, the dynamic increments due to a single-axle, sprung mass load $\left(\frac{b}{L} = 0\right)$ were found to be generally a conservative representation of the absolute maximum response for $\frac{b}{L} > 0$.
3. For conditions stated in the second observation, the dynamic increments due to a single-axle, sprung mass load were larger than the corresponding ones due to the constant force. However, these larger values were not critical because they were shown not to correspond to the maximum static effects.
4. The amplitude of the peak responses increases uniformly with the increasing values of the speed parameter α for given values of the other parameters.

The analysis of flexural-torsional response of horizontally curved bridges due to moving vehicles with sprung and unsprung mass is extremely complex because of its dependence on various physical parameters governing the response. However, the foregoing observations reveal that the constant-force solution can adequately predict the response. In what follows, the constant-force solution will therefore be used to illustrate the development of the impact factors.

Development of Impact Factors

For a single moving constant force, the maximum values of the dynamic increments for the bending moment, St. Venant's torque, warping torque, and bimoment can be approximated by Eqs. 9a and 9b. It is shown elsewhere (1) that, for two moving constant forces each of magnitude $\frac{P}{2}$ and with a relative spacing of $\frac{b}{L} \leq 0.5$, the maximum dynamic

increments for the bending moment, St. Venant's torque, warping torque, and bimoment can also be given by Eqs. 9a and 9b if expressed in terms of

$$\frac{PL}{\pi^2}\sum_{s=1}^{2}\frac{1+A^2K_{1s}}{\rho_{1s}RM_{1s}},\ \frac{PLA}{\pi^2}\cdot\frac{GK_t}{EI_x}\sum_{s=1}^{2}\frac{1+K_{1s}}{\rho_{1s}RM_{1s}},$$

$$PLA\,\frac{EI_w}{EI_xL^2}\sum_{s=1}^{2}\frac{1+K_{1s}}{\rho_{1s}RM_{1s}},\ \text{and}\ \frac{PL^2A}{\pi}\cdot\frac{EI_w}{EI_xL^2}\sum_{s=1}^{2}\frac{1+K_{1s}}{\rho_{1s}RM_{1s}},$$

respectively and if $\frac{\sqrt{\rho_{11}}}{\alpha}\frac{b}{L} = 2, 4, 6, 8, \ldots$. This allows the amplification factor for flexural behavior to be written as

$$AF_{flexural} = \frac{M,max}{M_{st,max}}$$

$$= \frac{M_{st,max} + \frac{PL}{\pi^2}\sum_{s=1}^{2}\frac{1+A^2K_{1s}}{\rho_{1s}RM_{1s}}\frac{\alpha}{(\sqrt{\rho_{1s}}-\alpha)}}{M_{st,max}} \tag{10}$$

For two forces each of magnitude $\frac{P}{2}$, $M_{st,max}$ can be expressed by the first term in the series solution as

$$M_{st,max} = \frac{PL\left(1+\cos\frac{\pi b}{L}\right)}{2\pi^2}\sum_{s=1}^{2}\frac{1+A^2K_{1s}}{\rho_{1s}RM_{1s}} \tag{11a}$$

Substituting Eq. 11a into 10 yields

$$AF_{flexural} = 1 + \frac{\sum_{s=1}^{2}\frac{1+A^2K_{1s}}{\rho_{1s}RM_{1s}}\frac{\alpha}{(\sqrt{\rho_{1s}}-\alpha)}}{\frac{1}{2}\left(1+\cos\frac{\pi b}{L}\right)\sum_{s=1}^{2}\frac{1+A^2K_{1s}}{\rho_{1s}RM_{1s}}} \tag{11b}$$

The impact factor, $I_{flexural}$, is then given by

$$I_{flexural} = \frac{\sum_{s=1}^{2}\frac{1+A^2K_{1s}}{\rho_{1s}RM_{1s}}\frac{\alpha}{(\sqrt{\rho_{1s}}-\alpha)}}{\frac{1}{2}\left(1+\cos\frac{\pi b}{L}\right)\sum_{s=1}^{2}\frac{1+A^2K_{1s}}{\rho_{1s}RM_{1s}}} \tag{12a}$$

Similarly, the impact factor associated with the torsional response may be written as

$$I_{torsional} = \frac{\sum_{s=1}^{2}\frac{(-1)^{s+1}(1+K_{1s})}{\rho_{1s}RM_{1s}}\frac{\alpha}{[\sqrt{\rho_{1s}}-(-1)^{s+1}\alpha]}}{\frac{1}{2}\left(1+\cos\frac{\pi b}{L}\right)\sum_{s=1}^{2}\frac{1+K_{1s}}{\rho_{1s}RM_{1s}}} \tag{12b}$$

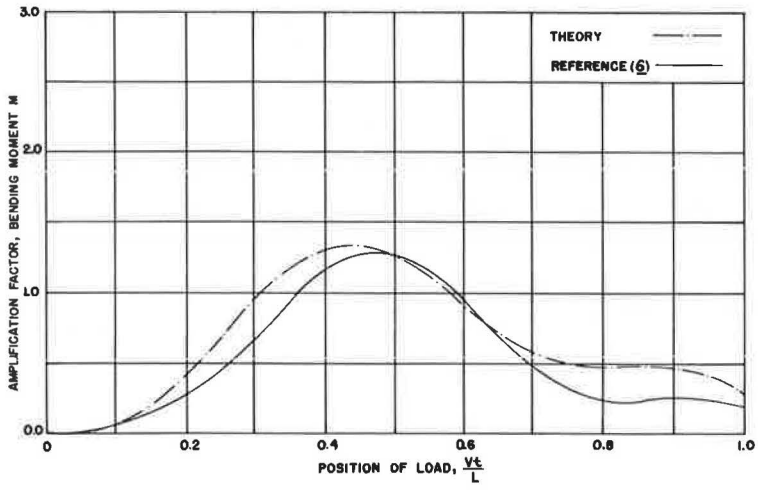

Figure 3. Comparison of amplification factor history curves for bending moment.

Comparison of Theory With Results From Literature

Figures 3 and 4 show a comparison of the results obtained by Eqs. 7 and 8 with those of Christiano (6). These figures represent the history curves for amplification factors associated with the bending moment and the warping torque. Christiano's theoretical results include more than one term of the series and are calculated using the physical properties of a laboratory bridge model that was tested. An inspection of these curves reveals that the agreement between the two results is good, and the normal mode solution, based on only the first term n = 1, is satisfactory. A comparison with results of field tests would be useful to prove the applicability of the analysis to field conditions; however, this is not possible because tests on curved bridges have not been conducted to date.

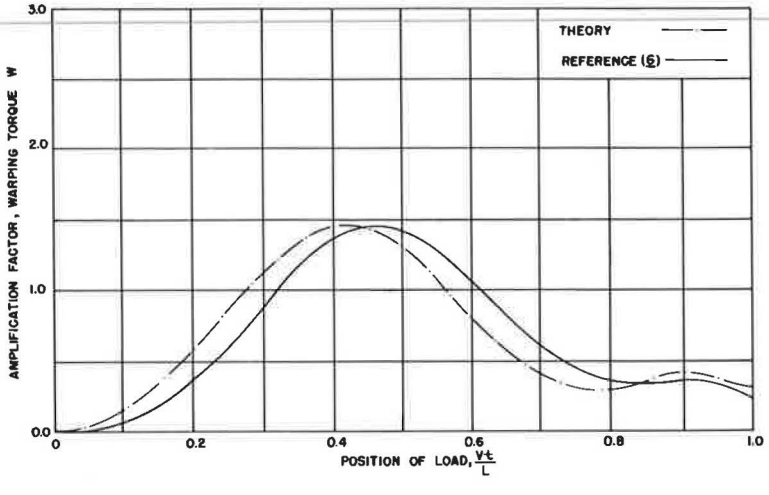

Figure 4. Comparison of amplification factor history curves for warping torque.

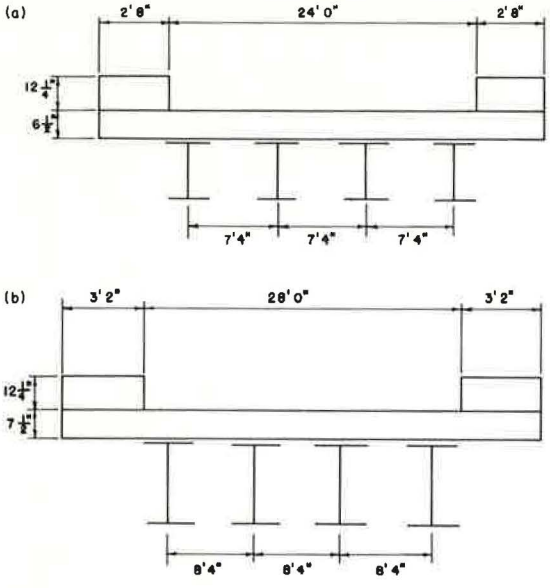

Figure 5. Cross section of (a) I-beam noncomposite BPR bridge and (b) welded girder composite BPR bridge.

Impact Factor Curves for BPR Bridges

Utilizing the expressions for impact factors given by Eqs. 12a and 12b, impact curves were prepared for two classes of bridges—the BPR standard bridges of the I-beam noncomposite and welded girder composite types with four girders supporting the concrete slab. The cross sections of both bridge types (9) are shown in Figure 5. These bridges are intended to be built on straight alignment. However, for the purposes of this study, they are assumed to be built on curved alignment by keeping the span length constant and varying the radius of horizontal curvature. The physical parameters relating the bridge and vehicle characteristics, which enter into Eqs. 12a and 12b, are the torsional-flexural frequency ratio $\frac{\omega_\phi}{\omega_V}$ (n = 1), the ratio of span length to polar radius of gyration about the shear center $D = \frac{L}{\pi\rho_o}$, the speed parameter α, the axle-spacing parameter $\frac{b}{L}$, and the central subtended angle parameter A. The designs of the bridges based on standard plans were analyzed previously (1) to evaluate the necessary parameters given in Table 1. The parameter A is directly proportional to the central subtended angle Δ, which varies between 15 and 75 deg, accounting for practical bridge construction. The present AASHO impact formula (10) does not reflect the effect of vehicle speed. However, it is clear from the fourth observation summarized previously that for maximum response the speed parameter α should be computed using a representative value of the maximum limit on the vehicle speed. In the present study, the

TABLE 1

BRIDGE AND VEHICLE PARAMETERS FOR IMPACT CURVES

Description	Span Length L, ft	$\frac{\omega_\phi}{\omega_V}$ (n = 1)	D	α at 60 mph	$\frac{b}{L}$
I-beam, noncomposite, 24 ft wide, H15-44 loading	20	0.9432	0.7536	0.116	0.500
	25	0.9519	0.9416	0.134	0.500
	30	0.9463	1.1274	0.133	0.500
	35	0.9505	1.3120	0.138	0.500
	40	0.9430	1.4916	0.136	0.500
	45	0.9466	1.6692	0.139	0.500
	50	0.9566	1.8369	0.138	0.500
	60	0.9845	2.1642	0.143	0.500
	70	1.1728	2.4234	0.147	0.500
Welded girders, composite 28 ft wide, H20-S16-44 loading	90	1.3046	2.3963	0.116	0.389
	100	1.4048	2.4759	0.118	0.350
	110	1.4260	2.4324	0.113	0.318
	120	1.4583	2.3785	0.111	0.292
	130	1.4440	2.3835	0.113	0.269
	140	1.4574	2.1751	0.109	0.250
	150	1.4426	2.0553	0.108	0.233
	160	1.4339	1.9342	0.106	0.219
	170	1.3819	1.8473	0.106	0.206
	180	1.3462	1.6325	0.102	0.195

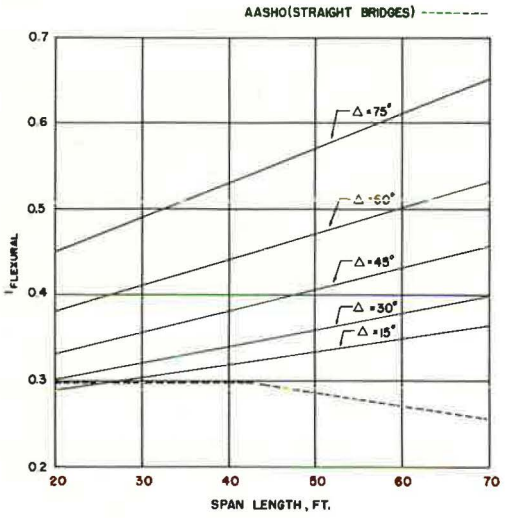

Figure 6. Flexural impact factor curves for I-beam noncomposite bridges.

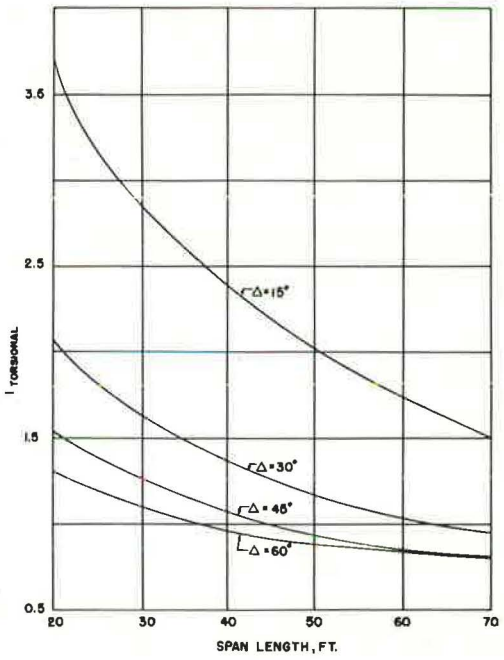

Figure 7. Torsional impact factor curves for I-beam noncomposite bridges.

values of α correspond to a maximum vehicle speed of 60 mph. In accordance with the dimensions of the trailer wheelbase of the AASHO H20-S16-44 design vehicle, the axle spacing b is varied between 14 and 35 ft, with $\frac{b}{L} \leq 0.5$. The value of the axle-spacing parameter $\frac{b}{L}$ is given in Table 1.

It is seen from data in Table 1 that the torsional-flexural frequency ratio $\frac{\omega_\phi}{\omega_v}$ (n = 1) is nearly constant and approximately equal to 0.95 for the I-beam type noncomposite bridges. For the welded girder type composite bridges, this ratio increases with span, attaining a maximum and then decreasing with span. The value of this ratio ranges from 1.30 to 1.46. The nondimensional parameter D increases approximately linearly with the span length for the I-beam type bridges and decreases for the welded girder type bridges. The parameter ranges from 0.75 to 2.43 for the I-beam type bridges and from 1.63 to 2.48 for the welded girder type bridges. The speed parameter α, which corresponds to a vehicle speed of 60 mph, is nearly constant for various span lengths of both types of bridges. The value of this parameter ranges from 0.116 to 0.147 for the I-beam type bridges and from 0.102 to 0.118 for the welded girder type bridges. The value of the axle spacing parameter $\frac{b}{L}$ is subject to the condition $\frac{b}{L} \leq 0.5$. Because of this, the maximum value of $\frac{b}{L} = 0.5$ applies for the I-beam type bridges, while for the welded girder type bridges the value of $\frac{b}{L}$ ranges from 0.195 to 0.389.

Figures 6, 7, 8, and 9 show the impact curves for the BPR standard bridges of the I-beam and welded girder types. These impact curves are based on the approximate expressions given by Eqs. 12a and 12b. Also included in Figures 6 and 8 is a plot of the AASHO impact formula (10) for flexural response of straight bridges.

The following procedure illustrates the use of the impact curves to predict the maximum dynamic response for an actual horizontally curved bridge due to two moving constant forces:

Step 1. Compute the maximum static values of the bending moment, St. Venant's torque, warping torque, and bimoment using conventional methods (11).

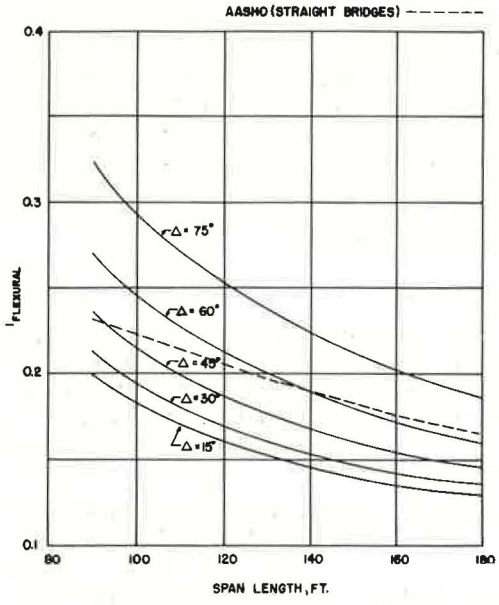

Figure 8. Flexural impact factor curves for welded girder composite bridges.

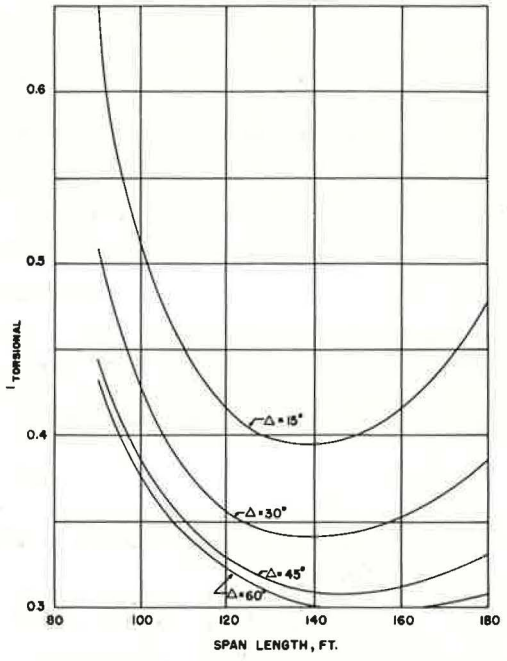

Figure 9. Torsional impact factor curves for welded girder composite bridges.

Step 2. For a given span length, L, enter Figure 6 or 8 to obtain the value of $I_{flexural}$ corresponding to the chosen value of the central subtended angle Δ.

Step 3. Repeat procedure of Step 2 to obtain $I_{torsional}$ from Figure 7 or 9.

Step 4. To obtain the maximum total value of the bending moment, multiply the corresponding static value obtained in Step 1 by $1 + I_{flexural}$.

Step 5. To obtain the maximum total values of the St. Venant's torque, warping torque, and bimoment, multiply the corresponding static values obtained in Step 1 by $1 + I_{torsional}$.

The method presented provides a working criterion for impact in preliminary bridge design. However, the final design should be verified using Vashi's analysis (1). It is seen from Figures 6 and 8 that the flexural impact factor increases as the value of Δ is increased. From Figure 6, it is clear that the AASHO impact formula cannot be used to predict the response of curved bridges of I-beam noncomposite type. However, Figure 8 shows that the AASHO impact formula is conservative up to Δ = 45 deg for the curved bridges of welded girder composite type. Figures 7 and 9 show that the torsional impact factor decreases as the value of Δ is increased. It should be remembered that large values of $I_{torsional}$ described in these figures relative to smaller values of the central subtended angle Δ are of no practical importance because these values correspond to small values of maximum static effects. However, for larger values of Δ, the torsional impact factors are important because they correspond to large values of maximum static effects. These results show that the impact factors associated with the torsional response may at times be more important than the impact factors associated with the flexural response, and, hence, the torsional response may be more decisive in governing the design of horizontally curved bridges.

SUMMARY AND CONCLUSIONS

A method is presented to analyze the dynamic response due to constant forces of a horizontally curved beam. The results of this analysis are utilized to develop impact

factors for flexural-torsional response of a curved beam. Particular emphasis has been placed on applying these impact factors for determining the general level of response that can be expected during the service life of the highway bridges. A procedure was proposed to determine impact for two classes of actual highway bridges of BPR standard designs. Study of the impact factor curves prepared for the BPR standard bridges of the I-beam and welded girder types indicates that the impact factors associated with the torsional response may at times be more important than the impact factors associated with the flexural response. Thus, the torsional response may be more decisive in governing the design of horizontally curved bridges.

ACKNOWLEDGMENTS

These equations and theory were used in a study sponsored by the State Roads Commission of Maryland and the U.S. Bureau of Public Roads. The entire development is part of a thesis presented in partial fulfillment of the requirements for the degree of Doctor of Philosophy at the University of Maryland Civil Engineering Department.

REFERENCES

1. Vashi, K. M. Dynamic Response of Simple-Span Horizontally Curved Highway Bridges to Moving Vehicles. PhD dissertation, Univ. of Maryland, College Park, 1969.
2. Vlasov, V. Z. Thin-Walled Elastic Beams, Second Edition. National Science Foundation, 1961, Ch. 12, p. 452.
3. Tan, C. P. Dynamic Response of a Horizontally Curved Bridge Subjected to Simulated Highway Loadings. PhD dissertation, Univ. of Pennsylvania, Philadelphia, 1966.
4. Tan, C. P., and Shore, S. Dynamic Response of a Horizontally Curved Bridge. Jour. Structural Div., ASCE, Vol. 94, No. ST3, March 1968.
5. Tan, C. P., and Shore, S. Response of Horizontally Curved Bridge to Moving Load. Jour. Structural Div., ASCE, Vol. 94, No. ST9, Sept. 1968.
6. Christiano, P. P. The Dynamic Response of Horizontally Curved Bridges Subject to Moving Loads. PhD dissertation, Carnegie-Mellon Univ., Pittsburgh, 1967.
7. Culver, C. G., and Christiano, P. P. Static Model Tests of Curved Girder Bridge. Jour. Structural Div., ASCE, Vol. 95, No. ST8, Aug. 1969.
8. Christiano, P. P., and Culver, C. G. Horizontally Curved Bridges Subject to Moving Load. Jour. Structural Div., ASCE, Vol. 95, No. ST8, Aug. 1969.
9. Standard Plans for Highway Bridges: Vol. II, Structural Steel Superstructures. U.S. Bureau of Public Roads, 1962.
10. Standard Specifications for Highway Bridges, Ninth Edition. American Association of State Highway Officials, 1965, p. 20.
11. Spates, K. R., and Heins, C. P. The Analysis of Single Curved Girders With Various Loadings and Boundary Conditions. Civil Engineering Dept., Univ. of Maryland, College Park, June 1968.

Appendix

NOTATION

The following symbols are used in this paper:

$A = \frac{L}{\pi R} \frac{\Delta}{180}$, central subtended angle parameter;

$AF_{flexural}$ = amplification factor associated with the flexural response;

b = axle spacing;

B = bimoment;

$D = \frac{L}{\pi \rho_o}$, ratio of span length to polar radius of gyration about shear center;

$DI_{flexural}$ = dynamic increment associated with the flexural response;
$DI_{torsional}$ = dynamic increment associated with the torsional response;
E = modulus of elasticity of the bridge material;
$f(z, t)$ = external load in the y-direction per unit length;
G = modulus of rigidity of the bridge material;
$G_{ns}(t)$ = a time-dependent nondimensional function;
$H_{1s}(t)$ = a time-dependent nondimensional function;
$I_{flexural} = AF_{flexural} - 1$, flexural impact factor;
$I_{torsional}$ = torsional impact factor;
I_x = moment of inertia of the bridge cross section;
I_w = warping constant;
K_{ns} = amplitude ratios;
K_t = St. Venant's torsional constant;
L = length of the curved beam along the centerline between the supports;
m_b = beam mass per unit length;
$m(z, t)$ = externally applied torsional moment per unit length;
M = bending moment;
n = an integer denoting the order of the natural mode of vibration;
P = magnitude of the traveling constant force;
R = radius of horizontal curvature of the bridge;
$RM_{ns} = \frac{1}{2}\left[1 + \left(\frac{AK_{ns}}{D}\right)^2\right]$, dimensionless ratio;
RS = ratio of the mass of the vehicle to the mass of the bridge;
S = St. Venant's torque;
t = time;
T_B = fundamental flexural natural period of a straight beam of the same length and rigidity as the curved beam;
V = speed of the vehicle;
W = warping torque;
x, y, z = three mutually perpendicular axes that are fixed in the beam cross section;
$\alpha = \frac{VT_B}{2L}$, speed parameter;
Δ = central subtended angle in degrees;
η = vertical displacement of the shear center in the y-direction;
θ = angle of twist of the beam cross section;
ρ_o = polar radius of gyration of the beam cross section about its shear center;
ρ_{n1}, ρ_{n2} = modification factors for coupled natural frequencies of the curved beam;
σ_v = ratio of the vehicle-suspension frequency to the bridge frequency;
ω_{ns} = coupled natural frequencies of the curved beam (s = 1 and 2 for each n = 1, 2, 3, . . . , ∞);
ω_v = nth uncoupled flexural natural frequency of a straight beam of the same length and rigidity as the curved beam; and
ω_ϕ = nth uncoupled torsional natural frequency of a straight beam of the same length and rigidity as the curved beam.

Upper Anchorage of Column Bars in Bridge Pylons

K. S. RAJAGOPALAN, Mullen and Powell, Inc., Dallas; and
PHIL M. FERGUSON, University of Texas at Austin

In single-column pylons having cantilevered arms supporting highway spans, a large tension may be induced in the column bars from unequal live loads on opposite arms. The upper anchorage of such large column bars, generally No. 14S and No. 18S, can be questioned because of the varying stress from the bending forces perpendicular to the bars, including possible tensile cracks parallel to the bar in the transverse beam. A specific detail currently being used in Texas was tested in full size and found adequate. Based on this test and reinforcing steel strain data collected, some conservatism in the anchorage length provided under ultimate strength design seems desirable.

•LARGE-DIAMETER BARS, No. 14S and No. 18S, are being used in bridge pylons consisting of a central column and cantilevered beams on opposite sides supporting the roadway girders, as shown in Figure 1. The column reinforcement will be subjected to significant tensile stresses caused by an unbalanced load on the cantilevers. Because the anchorage of the larger diameter column bars into the top beam is complicated by the varying stress conditions, analysis is uncertain. The upper part of the anchorage may be weakened by flexural cracks in the cantilever beam that could open along the plane of the column bars. The lower part of the anchorage is improved by perpendicular flexural compression from the same cantilever beams. The net effect of two such diverse factors is uncertain.

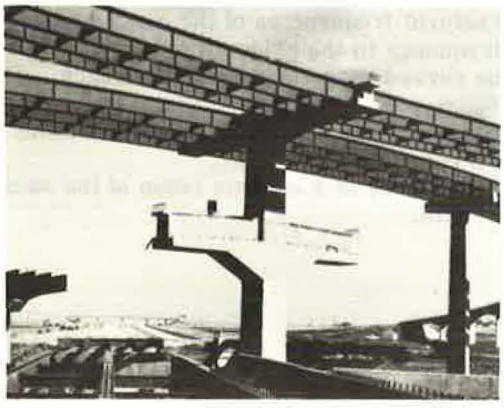

Figure 1. Pylon for construction in Dallas.

A test to determine the adequacy of a specific anchorage length currently used by the Texas Highway Department is reported here. Pertinent details of such a pylon bent with No. 14S bars as the main column steel are shown in Figure 2. With bond strength heavily involved, only a full-size model with No. 14S bars could be trusted. A model could be used only in the sense that a slice 1 ft thick could be used for the test instead of the 6-ft thickness used in the field.

TEST SPECIMEN

A slice of the balanced cross beams and the upper part of the pylon was constructed to full size, with dummy anchor beams built as the lower part of the specimen (Fig. 3). The cantilever beams were constructed without a sloping top and modified as to

Paper sponsored by Committee on Concrete Superstructures.

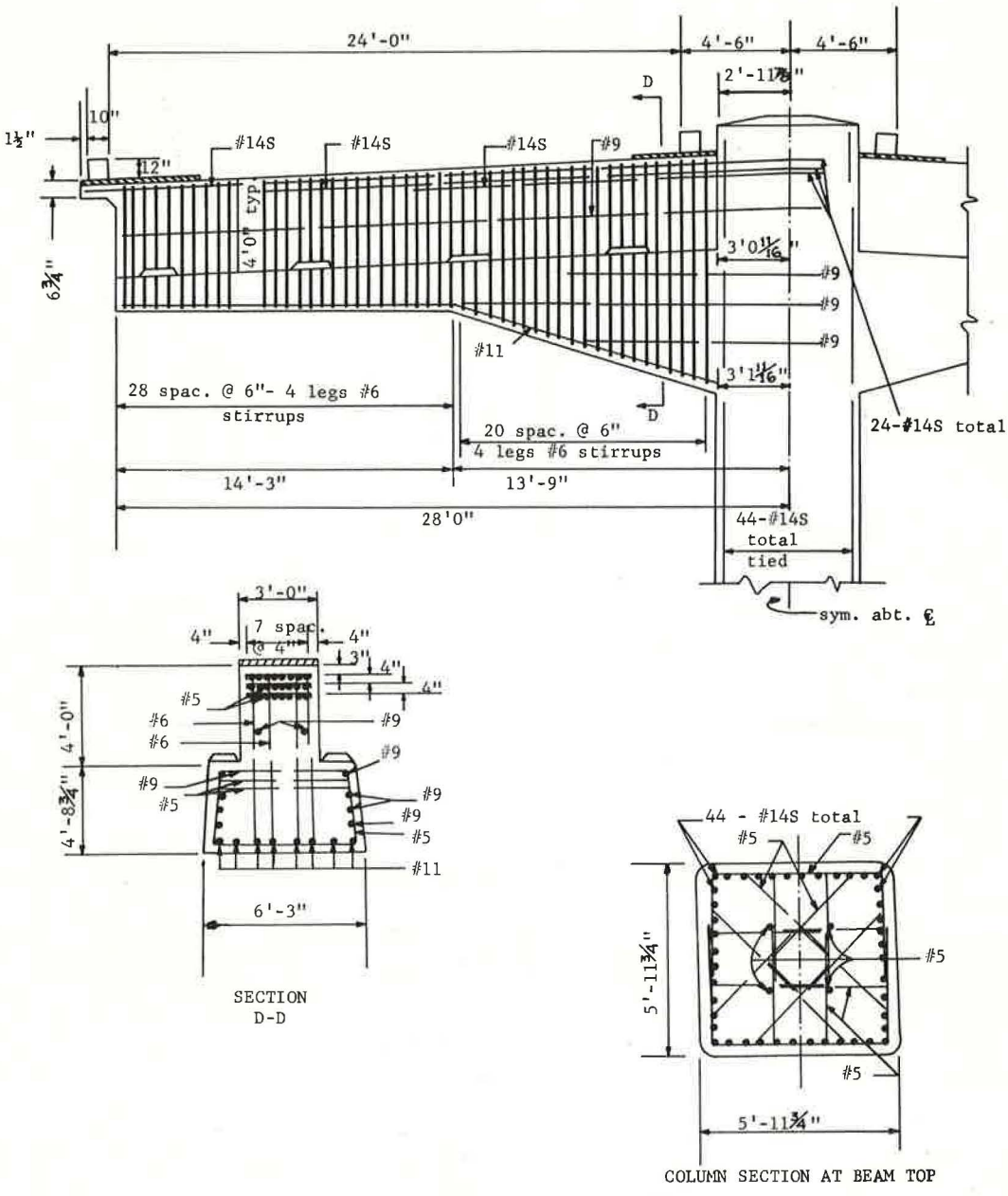

Figure 2. Details of pylon (prototype).

length to permit a single concentrated load to give essentially the proper ratio between moments and shears at the joint. The details of the test specimen are shown in Figure 3b.

The entire specimen (21 cu yd) was cast in the horizontal position, raised to allow insertion of bearing rollers, and tested while still in the same horizontal position. Vertical loads were applied by jacking the cross beams and anchor beams toward each other by means of hydraulic rams reacting against strap-type loading frames.

The test specimen, shown before concreting in Figure 4, departed in several minor details from being an exact model of the actual pylon beam, but differences were away

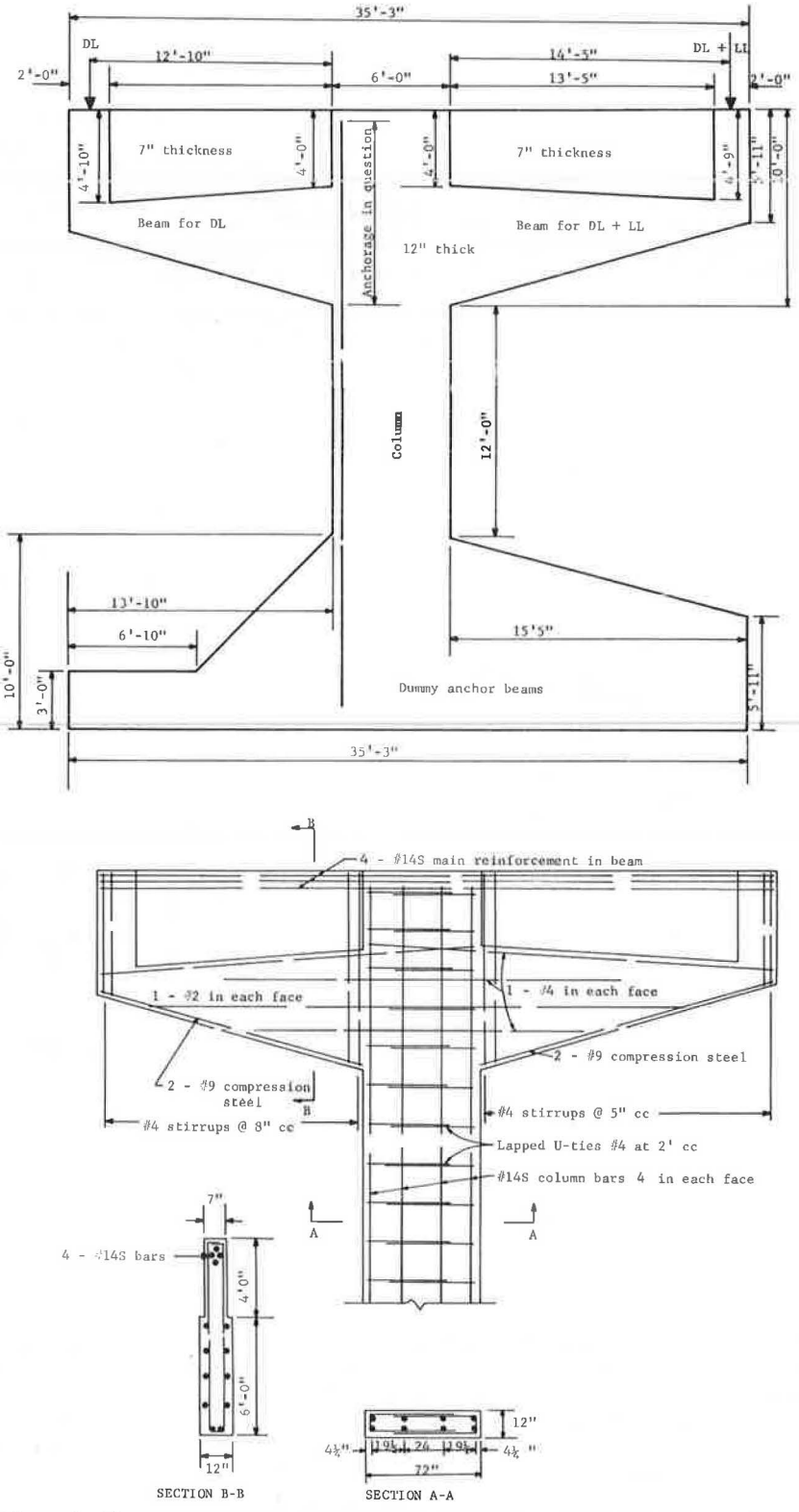

Figure 3. The test specimen with outline showing location of (a) critical bars and (b) detailed reinforcement.

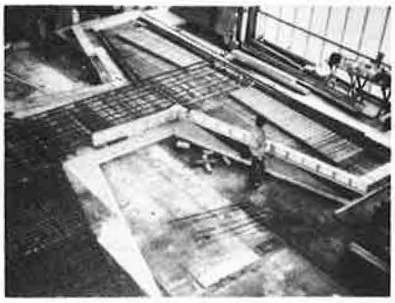

Figure 4. Most of reinforcement of test specimen in place.

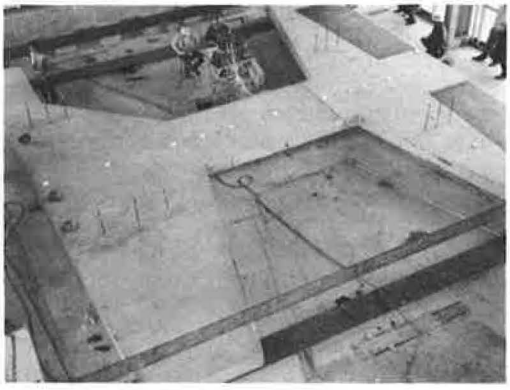

Figure 7. Overall view of the test.

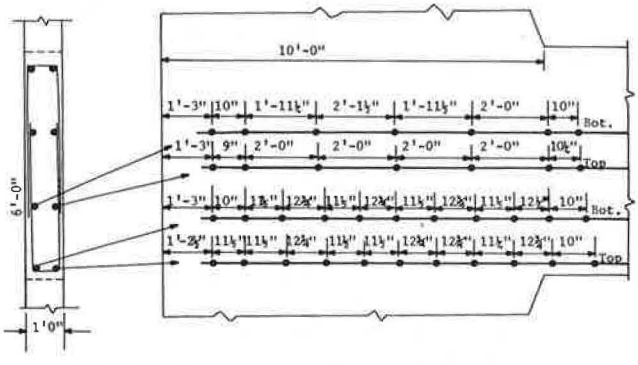

Figure 5. Location of strain gages on No. 14S bars.

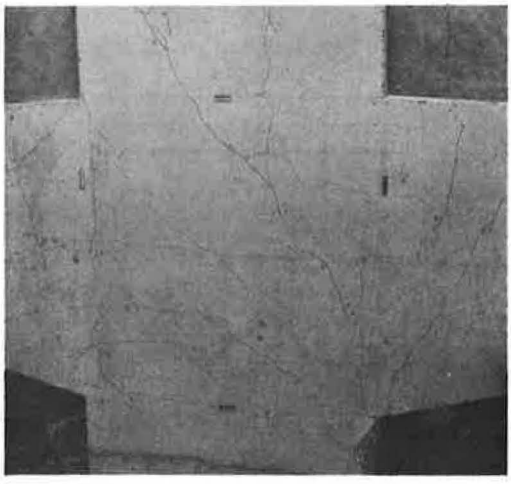

Figure 8. Cracking pattern at the junction of the pylon and crossbeam.

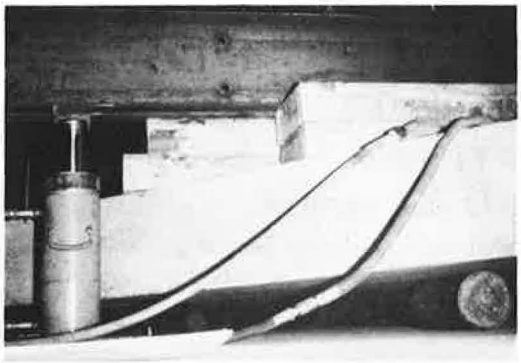

Figure 6. Lifting of the specimen and placing on rollers.

Figure 9. Final failure in secondary compression after yielding of steel in tension.

from the critical column and joint. The test was deliberately changed from the prototype by using A 432 steel for the No. 14S bars in column and beam (yield strength at 0.005 strain of 62.7 ksi) instead of intermediate-grade steel as designed. The beam web steel was strengthened to match.

Electrical resistance strain gages were attached to each No. 14S bar on the tension side of the column, 11 on each outer bar and 7 on each inner bar, as shown in Figure 5. These gages were distributed over the entire anchorage length of the bars and about a foot into the top of the column below the transverse cantilever beams. Concrete made with Type III cement was placed from a transit mixer and the specimen was cast in two parts, with a construction joint just below the transverse beams to simulate construction in the field.

TEST PROCEDURE

After curing for 5 days, the test specimen was lifted from the floor by using as a strongback a pair of steel channels attached to bolts through the specimen. Lifting was carried just far enough to permit the placement of 7-in. rollers made from concrete-filled steel pipe (Fig. 6). One of the loading cantilevers was cracked by an accidental torque loading during lifting (shown by the cracks specially marked in Fig. 10); these cracks had no observable influence on the failure. The loading arm functioned precisely as planned.

The lifting rods are still in place in Figure 7, which shows the general setup for the test. The dark steel straps in the foreground and in the background are the loading straps that frame into vertical channels. Load was applied by jacking between the cantilever arms and the channels.

The transverse cantilever beams were first loaded to dead load plus 1.25 live loads (DL + 1.25LL) to produce flexural cracking and then were unloaded. (Throughout this report live load is considered as the sum of the live and impact loads and is noted by the abbreviation LL.) For the test proper, the equivalent of dead load was applied to each arm, and then the right arm was loaded progressively by steps up to the equivalent of dead load plus 5.5LL. At this load the loading system at the heavily loaded end became unstable and released the load, bringing the first part of the test to an end. The strains still remaining in the bars after unloading were recorded.

Four days later, after some correction to the loading system, the testing was resumed in a similar manner to a level of dead load plus 6.75LL on the heavily loaded beam when failure occurred that was equal to 2.54 (DL + LL). The failure was the result of yielding of the vertical tensile steel in the column and the subsequent secondary compression failure at the opposite face of the column above the construction joint. The crack pattern in the joint at this stage is shown in Figure 8, where the crushing of the concrete at the right foreground indicates the start of the compression failure. Straining at the same load was continued until the compression concrete outside the compression steel completely failed from secondary compression, as shown in Figure 9.

The final crack pattern over the joint is shown in Figure 10. Vertical splitting had occurred over the lower half of the anchorage of the higher stressed column tension bar where it projected into the beam. It will be noted, however, that splitting did not continue all the way to the top even at this final stage. There was no bond or anchorage failure.

One of the practical difficulties of this test was the removal of the specimen. It had to be broken up into truck-sized units as shown in Figure 11.

DATA AND ANALYSIS OF TEST RESULTS

The change to A 432 reinforcement steel with extra stirrups permitted the beam loading to go beyond the design value. The primary purpose of the test was to check the anchorage (or development length) of the No. 14S tension bars in the pylon column where these extended into the upper cross beam. With f'_c = 4,200 psi, the construction carried dead load on each arm and 6.75LL on the right arm without any failure in anchorage or development length, a load equivalent to 2.54 (DL + LL). At the face of the column (on the 1-ft thickness), the design moments were DL M = 1,122 kip-ft and LL M = 430 kip-ft

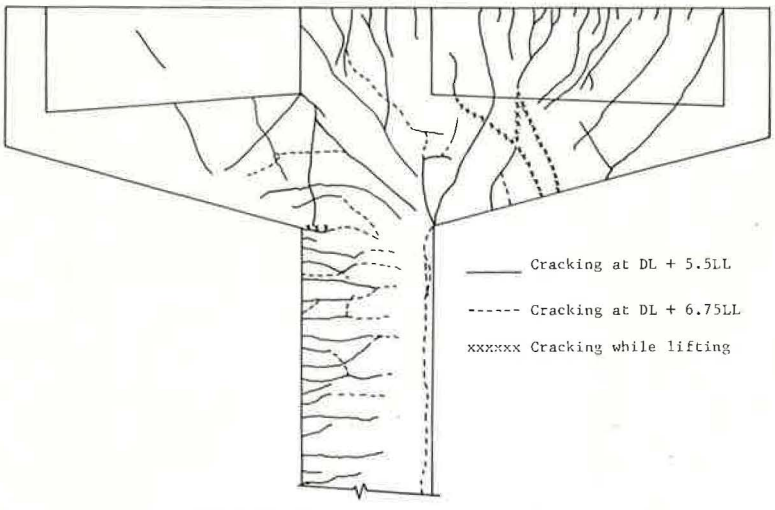

Figure 10. Crack pattern of the specimen.

(including impact). The column continued to function until flexural failure in secondary compression, after the A 432 No. 14S bars yielded. Although the strain gage record is not good at this level, it appears that the outside tension bars were stressed to at least 65 ksi and at least one of the inner bars (at about the quarter point of the column depth) was at 58-ksi stress.

The bent design was for intermediate-grade steel. At DL + 4.5LL, equivalent to 1.97 (DL + LL), the steel stress in the outer bars was 43 ksi and in one of the inner bars was 37 ksi. This indicates an overall factor of safety of nearly 2 for a design based on intermediate-grade steel. Although there was some splitting (Fig. 10), it is not certain that the anchorage was in serious danger at the ultimate load.

Strain Gage Data

The chief subsidiary data were strain gage readings on four bars shown in Figure 5. These were interpreted into stresses and are shown in Figures 12 through 15; the bottom of the beam is indicated by the hatched corner outline. The data in each case are in two parts: an upper set of curves representing the first loading (before it became unstable) and a lower set representing the data during the final load test, including the locked-up strains from the first loading.

Figure 11. Specimen broken up for removal.

Interpretation of Bar Strain Data

Stresses were obtained by using the bar stress-strain data in Figure 16. Some of the gage data are missing or should be questioned; these cases are shown by dashed lines. In Figure 12 it is obvious that at gage 9 the steel has reached the yield stress and must be more highly stressed at gages 10 and 11. The bulge in the stresses in the area of gage 5 probably occurred because a diagonal crack opened in that vicinity, the crack being directed radially toward the inner corner between the compression faces of the column and heavily loaded beam. The inner bar stresses in Figure 14 drop sharply as the bar leaves

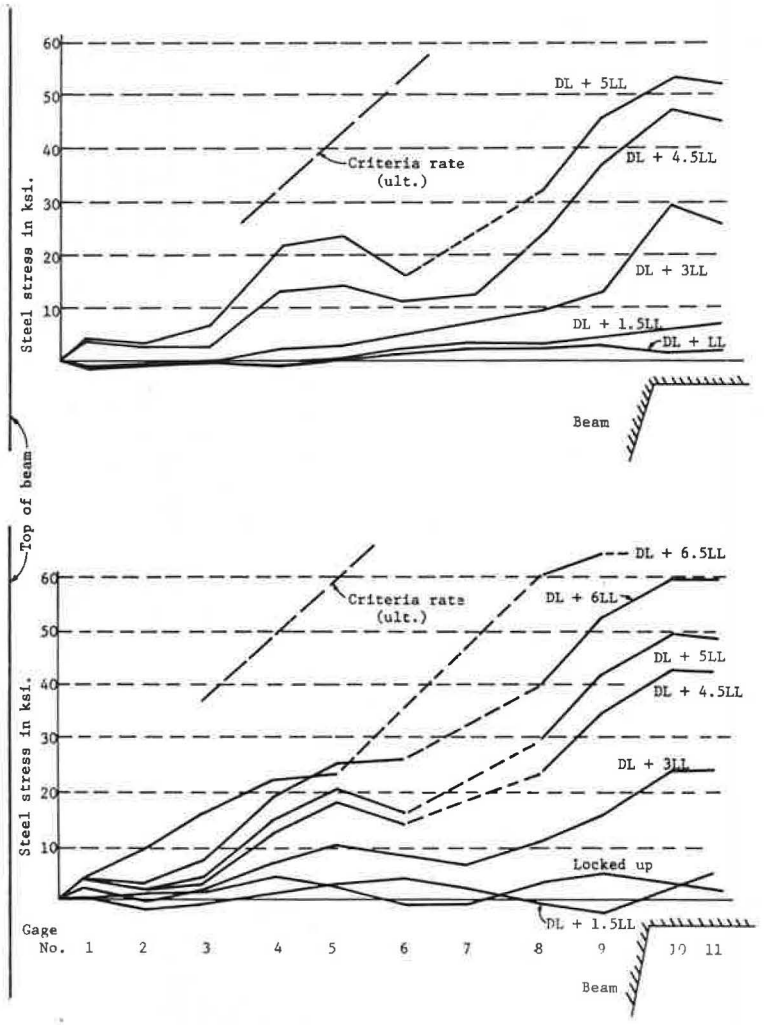

Figure 12. Steel stress distribution in outer bottom bar.

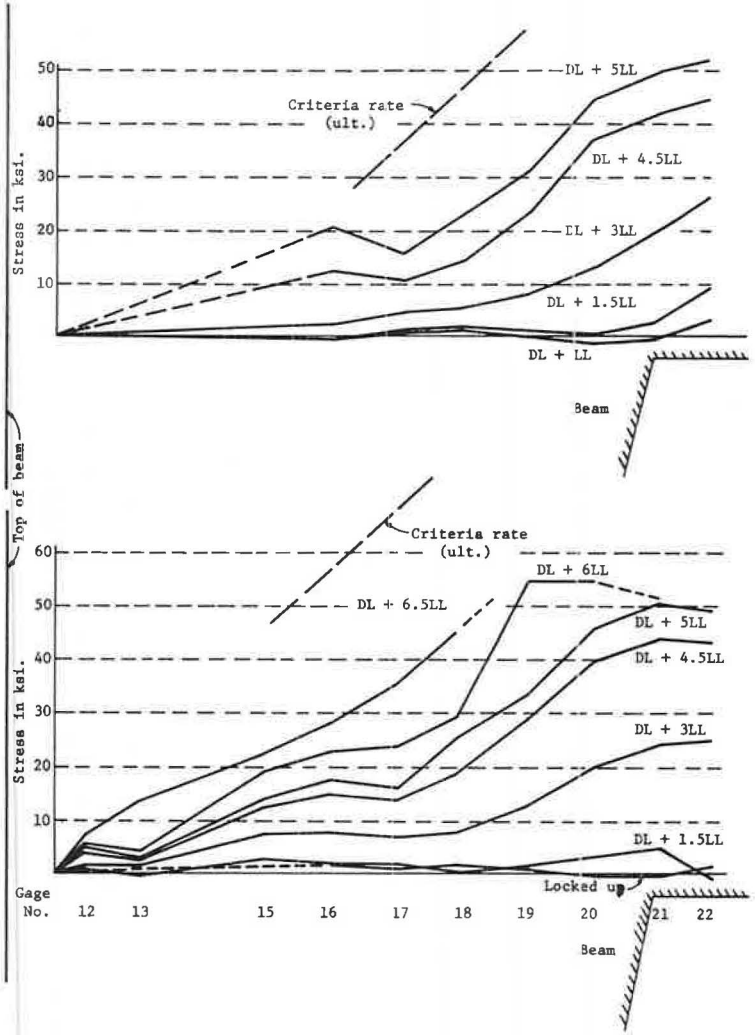

Figure 13. Steel stress distribution in outer top bar.

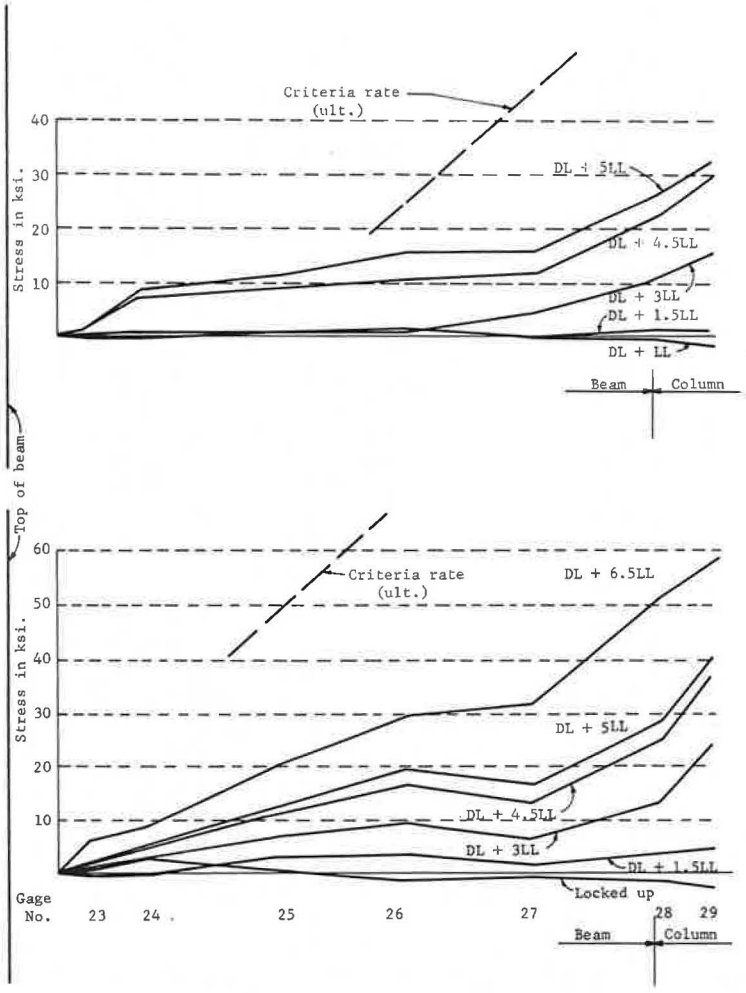

Figure 14. Steel stress distribution in inner top bar.

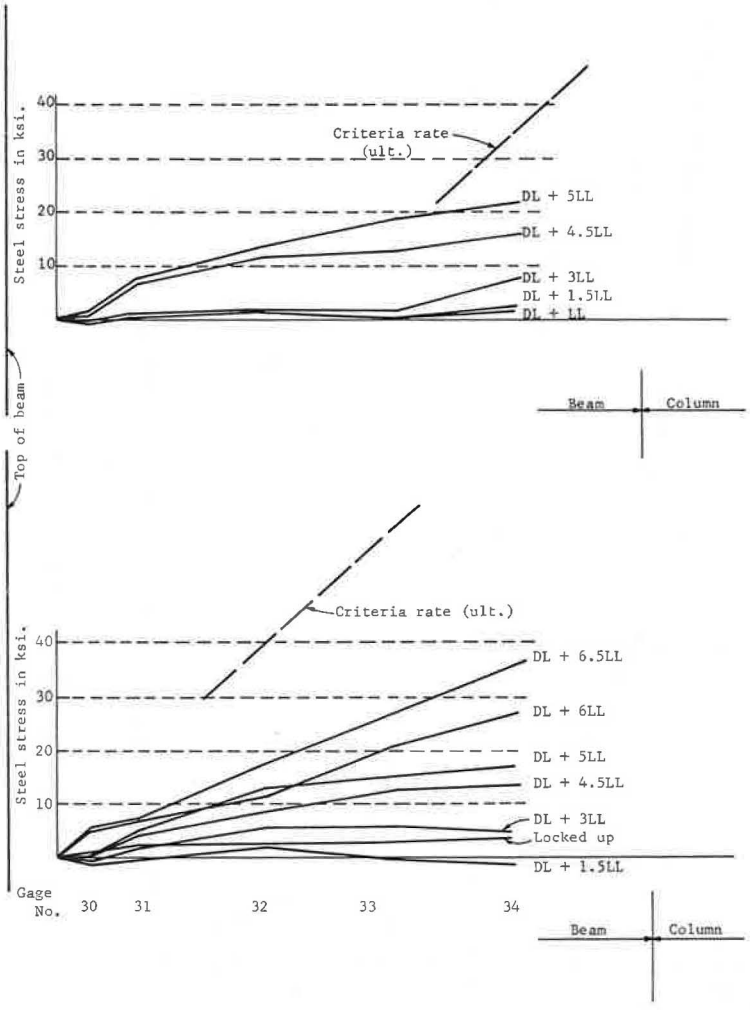

Figure 15. Steel stress distribution in inner bottom bar.

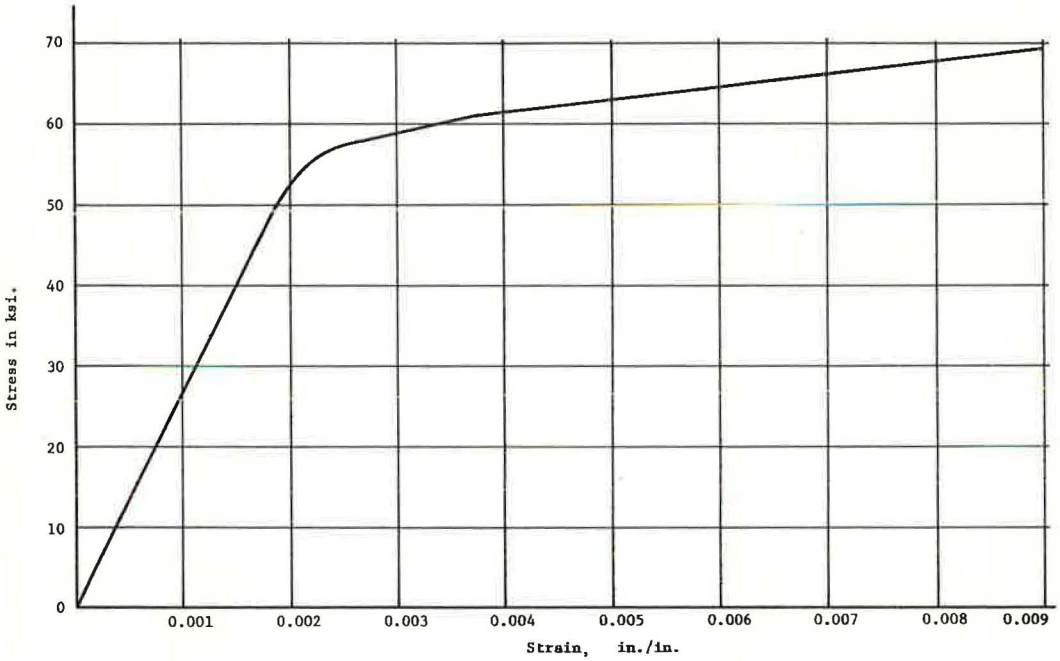

Figure 16. Steel stress-strain curve for No. 14S bar.

the simpler stress pattern at the top of the column and enters into the more complex beam and joint area.

So far as end anchorage is concerned, these inner bars could apparently be stopped off somewhat shorter than the outside bars, possibly at about two-thirds of the anchorage length of the outer bar. However, the longer length serves a very necessary function in controlling the diagonal cracking that occurs within the joint, as marked by the bulge in stress at station 26. The crack pattern in Figure 10 indicates the need for a reinforcing grid to control cracking throughout the joint, that is, the area common to the beams and column.

Effective Bond Resistance

The ultimate design stresses in bond are the same in the Bureau of Public Roads criteria for ultimate strength design (1) and in the 1963 ACI Building Code (2); that is, $6\phi\sqrt{f'_c}$. For these bars (and $\phi = 1$ for a known f'_c of 4,200 psi) this allowable stress predicts the rate of change of bar stress indicated by the slope of the lines marked "criteria" in Figures 12 through 15. The inner bar in Figure 14 reaches this rate only in the short section that was gaged below the beam; Figure 15 does not cover the corresponding length. The exterior bars (Figs. 12 and 13) on the first unbalanced loading reached this approximate rate of change in stress and in the final loading seem to have exceeded it at least locally.

This degree of encouraging correlation must be viewed with the added fact that a long splitting crack did occur over about half of the anchorage length (Figs. 8 and 10), despite an ultimate bond stress (averaged over the entire anchorage length) of only 280 psi compared to the 388 psi that the BPR criteria and ACI Code permit. The exact extent of untapped bond strength is not precisely known, but it is thought to be very limited. The close spacing of No. 14S bars (at 6-in. centers) probably lowered the bond resistance, although the acting beam compression should have reduced the net splitting.

Although no conclusive evidence about the ultimate bond strength capacity has been established, the test indicates that in this type of situation it may be advisable to be conservative and count only 75 percent of the specified bond stress over the full anchorage length.

CONCLUSIONS

The test indicated that this specific detail was adequate in bond resistance, but that bending forces perpendicular to a bar may lower its bond strength. The column failure was in flexural tension with a secondary failure in flexural compression, the most desirable type of failure because of the adequate warning and the large amount of toughness it provides. The cracking in the joint area common to beam and column justifies a grid of reinforcing steel at least equal to that furnished by ties and column steel.

ACKNOWLEDGMENTS

The authors wish to acknowledge the financial support of the Texas Highway Department for this study.

REFERENCES

1. U. S. Bureau of Public Roads. Strength and Serviceability Criteria, Reinforced Concrete Bridge Members, Ultimate Design. U. S. Govt. Printing Office, Aug. 1966.
2. Building Code Requirements for Reinforced Concrete (ACI 318-63). American Concrete Institute, Detroit, 1963.

The Bump at the End of the Bridge

T. C. HOPKINS and R. C. DEEN, Division of Research,
Kentucky Department of Highways

ABRIDGMENT

•THE NATURE and causes of the differential settlements between a bridge deck and the adjoining highway approach pavement have been the subject of an increasing number of investigations in recent years. This settlement of the highway approach pavement not only presents a hazardous condition to rapidly moving traffic, but creates a rough and uncomfortable ride. These defects of the pavement surface require costly maintenance and, where a heavy traffic flow exists, these maintenance operations may tend to impede the normal flow.

Bridge abutments in Kentucky are usually founded on a relatively stable foundation, such as rock or point-bearing piles to rock, and, practically speaking, cannot settle. Highway approach pavements, on the other hand, are located on an embankment and foundation that are potentially free to settle. The extent to which either settlement of the embankment or foundation contributes to the approach settlement will obviously depend on the particular conditions at any given bridge site. Data obtained from a survey of existing bridge approaches conducted in the summers of 1964 and 1968 have provided general information as to the prevalence of the problem in Kentucky. In addition, these data imply that there is a general relationship between development of the approach fault and such possible causative factors as the type of abutment, geological conditions, and soils conditions. This report summarizes the general relationship between the occurrence of bridge approach settlement and various conditions at the bridge sites.

The approaches were classified according to one of the following settlement categories:

Group 1 settlement—no maintenance necessary and no approach fault noticeable.

Group 2 settlement—no maintenance performed; however, an approach fault was observed.

Group 3 settlement—maintenance performed on the approach.

The criterion used to distinguish between groups 1 and 2 was whether or not a bump was evident when an automobile passed onto or off the bridge deck. Additional information was obtained by visually inspecting each approach. In addition, the ages (approximate dates opened

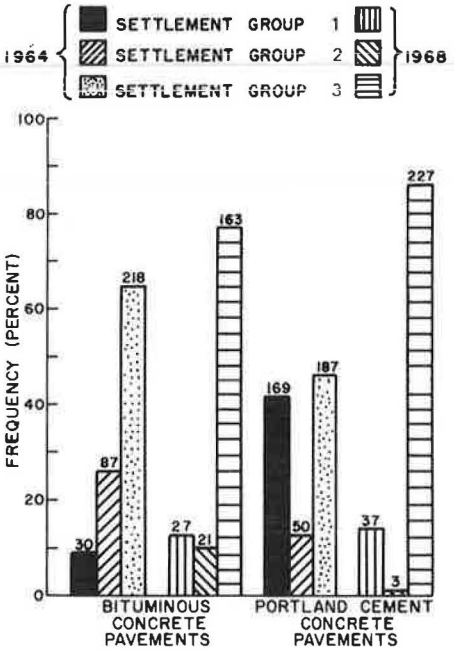

Figure 1. Comparison of bridge approaches by pavement type.

Paper sponsored by Committee on Substructures, Retaining Walls and Foundations.

to traffic) of the approaches were noted. The majority of approaches were at least 2 years old in the 1964 survey. From these data, it is evident that present design and construction procedures are not sufficient to guarantee smooth bridge approaches.

A comparison of portland cement concrete and bituminous concrete approaches (Fig. 1) shows a markedly higher percentage of bituminous concrete approaches with patching than rigid approach pavements with mudjacking in 1964. In addition, there was a much greater percentage of smooth approaches (group 1) for concrete approaches than for bituminous approaches. However, in 1968, the difference in percentage of mudjacked and patched approaches, as well as smooth approaches, was almost insignificant. Furthermore, the 1968 data, when compared with 1964 data, showed that there was an appreciable percentage decrease in smooth approaches and an increase in maintained approaches for both types of pavements. Apparently, at least for a short period of time, the rigidity of portland cement concrete pavement reduced the occurrence of the approach fault by bridging the presumed depression behind the abutment. Generally, the approach settlement appeared to be confined within 100 ft of the end of the bridge, and settlement of the approach pavement seldom exceeded 6 in.

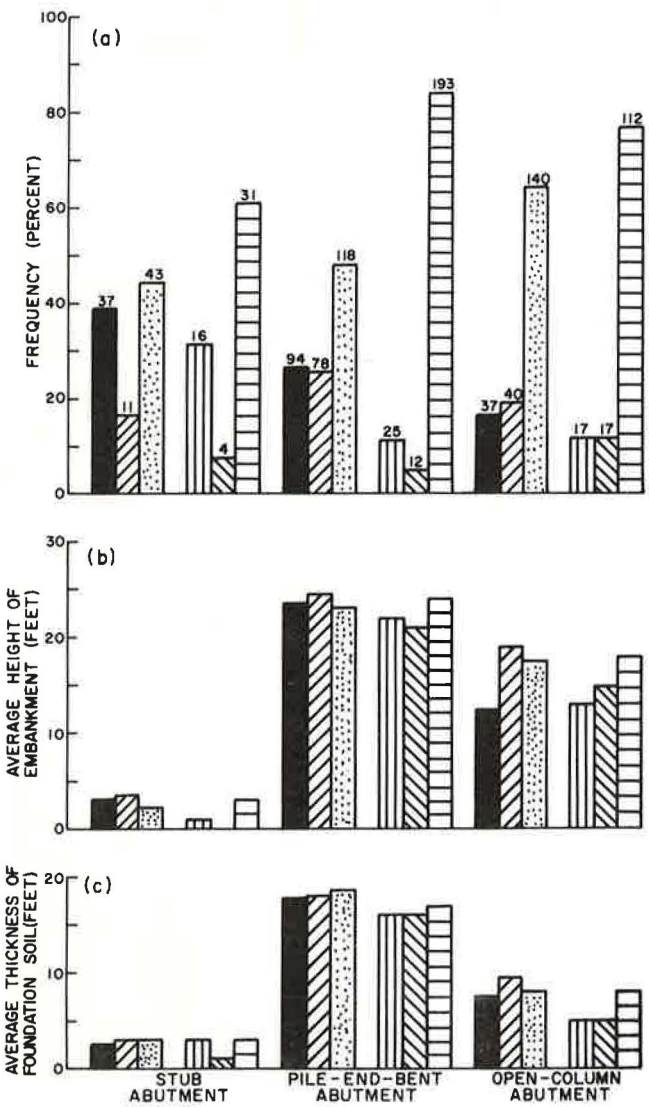

Figure 2. Comparison of bridge approaches by abutment type.

A comparison of the most commonly used types of abutments with respect to the three settlement groups (Fig. 2) revealed that the open-column (open-end) type was more commonly associated with settlement group 3 than either the pile-end-bent (open-end) type or stub (closed-end) type in 1964. The relationship between average height of embankment, average thickness of foundation soil, and type of abutment with respect to settlement groups is shown in Figure 2b and 2c. Notice that stub abutments are associated with smoother bridge approaches, smaller average heights of embankment and thinner foundation soils. The pile-end-bent abutments had greater average heights of embankment and thicknesses of foundation soils than the open-column abutment, but the pile-end-bent abutments had better bridge approaches. The better performance of approaches located behind stub abutments may be attributed to smaller settlements associated with shallower embankments and foundation soils. The comparatively larger time for consolidation before construction of the pavement and the need for less hand com-

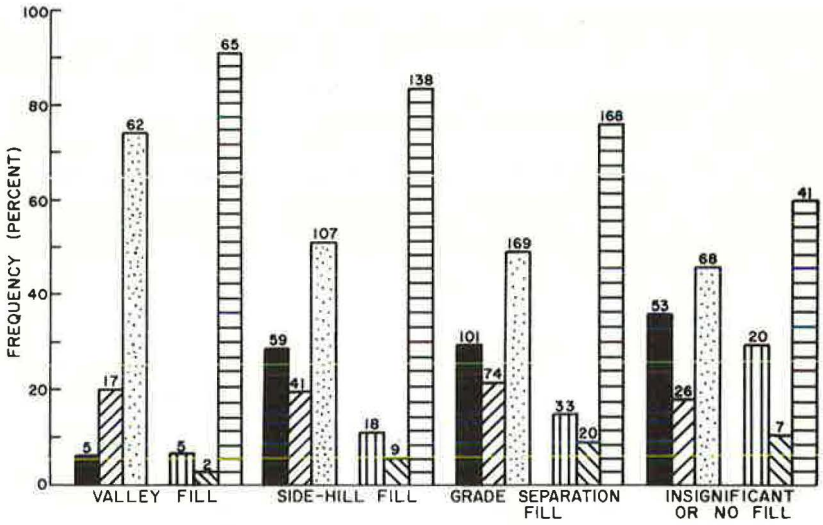

Figure 3. Comparison of bridge approaches by type of embankment.

paction near the abutment may account for the better performance of approaches associated with pile-end-bent abutments than those approaches at open-column abutments. However, in 1968 there was an increase in percentage of faulted approaches for all types of abutments with the percentage for pile-end-bent types increasing the most. There were small differences in percentages between the pile-end-bent and open-column abutments. Although the percentage of faulted approaches increased, stub abutments still had a comparatively high percentage of smooth approaches in 1968. For both surveys, there was a large number of defective bridge approaches associated with all types of abutments.

Different types of embankments were studied with respect to the settlement groups. These data (Fig. 3) show that embankments located in valleys of major streams had a much greater percentage of settlement group 3 approaches than embankments at other locations. Side-hill fills were considered to be those embankments that were generally part fill and part cut. Grade separation embankments were those considered to be built-up on a relatively flat plain. It is reasonable to assume that valley fills were located on foundations that were thicker than the other types of fills. Hence, these data probably reflect the importance of the foundation as a variable in bridge approach settlement. Those faulted approaches with embankments 3 ft or less in height may reflect improper backfill placement and compaction and such other causative factors as erosion or swelling and shrinkage.

At 54 bridge approaches located on Interstate 64 between Frankfort and Louisville, the approach embankments were constructed of a special granular fill material extending approx-

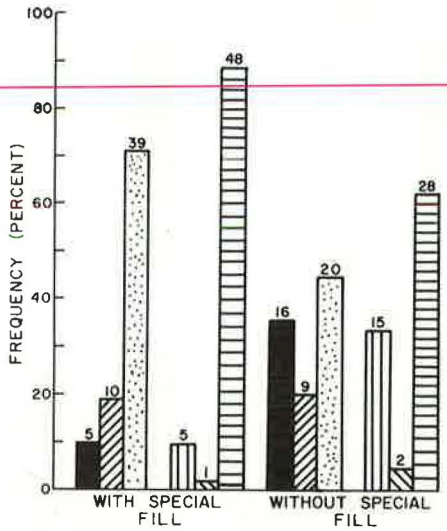

Figure 4. Comparison of bridge approaches by use of special backfill material.

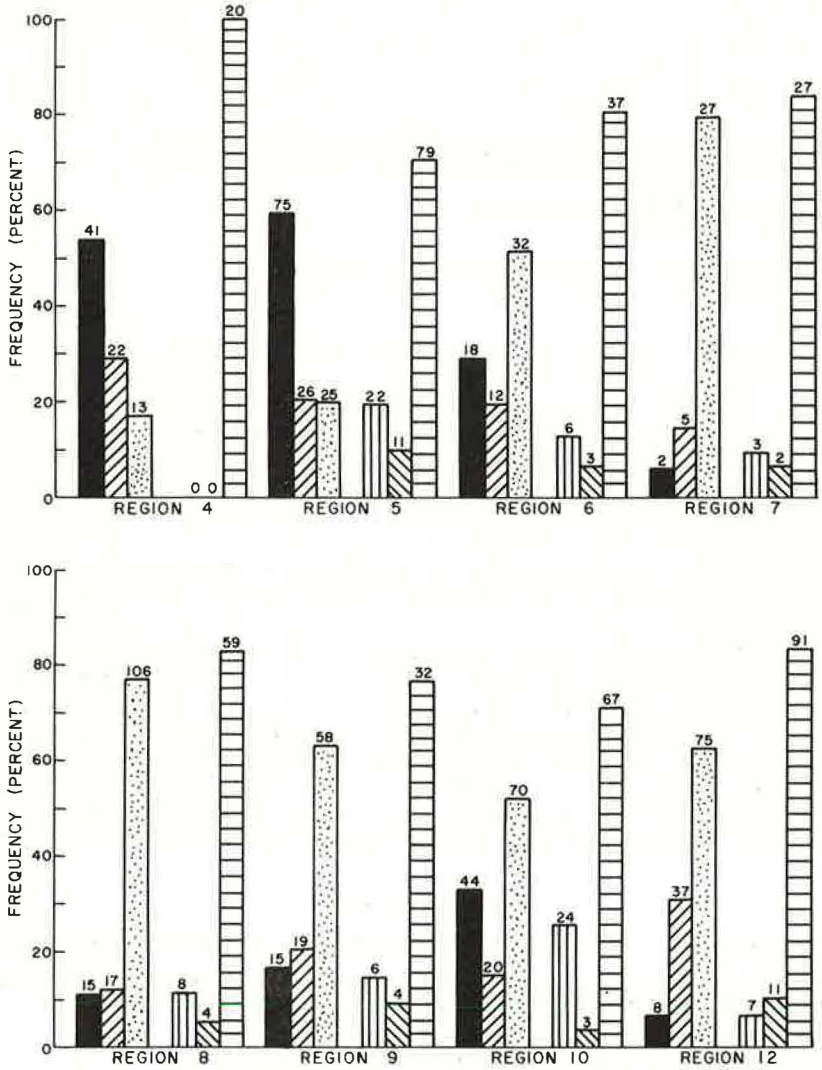

Figure 5. Comparison of bridge approaches by physiographic regions.

imately 20 to 60 ft behind the abutments. The special fill was formed and placed around the abutments, primarily open-column, in accordance with Kentucky Standard Drawing SF-1, which is no longer in use. The performance of bridge approaches associated with the special granular backfill is shown in Figure 4 and is compared with bridge approaches not associated with the special backfill on the same route. The data show that backfilling behind abutments in a manner specified by Kentucky Standard SF-1 did not check the development of faulted approaches. Moreover, for cases involving the special backfill when compared with cases without the special fill, there was an increase in frequency of faulted approaches.

A general relationship between approach settlement and different geological and soil conditions (Fig. 5) seemed apparent in 1964. Approaches passing through areas of soils containing large amounts of granular material did not fault as frequently as approaches passing through areas of soils with large amounts of plastic clays. However, in 1968 the influence of different geological and soil conditions was only slightly noticeable.

Estimated and Observed Settlements of Bridge Approaches

T. C. HOPKINS and G. D. SCOTT, Division of Research,
Kentucky Department of Highways

•AS NOTED in the previous paper, differential settlements between bridge decks and the adjoining highway pavement have been the subject of a number of investigations in recent years. Although evidence suggests that improper placement and compaction of material in the approach embankment produces the bridge approach fault, nothing conclusive has been presented to show that this is the primary source of settlement. Jones (1), Bishop (2), and Deen (3) suggest that differential settlement between bridge deck and approach pavement may be caused in part by volume change of the embankment and in part by consolidation of the embankment foundation.

To determine if the settlement at bridge abutments is primarily a result of volume changes in the embankment and/or foundation and to compare observed and predicted foundation settlements, mercury-filled settlement gages (4) were installed on the original ground of the approach embankment foundation at four selected bridge sites; settlement plates were installed at one other bridge site. By continually obtaining elevations of points located on the pavement, settlement of the pavement (the total settlement of the embankment and foundation) was obtained. Embankment settlement was taken as the difference between pavement settlement and foundation settlement. Undisturbed (Shelby tube) soil samples were collected from the foundation soils at each of the five sites, and consolidation tests were performed on these samples. These data and Terzaghi's theory of consolidation were used to calculate expected foundation settlements.

CASE STUDIES

Field and laboratory settlement investigations were conducted at five sites:

1. Lexington Relief Route, bridge over Parkers Mill Road in Fayette County;
2. I-64, bridge over Slate Creek in Bath County;
3. I-71, bridge over Kentucky River in Carroll County;
4. I-64, bridge over Bull Fork Creek in Rowan County; and
5. I-24, bridge over Eddy Creek in Lyon County.

For each case, a general summary of the physiography and geology is presented along with detailed soil profiles. Data resulting from laboratory settlement analyses are compared with actual measurements made in the field. Finally, the performance to date and the projected future performance are discussed. All sampling and testing were performed in accordance with ASTM standard procedures. Complete test results and detailed descriptions of equipment and procedures are presented elsewhere (5).

Lexington Relief Route, Fayette County

Parkers Mill overpass is located on the Lexington peneplain, a mildly karstic and gently rolling plain containing no prominent knobs or hills in the Inner Bluegrass Region of central Kentucky. This site is situated approximately 2 miles southwest of downtown Lexington.

Paper sponsored by Committee on Embankments and Earth Slopes.

In the vicinity of the crossing, the silty clay embankments are approximately 20 ft in height and the depth of foundation is 12 ft. The foundation soils at the site are residual clays developed mainly from limestones or calcareous shales. Soils in the upper portion of the profile were classified according to the Unified System as CL; those in the lower portion were SC (Fig. 1). Natural moisture contents of these soils varied from 28 to 43 percent. Although these soils are relatively plastic, they are well drained because the joints, cracks, and solution channels of the bedrock allow water to escape rapidly.

A single-point, mercury-filled settlement gage was installed on the centerline of the original ground on the northeast approach foundation, about 50 ft from the end of the bridge. Consolidation test data indicated that ultimate settlement of the approach embankment foundation would be less than 4 in. and that settlement would occur rapidly. The void ratio-log pressure curves showed that the foundation is composed of two clay layers that exhibit different consolidation characteristics; that is, the top 6 ft of this foundation is more compressible than the lower 6 ft. The preconsolidation pressures indicated the two layers to be over consolidated, apparently because of desiccation. Generally, the coefficients of consolidation were relatively high, ranging from approximately 0.5 to 3 sq ft per day.

A comparison of the predicted and observed settlements (Fig. 1) of the northeast approach foundation showed poor agreement. Observed settlement occurred rapidly, but was slower than the predicted rate. Approximately half of the northeast approach embankment was completed between May 5 and May 20, 1966, and the entire embankment was not completed until September 10, 1966. Approximately a month later, the abutments, which were placed on end-bent piles driven to bedrock, were completed. In the latter part of November 1966, the approach pavements were placed. Thus, the approach embankment and its foundation had roughly 8 months to consolidate with approximately half of the embankment completed and 4 months to consolidate under the load of the entire embankment. Recent measurements indicate primary consolidation of the foundation has ceased.

Initial elevations of points located on the northeast approach pavement were obtained December 1, 1966, and a subsequent set of elevations of these points was obtained June 4, 1968 (Fig. 1). These data show that the approach pavement has settled approximately 0.3 to 0.5 in. Examination of the observed time-settlement curve reveals that the foundation settled approximately 0.2 in. after placement of the approaches. At present

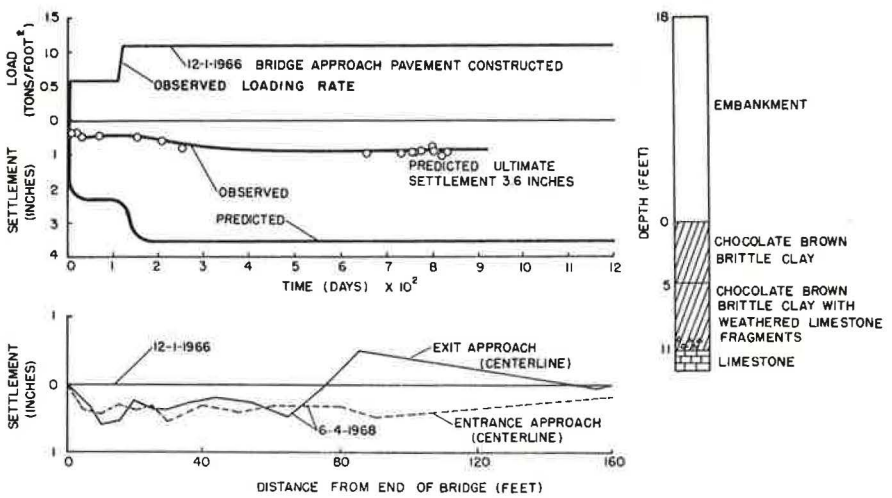

Figure 1. Settlement and loading curves, Parkers Mill overpass.

it appears that the approach settlement at this site is caused by settlement of the foundation and in part by settlement of the embankment.

I-64 Over Slate Creek, Bath County

I-64 crosses Slate Creek over twin bridges in the Knobs Region of Kentucky, approximately 2 miles south of Owingsville. The floodplain on the east side of the river is relatively flat and wide, and original ground elevation is near 705 ft. The east approach embankment is approximately 55 ft high.

The embankment is composed mainly of a greenish shale with some limestone rocks and, to facilitate pile-driving, a clay core. The shale in the embankment appears to be of the Crab Orchard formation (Silurian period). Borings in the east approach foundation apparently penetrated the lower portion of the Maysville limestone at an elevation of 692 ft. The foundation soil (approximately 12 ft thick) is composed of water-deposited, transported soils (recent alluvium of the Pleistocene epoch) composed of slightly sandy, silty clays with a few small pebbles (Fig. 2). Natural moisture contents of the foundation soils are low, ranging from 20 to 25 percent. The soils classify as ML according to the Unified System.

A single-point, mercury-filled settlement gage was installed 42 ft right of centerline and 42 ft from the east end of the bridge. The bridge abutments rest on end-bent piles that were driven through constructed earth cores.

Consolidation data indicated that settlement on the order of 8 in. could be anticipated for the east approach foundation and the rate of consolidation would be fairly rapid. Construction of the embankment began November 23, 1965; however, only a small amount of fill was placed in the first 125 days. Most of the fill was placed during the last 80 days. The predicted rate of settlement was adjusted to the last 80 days in accordance with a procedure recommended by Terzaghi (6), and a linear loading rate was used to approximate the actual loading rate. Unfortunately, only a few observed settlement readings have been obtained at this site because this gage has not always been operative. However, the observed readings shown in Figure 2 indicate that settlement of the approach foundation had ceased before placement of the approach pavements on July 14,

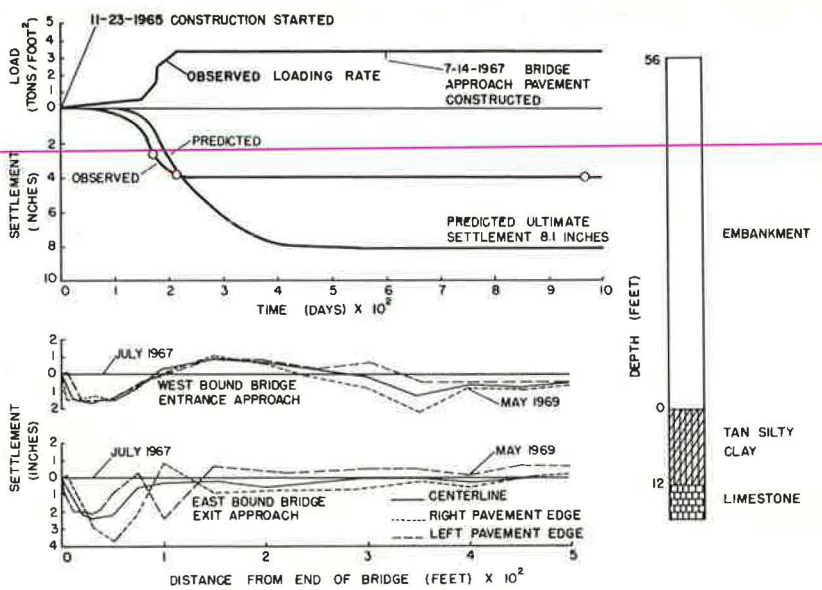

Figure 2. Settlement and loading curves, station 622+97, 42 ft right of centerline, I-64 over Slate Creek, Bath County.

1967, 584 days after embankment construction started. Subsequent elevations obtained May 22, 1969, show that the east approach pavements have settled roughly 1.5 to 3.5 in. The greatest amount of settlement occurred within approximately 100 ft of the end of the bridge. Apparently most of the approach pavement settlement is caused by a volume change of the embankment, primarily the earth cores.

I-71 Over Kentucky River, Carroll County

I-71 crosses the Kentucky River over twin bridges, station 2111+85 to station 2119+85, approximately 3 miles southwest of Carrollton and the junction of the Kentucky River with the Ohio River. This site is located in the Outer Bluegrass Region of northern Kentucky. The elevation of original ground on the southwest side of the broad, flat floodplain is approximately 465 ft. The approach embankment was constructed of clay and ranges in height from 36 to 56 ft at station 2111+50. The thickness of the foundation soil at this station varies from about 80 to 100 ft (Figs. 3 and 4). The embankment and foundation are uniform in thickness and depth from the end of the bridge, station 2111+85, to station 2101+85.

The approach foundation material is composed of recent alluvial deposits of clay, sandy clay, loose and very fine sand, and some silt. Unified classifications of these soils are CL, ML-CL, SP, and SM respectively. Natural moisture contents varied from 19 to 31 percent.

Two single-point, mercury-filled settlement gages were installed at station 2111+50, one 42 ft left and the other 65 ft right of centerline. Settlement estimates of approximately 2 ft were based on consolidation tests performed on undisturbed soil samples and detailed information on the foundation conditions.

Time-settlement curves for station 2111+50, 42 ft left and 65 ft right of centerline, are shown in Figures 3 and 4 respectively. The settlement curve in Figure 3 shows that primary compression of the foundation soil has been completed. In Figure 3 it can be seen that the observed rate of settlement proceeded faster than the predicted rate, while in Figure 4 the predicted and observed settlement rates agree rather well. For both cases the predicted and observed ultimate settlements are in good agreement.

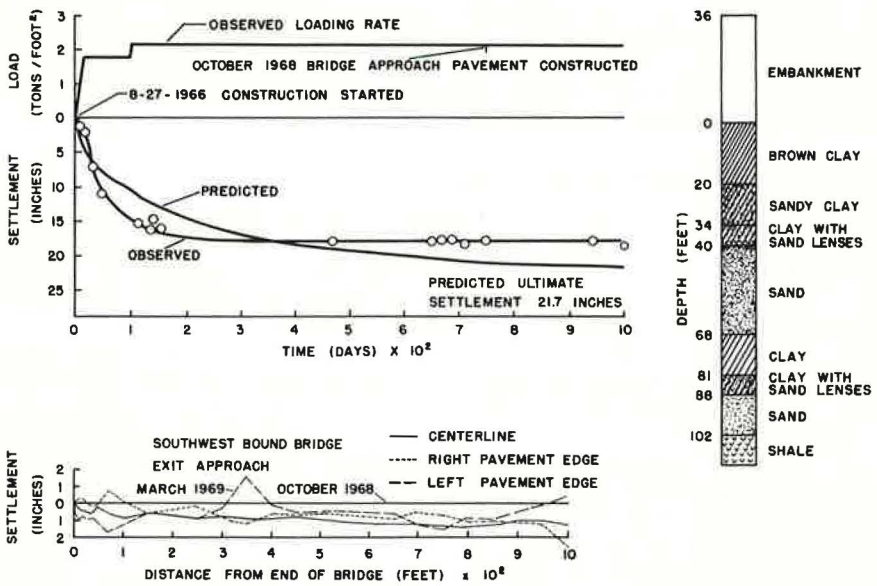

Figure 3. Settlement and loading curves, station 2111+50, 42 ft left of centerline, I-71 over Kentucky River, Carroll County.

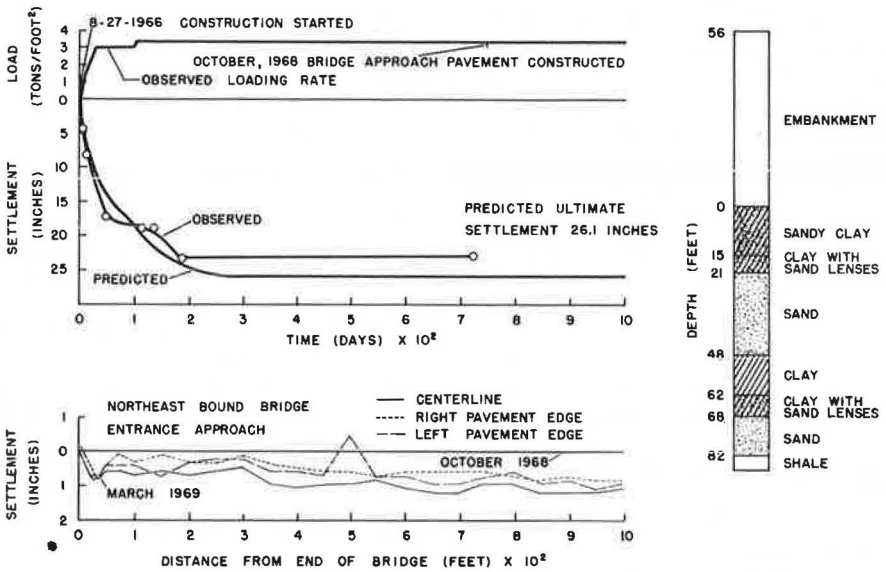

Figure 4. Settlement and loading curves, station 2111+50, 65 ft right of centerline, I-71 over Kentucky River, Carroll County.

Construction of the southwest embankment began August 26, 1966, and was completed October 15, 1966. Approximately a month later, excavation for pile-end-bent abutments was completed and a month later the abutments were constructed. The bridge approach pavements were constructed in October 1968, and pavement elevations were obtained at that time. Hence, there had been a time lapse of approximately 2 years between the time the embankment was completed and the time the approach pavements were constructed. Apparently, this was sufficient time for consolidation of the foundation to cease. However, pavement elevations obtained in March 1969 show that the approach pavements have settled on the order of 0.8 to 1.8 in. (Figs. 3 and 4). This pavement settlement extends back about 1,000 ft from the end of the bridge and appears to be a result of volume change of the embankment.

I-64 Over Bull Fork Creek, Rowan County

I-64 crosses Bull Fork Creek on twin bridges, station 2396+56 to station 2400+82, in the Knobs Region of northeastern Kentucky. In the vicinity of the crossing, the east approach embankment is on the order of 65 ft high; the west approach is approximately 75 ft high. The floodplain on the west side of the bridge is relatively flat, whereas the east floodplain rises at an approximate grade of 4 percent.

The Bull Fork basin is filled with water-lain, transported soils (recent alluvium) consisting of black shale and yellow sandstone gravels and sand intermingled with silts and clays. These are generally classified as SW, SM, and GW according to the Unified System. Natural moisture contents ranged from 18 to 55 percent. The three borings on the west approach foundation and the two borings on the east foundation penetrated black shale approximately 18 ft below ground elevation. The approach embankments, with the exception of the clay cores, were constructed of a greenish shale and sandstone obtained from the Waverly formation.

Instrumentation included three double-tubed, porous-tube piezometers in the west approach foundation and a single-point, mercury-filled settlement gage located at ground elevation. A single-tube, porous-tube piezometer was installed in the east approach foundation, and a multiple-point (three points), mercury-filled settlement gage was

located at ground elevation. Pore pressures were observed as the water level in vertical extensions of the piezometer tubing.

Consolidation test data indicated that ultimate settlements on the order of 1 ft or slightly greater could be expected and that the settlement of the basin material would proceed rather rapidly. Predicted and observed ultimate settlements are in fair agreement, but the observed rate of settlement proceeded faster than predicted for the west approach foundation (Fig. 5). Recent readings indicate that consolidation of this embankment foundation has ceased.

A typical settlement curve for the east approach foundation is shown in Figure 6 (unit 1 of the multiple-point, mercury-filled settlement gage). Predicted and observed ultimate settlements as well as rate of settlements are generally in fair agreement. Apparently, consolidation of this foundation is essentially complete. Pore pressure measurement data are commensurable with the observed settlement readings; that is, they showed almost instantaneous dissipation, just as the settlement was almost instantaneous.

The approach pavements at this site were placed in August 1968. Construction of the west embankment began January 6, 1967, and was completed July 20, 1967. Approximately 2 months later, pile-end-bent abutments were completed. Thus, this embankment and its foundation had approximately 1½ years to consolidate before the placement of the approach pavements. Construction of the east embankment began August 2, 1967, and was completed October 5, 1967. The pile-end-bent abutments were completed in November. This embankment and its foundation had approximately a year to consolidate before placement of the approach pavements. Judging from observed settlement data and pore pressure measurements of the approach foundations, an approach fault should not develop at any of the approach pavements as a result of consolidation of the foundation. Pavement elevations obtained in May 1969 show that the west approach pavements have settled from 0.2 to 0.5 in. within 75 ft of the end of the bridge. The east

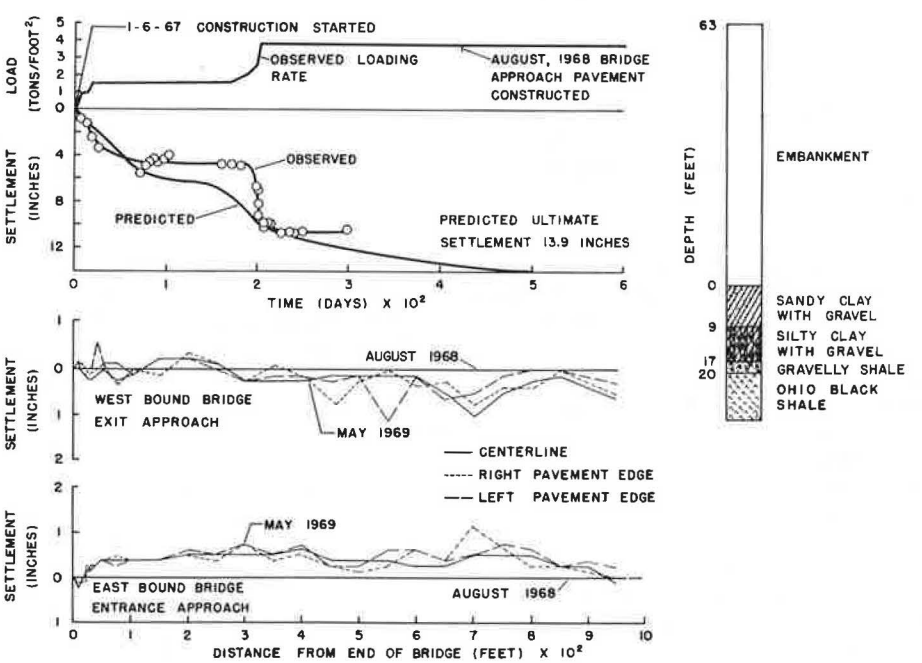

Figure 5. Settlement and loading curves, station 2396+00, centerline, I-64 over Bull Fork Creek, Rowan County.

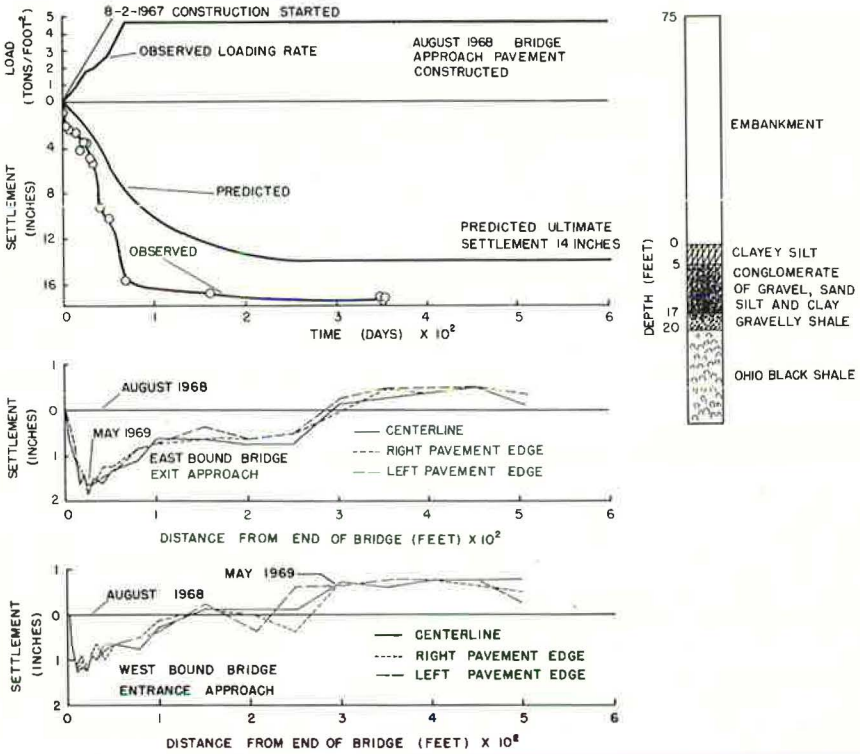

Figure 6. Settlement and loading curves, point 1, station 2401+25, 66 ft right of centerline, I-64 over Bull Fork Creek, Rowan County.

approach pavements have settled from 0.4 to 1.8 in., the settlement occurring within approximately 250 ft of the end of the bridge. Hence, most of the approach settlement at this site is apparently caused by a volume change of the embankment, mainly the earth (clay) cores.

I-24 Over Eddy Creek, Lyon County

I-24 crosses the Eddy Creek basin in western Kentucky approximately 6 miles southeast of Eddyville and 4 miles east of Barkley Lake. Physiographically, the dominant feature of the area surrounding the site is Barkley Lake, which was formed within the last decade by damming the Cumberland River near Gilbertsville. Eddy Creek is situated in the Western Pennyroyal, a division of the Mississippian Plateau, and it is a prominent tributary of Barkley Lake. The area called "land between the lakes," positioned to the west of the site and Barkley Lake, constitutes a transition in geology between Cretaceous and Tertiary sediments of the Jackson Purchase Region and outcrops of Mississippian limestone of the Western Pennyroyal Region. The mildly rolling karst topography of the area lying close to the site is dotted with limestone sinkholes and contains small local relief. The landscape reflects intense faulting. In 1965 the basin was inundated by impounded waters of Barkley Lake.

In the immediate vicinity of the I-24 crossing, the basin is about 1,400 ft wide. The depth of water in the basin measured 8 ft at normal pool elevation of 359 ft. The material of the basin is composed of recent alluvial deposits ranging in thickness from 20 to 40 ft. Most of these materials are generally classified according to the Unified System as OL and CL.

Shelby tube and split-spoon samples were obtained from five drill holes. Sampling was performed with a mobile drill rig mounted on a barge. An inspection of these samples revealed that the upper 40 ft of the foundation soil was composed of wet to saturated, soft, slightly organic silts and clays with some sand, apparently in lenses. Because of the limited number of borings, the horizontal extent of the sand lenses could not be determined. The silts and clays were underlain by what appeared to be a gravel hardpan having standard penetration values in excess of 100. Natural moisture contents of the foundation material ranged between 17 and 63 percent.

From older to younger, the geological formations near the site are the St. Louis and Ste. Genevieve limestones (Meramec series) of the Mississippian system and loess (Pleistocene series) and alluvium of the Quaternary system. The five borings apparently penetrated the lower member of the St. Louis limestone.

Unconfined compression tests, consolidated-undrained triaxial tests with pore pressure measurements, and one-dimensional consolidation tests were performed on specimens trimmed from Shelby tube samples. Stability analyses were made for various conditions of loading and foundation consolidation. It was concluded that the embankment could be constructed at a normal rate without sand drains with little risk of failure.

The calculated average ultimate settlement was on the order of 16 in. The time required for the embankment to set prior to constructing a permanent pavement, in order to keep settlement at the bridge approaches within a tolerable range, was about 4 months and 20 months, with and without sand drains respectively. Therefore, the consolidation analysis indicated that, without sand drains, an objectionable amount of settlement would occur if a permanent pavement were constructed sooner than about 1.5 years after construction of the embankment.

Based on the results of the stability and consolidation analyses, the following construction procedures were adopted for the construction of 35-ft high embankments across the lake area:

1. The embankment and berms were constructed without sand drains and piezometers were installed along the centerline at about 200-ft spacings.
2. No pavement was to be constructed before the foundation consolidation was at least 75 percent completed as indicated by settlement platforms and gages along the centerline at 200-ft spacings.
3. Early construction of the project was specified in order to increase the consolidation period prior to paving.
4. The contractor was prepared, if necessary, to use a controlled loading rate.

In the latter part of April 1967, six settlement platforms were installed by the contractor at the following locations:

1. Station 3683+50 on centerline;
2. Station 3688+00, 72 ft left of centerline;
3. Station 3688+00, 72 ft right of centerline;
4. Station 3688+00 on centerline;
5. Station 3691+00 on centerline; and
6. Station 3692+00 on centerline.

These platforms consisted of a 3-ft square steel base and screwed extensions of 2.5-in. diameter steel pipe that were approximately 5 ft in length.

Construction of the approach embankments across the lake area began in the early part of May 1968. The first stage of construction involved building the rock fill that formed the outer perimeter of the berms. The rock fill was located approximately 170 ft right and left of centerline. Approximately 56,977 tons of limestone was trucked to the project for this purpose. The second stage of construction consisted of placing 131,731 cu yd of a mixture of sand and gravel fill inside the rock embankment to an elevation of 364 ft. Approximately 54,847 cu yd of the granular fill (sand) was delivered to the site by barges. The remainder of the granular material was composed of a blend of locally available bank gravel and sand with a clay content of less than 10 percent. Early in October 1968, the top portion of the south approach embankment was completed, but the north approach embankment was not completed until late December 1968.

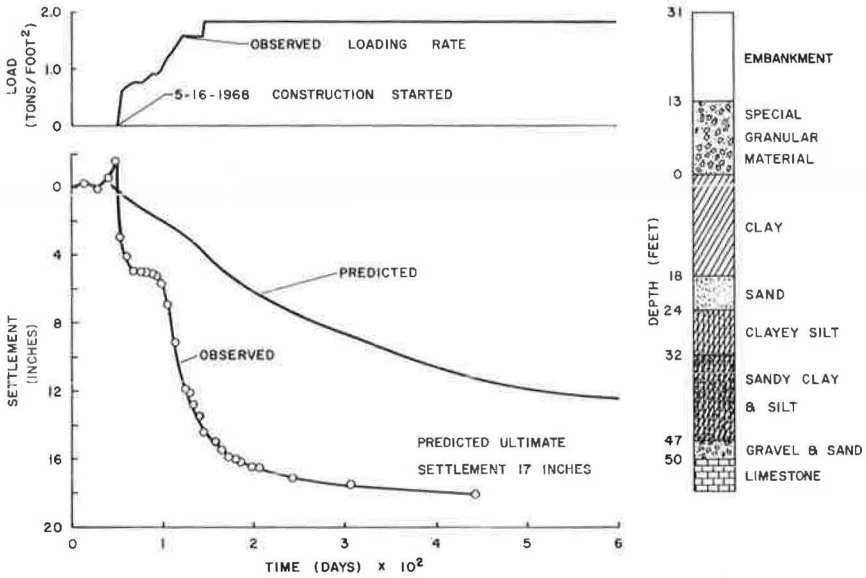

Figure 7. Settlement and loading curves, station 3688+00, I-24 over Eddy Creek, Lyon County.

Typical settlement curves, representing about 430 days of settlement observations, are shown in Figures 7 and 8 for the south approach foundation. The latest settlement measurements have ranged from 7 in. at station 3683+50 to 18 in. at stations 3691+00 and 3692+00. At station 3688+00, observed settlements have ranged from 12 in. at centerline to 17 in. at a point 72 ft left of centerline. The ultimate predicted settlements for stations 3683+50 and 3688+00 were 13 and 17 in. respectively. For stations

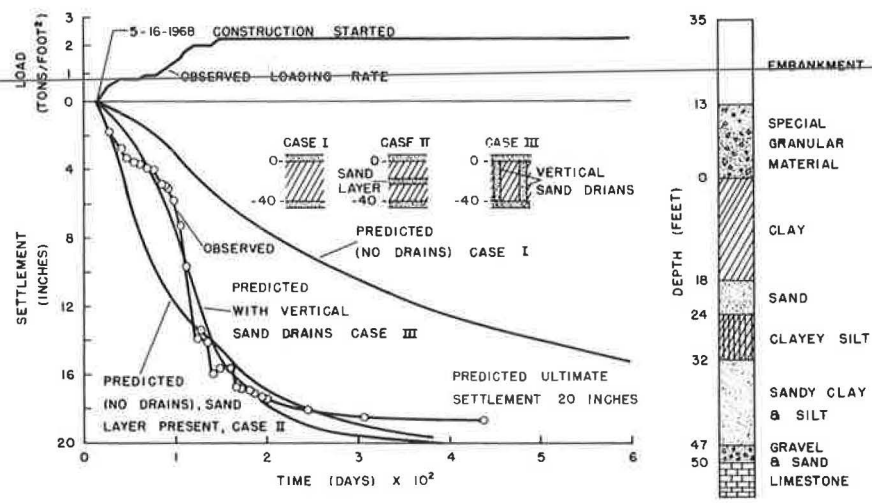

Figure 8. Settlement and loading curves, station 3692+00, I-24 over Eddy Creek, Lyon County.

3691+00 and 3692+00, the ultimate settlement was predicted to be 20 in. Thus, there is good agreement between observed and predicted ultimate settlements.

The observed rate of settlement of the foundation proceeded faster than predicted. Rapid pore pressure dissipation is generally confirmed by pore pressure measurements obtained from piezometers. These readings show that the water level in the piezometer tubes never rose above the elevation of the berm, 364 ft, whereas the critical elevation was 380 ft, which corresponded to a factor of safety against failure of 1.35. The settlement data indicate that primary consolidation of the foundation is nearly complete.

Apparently, the sand lenses encountered during the drilling operation were of a greater horizontal extent than assumed in the consolidation analysis. In the analysis, the sand lenses were ignored and assumed to have no influence on the rate of settlement. However, if it is assumed that a sand layer was sandwiched between two clay layers (case II, Fig. 8), then there is good agreement between the observed and predicted rates of settlement. The influence of vertical sand drains is also shown (case III, Fig. 8).

Based on field and laboratory observations to date, failure of the embankment and foundation at this site is unlikely, and future foundation settlements will probably not exceed 3 in. Most of the future foundation settlement will be in the form of secondary consolidation, which proceeds slowly. However, the foundation will probably be stabilized by the time of paving.

CONCLUSIONS

The following conclusions are substantiated by findings from field and laboratory investigations reported herein:

1. The analysis procedures employed in this study are quite adequate for predicting embankment foundation settlements. Data generally show that there was only fair agreement between predicted and observed rates of settlement, predicted rates generally exceeding observed rates by as much as 100 percent. However, there was generally good agreement between predicted and observed ultimate settlements, with predicted settlements usually exceeding observed settlements by about 10 percent. The above discrepancies originate from the fact that (a) perfectly undistrubed soil specimens cannot be obtained in any practical manner, (b) Terzaghi's theory of consolidation is not totally applicable to the partially saturated soils that usually make up a portion of embankment foundations, and (c) the field drainage boundary conditions do not fit the assumptions of the theory or are too complex to determine accurately.
2. Settlement of the approach foundation can contribute significantly to settlement of bridge approaches; the amount contributed is highly dependent on the time at which the approach pavement is constructed. Both field and laboratory data show that time-settlement characteristics of foundation soils vary greatly. The estimated time for consolidation to cease ranged from a few days to approximately 3 years; this was generally confirmed by field observations. Measurements made to date at three sites show that sufficient time existed for the completion of foundation consolidation before placement of the approach pavements.
3. Settlement of the embankment can contribute significantly to settlement of the approach pavements. Data obtained at four sites strongly indicate that, where embankments are composed in part or entirely of compressible materials, consolidation of the embankment can contribute to approach settlement; pavement profiles show that embankments to consolidate even when compacted according to specifications. This strongly emphasizes the need for studying the consolidation characteristics of embankment materials.
4. The results of settlement investigations performed at the sites of proposed bridge construction projects can provide a much-needed basis for design to control or minimize the effect of approach settlement. For cases where the calculated ultimate settlement is large or the rate of settlement is slow, relatively elaborate countermeasures are warranted. The embankment could be constructed early and allowed to consolidate if time permits, or a temporary pavement could be constructed and periodically maintained until the embankment and foundation are stabilized, at which time a permanent pavement could be constructed. Alternatively, some means of bridging, such as extending the

structure and/or providing heavily reinforced concrete approach slabs, could be used. For cases where the calculated ultimate settlement is small or the rate of settlement is very fast, such elaborate precautions would not be warranted. Estimates of embankment consolidation based on consolidation tests performed on compacted specimens should be included in the settlement calculations. Other indeterminate factors such as the effect of creep or internal erosion (7) preclude the exact calculation of total settlement. Nevertheless, in many cases consolidation is the major cause of settlement and its control would constitute a significant partial solution of the bridge approach settlement problem.

REFERENCES

1. Jones, C. W. Smoother Bridge Approaches. Civil Engineering, June 1959.
2. Bishop, G. F. Design of Bridge Approach Slabs. Proc. Kentucky Highway Conference, Engineering Experiment Station Bull. 78, Jan. 1966.
3. Deen, R. C. Camber Design Study for Concrete Pipe Culvert. Highway Research Record 116, 1966, pp. 20-35.
4. Hopkins, T. C., and Deen, R. C. Mercury-Filled Settlement Gage. Division of Research, Kentucky Dept. of Highways, 1969.
5. Hopkins, T. C. Settlement of Highway Bridge Approaches and Embankment Foundations. Division of Research, Kentucky Dept. of Highways, Feb. 1969.
6. Terzaghi, K., and Peck, R. B. Soil Mechanics in Engineering Practice. John Wiley and Sons, New York, 1964.
7. Hopkins, T. C., and Deen, R. C. The Bump at the End of the Bridge. Division of Research, Kentucky Dept. of Highways, June 1969. Abridgment included in this Record.

Practical Aspects of Cantilever Retaining Wall Design

JOHN W. STILES, Bureau of Public Roads, Federal Highway Administration, U. S. Department of Transportation

The Bureau of Public Roads publication, "Typical Plans for Retaining Walls" (1), contains a new and simple approach to the relationships between footing dimensions and bearing pressures. A series of graphs show how changes in toe and heel length affect the bearing pressures. These graphs, their construction, and their use are discussed. The graphs, when used in conjunction with the wall dimensions in the typical plans, give the designer a "feel" of how bearing pressure varies with changes in footing width without his becoming involved in computations. Several loading cases are given and the problems associated with each are discussed.

•THE PROCEDURE used in developing the Bureau of Public Roads "Typical Plans for Retaining Walls" (1) is described in this paper. Copies of these "typical plans" may be obtained from the Superintendent of Documents, U. S. Government Printing Office.

The BPR typical plans present retaining wall dimensions for wall heights from 6 to 30 ft. The first type of retaining wall shown is the cantilever retaining wall on a spread footing. Also shown are pile-supported cantilever walls and counterfort walls. For our discussion we will refer only to the cantilever retaining walls on spread footings. Four loading conditions are shown: case I, level backfill, no surcharge; case II, level backfill with a 2-ft live load surcharge; case III, backfill on a 2:1 slope, and case IV, backfill on a 1½:1 slope. For the various design dimensions presented, the maximum bearing pressure is also indicated, as shown in Figure 1. (Note that Figure 1 is not the complete sheet from the typical plans but is only that portion pertaining to this paper. Bar lists, reinforcement layout, and other details have been deleted for clarity.) Because the bearing pressure for a given situation may be intolerable, graphs were included in the BPR plans. These graphs allow the designer a greater "feel" of how the bearing pressures will vary with changes in the width of the retaining wall footing. It is our purpose to explain how to use these graphs, as well as to describe how they were constructed. Appexdix C to this paper includes the notations used.

The graphs, as shown, should only be used in conjunction with the dimensions given in the BPR plans. Any change in the dimensions given, especially in the placement of the stem on the footing, will give erroneous answers. To illustrate the use of the graphs, assume that we have a 30-ft cantilever retaining wall supporting a horizontal backfill. At the site, the maximum allowable bearing pressure is 4 kips per sq ft. In Figure 1 we see that, for the dimensions shown, the maximum bearing pressure is 4.65 kips per sq ft. Because this exceeds the allowable bearing pressure, we must change the footing dimensions so that the allowable pressure is not exceeded. Entering the graph with a bearing pressure of 4 kips per sq ft and proceeding upward until we reach the H = 30 ft curve, then going horizontally, we see that an increase in toe length of 11 in. will satisfy the requirements. Adding this to the footing width in the table of wall dimensions, we obtain a new footing width of 17 ft 9 in. If the bearing pressure at the heel is needed, it can be obtained by proceeding downward from the point where the

Paper sponsored by Committee on Substructures, Retaining Walls and Foundations.

WALL DIMENSIONS			
H	B	T	D
6	2'-10"	0'-9"	1'-3"
7	3-6	1-0	1-3
8	4-0	1-0	1-3
9	4-9	1-3	1-3
10	5-3	1-3	1-3
11	5-11	1-6	1-6
12	6-5	1-6	1-6
13	7-1	1-9	1-6
14	7-7	1-9	1-6
15	8-4	2-0	1-6
16	8-10	2-0	1-6
17	9-7	2-3	1-6
18	10-1	2-3	1-6
19	10-8	2-6	1-9
20	11-2	2-6	1-9
21	11-10	2-9	2-0
22	12-3	2-9	2-0
23	12-10	2-9	2-0
24	13-5	3-0	2-3
25	13-11	3-0	2-3
26	14-6	3-3	2-6
27	15-1	3-3	2-6
28	15-9	3-6	2-9
29	16-3	3-6	2-9
30	16-10	3-9	3-0

QUANTITIES PER LIN. FT. OF WALL		MAXIMUM BEARING PRESSURE	H
Concrete	Reinforcing Steel		
Cu. Yd	** Lb.	Kips/Sq. Ft.	
0.325	16.6	1.09	6
0.401	19.3	1.13	7
0.470	22.0	1.37	8
0.553	24.7	1.39	9
0.626	29.9	1.63	10
0.750	32.2	1.70	11
0.830	38.2	1.93	12
0.922	48.5	1.98	13
1.005	56.0	2.21	14
1.104	64.2	2.24	15
1.190	79.5	2.47	16
1.292	94.3	2.50	17
1.381	112.7	2.73	18
1.560	132.8	2.85	19
1.657	146.3	3.05	20
1.998	144.9	3.15	21
2.111	166.7	3.40	22
2.239	191.1	3.62	23
2.471	214.7	3.71	24
2.601	223.8	3.95	25
2.852	248.2	4.03	26
2.999	274.7	4.26	27
3.277	308.2	4.34	28
3.425	338.8	4.56	29
3.714	372.7	4.65	30

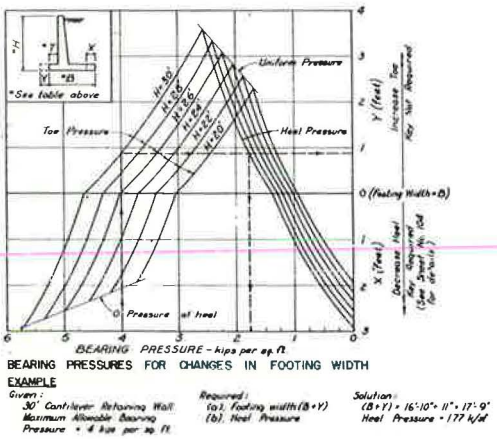

Figure 1. Typical plans for retaining walls.

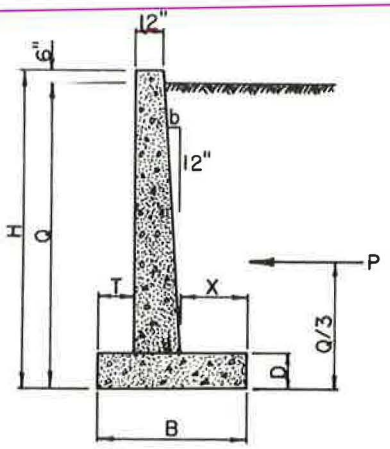

Figure 2. Cross section of case I wall.

horizontal line crosses the curve for heel pressure; in this case the pressure is 1.77 kips per sq ft. From this information, the steel requirement for the footing can be modified to meet actual conditions.

SOIL ASSUMPTIONS

The Rankine method was used in determining the soil force acting on the walls. In all cases a well-graded, free-draining backfill material is specified in the plans. This is important because a plastic material could increase the soil force up to 300 percent of the assumed value. Also necessary are weep holes or another method of draining the backfill. The backfill material was assumed to have an angle of internal friction equal to 33 deg 41 min, and a unit weight of 120 lb per cu ft.

Using these assumptions, the value of Rankine's constant, ϵ, was determined. The respective values of the soil force, P, were thus determined. In the cases of an inclined backfill, both the horizontal and vertical components of the soil force were used in the analysis. The soil in front of and covering the toe of the wall was neglected because in some cases it would be nonexistent. This would, in most cases, give an added factor of safety against sliding. If the foundation is a substantial distance below the ground surface, this wedge of soil should be considered.

DEVELOPMENT OF CASE I CURVES

In developing the curves in the typical plans, a series of relationships were derived from the wall geometry and loading conditions. A cross-sectional view of a case I wall and loading is shown in Figure 2.

The generalized equations were derived in terms of known dimensions H and Q, the soil force, P, and the assigned dimensions D, T, and b. By summing moments of the weight of the areas about the toe of the footing (Fig. 3), we obtain the relationships given in Table 1.

When all of the weights are summed, the expression will take the form of $\Sigma W = YB - M$, where Y and M will be constants for this particular wall. After multiplying the weights by the appropriate moment arm, a′, and summing, we obtain an expression in the form of $\Sigma Wa' = NB^2 - R$. It is noted that, between the weight summation and the moment summation, all terms

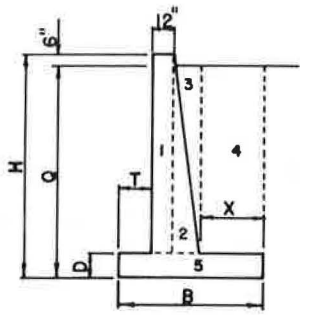

Figure 3. Case I weights and moment arms.

TABLE 1
CASE I WEIGHTS AND MOMENT ARMS

Area No.	Weight	Arm
1	0.15(H - D)	T + 0.5
2	0.00625(H - D)²b	$T + 1 + \left(\frac{H - D}{36}\right)b$
3	0.12(Q - D)X	$B - \frac{X}{2}$
4	0.005(Q - D)²b	$T + 1 + \frac{0.5b}{12} + \left(\frac{Q - D}{18}\right)b$
5	0.15BD	0.5B

containing B are multiplied by B/2; therefore, Y = 2N. This will be necessary in simplifying the general equation in the derivation.

By summing forces and moments, $\Sigma W/A \pm Mc/I$, about the center of the footing, we obtain

$$\frac{\Sigma W}{B} \pm \frac{6\,\Sigma W\,(a - B/2)}{B^2} \pm \frac{2PQ}{B^2} = 0$$

where a is the distance from the toe of the footing to the centroid of the total mass, $M = \Sigma Wa$, $c = B/2$, and $I = B^3/12$.

For the condition of zero heel pressure,

$$F_h = \frac{\Sigma W}{B} + \frac{6\,\Sigma W\,(a - B/2)}{B^2} - \frac{2PQ}{B^2} = 0$$

Because ΣW is in the form of $YB - M$ and $\Sigma Wa'$ is in the form of $NB^2 - R$, we obtain

$$F_h = YB^2 - MB + 6NB^2 - 6R - 3YB^2 + 3MB - 2PQ = 0$$

Substituting $Y = 2N$ and solving for a B that will give a heel pressure of zero, we obtain

$$B = \sqrt{\frac{2PQ}{Y} + \frac{6R}{Y} + \left(\frac{M}{Y}\right)^2} - \frac{M}{Y}$$

By going back to the general equation for any pressure under the footing and applying the correct signs, we obtain a toe pressure equal to

$$F_t = \frac{4\,\Sigma W}{B} - \frac{6\,\Sigma Wa'}{B^2} + \frac{2PQ}{B^2}$$

Because the footing width, B, found here is for a heel pressure of zero, let us now see what happens when the heel is increased by a distance, S, added to the heel. The additional weight of concrete and soil to be considered is equal to $K = 0.15SD + 0.12(Q - D)S$, where the unit weight of soil = 120 pcf, and $K = 0.12Q + 0.03D$ for each 1-ft increment added. Referring to Figure 2 and again summing moments about the midpoint of the new footing width, we obtain

$$F_t = \frac{4\,(\Sigma W + KS)}{(B + S)} - \frac{6\,\Sigma Wa' + 6KSB + 3KS^2 - 2PQ}{(B + S)^2}$$

$$F_h = -\frac{2(\Sigma W + KS)}{(B+S)} + \frac{6\Sigma Wa' + 6KSB + 3KS^2 - 2PQ}{(B+S)^2}$$

The B found above, for $F_h = 0$, is less than the width required to prevent sliding. Because an increase in the heel length will affect the sliding characteristics more than an increase in the toe length, the heel should be increased up to the point where sliding is impending.

By using a coefficient of friction against sliding of concrete on undisturbed soil of 0.45, we obtain the expression $P = 0.45\,\Sigma W$ for the impending of sliding. By applying a factor of safety of 1.5 against sliding, we obtain a $P \leq 0.30\,\Sigma W$. Any B that gives a value of ΣW less than 3.33P will have to have a key to prevent sliding. For the case I walls shown in the typical plans, the value of B given is one that will give $\Sigma W \approx 3.33P$; no key is required.

Consideration should now be given to the pressure under the toe. Any increase in the toe length will reduce this pressure more substantially than a further increase in the heel length. For these reasons let us now see what effect an increase in the toe length will have on the soil pressures.

Summing moments about the midpoint of the footing width at which sliding is impending, plus any increase in the toe length, we obtain

$$F_t = \frac{4(\Sigma W + 0.15SD)}{(B+S)} - \frac{6\Sigma W(a+S) + 0.45S^2D - 2PQ}{(B+S)^2}$$

$$F_h = -\frac{2(\Sigma W + 0.15SD)}{(B+S)} + \frac{6\Sigma W(a+S) + 0.45S^2D - 2PQ}{(B+S)^2}$$

By setting the limit of toe pressure equal to heel pressure, with the increases in toe length we obtain a maximum

$$S = \frac{B\Sigma W - 2\Sigma Wa' + 0.67PQ}{\Sigma W - 0.15BD}$$

SAMPLE CASE I SOLUTION

A sample problem is solved in Figure 4. The solution is as follows:

1. Determine the dimensions H and Q. Assume a footing thickness D (approximately 1/10 H, 1 ft 3 in. minimum), and distance T (approximately 6 in. + H/10).
2. Solve the footing width at $F_h = 0$. In this example B = 9 ft 2 in.
3. Increase the heel length up to the footing width at which sliding is impending (B in the plans) and solve for the corresponding bearing pressures. The width at which sliding is impending is equal to 11 ft 2 in.
4. Using the footing width at which sliding is impending, 11 ft 2 in., increase the toe length up to the point at which the bearing pressure is uniform.
5. Plot the bearing pressures versus footing width for the various increments of increases in footing width, thus obtaining the curves shown in Figure 5.

A sample worksheet is shown in Appendix A for each of the other three cases.

DEVELOPMENT OF CASES II, III, AND IV CURVES

The case of the horizontal backfill is by far the simplest loading on a retaining wall. As surcharges of different shapes and magnitudes are added, the soil force becomes more complicated. If a uniform surcharge is assumed, as in case II, the soil force is increased by an amount $P_1 = \gamma h_s Q \epsilon$. This force, as shown in Figure 6, is applied at half the height of the wall. By considering this loading condition and reducing it to an equivalent loading system applied at one-third the height, we can use the case I equations by substituting $P' = P + P_1$.

CASE I

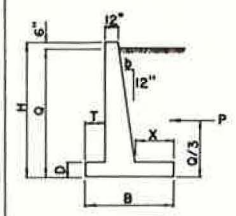

H = 20'
D = 1.75'
T = 2.5'
Q = 19.5'
P = E.F.P. $\frac{Q^2}{2}$ = 6.6544 k
X = B − T − 1 − b($\frac{H-D}{12}$) = B−4.2604

Equivalent Fluid Pressure = 0.035 ksf

Batter
b = $\frac{3}{4}$" for (H−D) > 20'
b = $\frac{1}{2}$" for (H−D) ≤ 20'

If P < 0.3(ΣW) = 6.6539 for B=11'-2"
F.S. against sliding > 1.5

If P < $\frac{1.5\Sigma Wa'}{Q}$ = 7.4191 for B=9'-2"
F.S. against overturning > 2.0

W	o'	Wa'
.15(H−D) = 2.7375	T+0.5 = 3.0	8.2125
.00625(H−D)²b = 1.0408	T+1+($\frac{H-D}{36}$)b = 3.7535	3.9066
.12(Q−D)X = 2.138−9.075	B−$\frac{X}{2}$ = 0.5B+2.1302	1.065B²−19.331
.005(Q−D)²b = 0.7877	T+1+$\frac{5b}{12}$+($\frac{Q-D}{18}$)b = 4.0139	3.1617
.15BD = 0.2625 B	.5B = 0.5B	0.1312 B²
ΣW = YB−M = 2.39B−4.5087		ΣWa' = NB²−R = 1.196B²−4.0501

U = $\frac{(\Sigma W + YS)}{(B+S)}$

V = $\frac{(6\Sigma Wa' + 6YSB - 2PQ + 3YS^2)}{(B+S)^2}$

A = $\frac{(\Sigma W + 0.15SD)}{(B+S)}$

C = $\frac{(6\Sigma W(o+S) + 0.45DS^2 - 2PQ)}{(B+S)^2}$

B = $\sqrt{\frac{2PQ}{Y} + \frac{6R}{Y} + (\frac{M}{Y})^2} - \frac{M}{Y}$ = $\sqrt{108.473 + 10.157 + 3.551} - 1.8845$ = 9.169 ft.
Use B = 9'-2"

$F_1 = \frac{4\Sigma W}{B} - \frac{6\Sigma Wa'}{B^2} + \frac{2PQ}{B^2}$ = 7.6203 − 6.8935 + 3.0331 = 3.7599 kips/ft²

Effect on soil pressure when B is increased by increment S

to heel

$F_1 = 4U - V$
$F_h = V - 2U$
B = 9'-2"

S	U	V	F_1	F_h
0			3.76	0
1	1.9465	4.4290	3.36	0.54
1.99	1.9859	4.8938	3.05	0.92

to toe

$F_1 = 4A - C$
$F_h = C - 2A$
B = 11'-2"

S	A	C	F_1	F_h
1	1.846	5.034	2.350	1.34
2	1.726	5.079	1.82	1.63
2.296	1.694	5.080	1.70	1.70

Figure 4. Sample solution for minimum width footing for case I retaining wall.

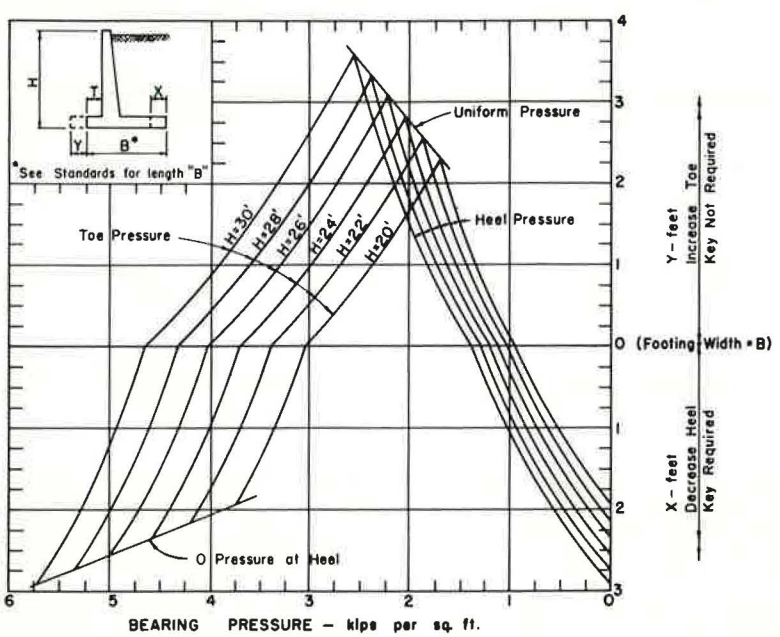

Figure 5. Bearing pressures for changes in footing width for case I retaining wall.

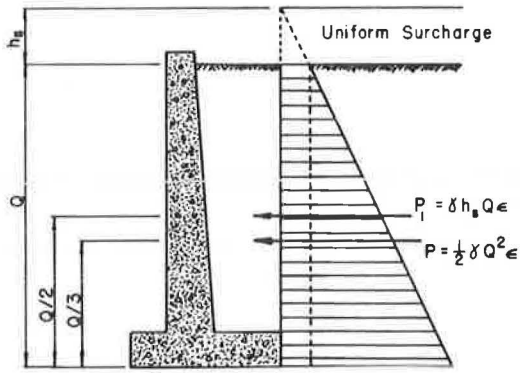

Figure 6. Cross section of case II loading.

In the first two cases considered, a relatively simple relationship for the minimum base width can be obtained. For the case of a sloping backfill, the solution is not so simple. The basic equations for the sloping backfill must consider the sloped soil force. Both the horizontal and vertical components of this force were considered in our analysis. Even though some design offices do not consider the vertical force, we felt that a more realistic condition of loading was obtained when this force was considered.

The basic P/A ± Mc/I equations, for this condition, were derived and, after seeing that the solution would be complicated, a minimum base width was not solved for. Instead, a value for the base width was assumed and the values for heel and toe pressure were computed. The equation for the bearing pressures, for any backslope, are

$$F_t = \frac{P \sin\theta + \Sigma W}{B} - \frac{6\Sigma W(a - B/2)}{B^2} - \frac{3P \sin\theta}{B} + \frac{2P \cos\theta h}{B^2}$$

$$F_h = \frac{P \sin\theta - \Sigma W}{B} + \frac{6\Sigma W(a - B/2)}{B^2} + \frac{3P \sin\theta}{B} - \frac{2P \cos\theta h}{B^2}$$

For an increase, S, in the length of the toe, with a 2:1 slope, the bearing pressures are

$$F_t = \frac{4\Sigma W + 0.15DS - 0.8944P}{(B + S)} + \frac{1.7888Ph - 6\Sigma Wa' - 6S\Sigma W + 0.45DBS}{(B + S)^2}$$

$$F_h = \frac{1.7888P - 2\Sigma W + 0.15DS}{(B + S)} + \frac{6\Sigma Wa' + 6S\Sigma W - 0.45DBS - 1.7888Ph}{(B + S)^2}$$

and with a 1½:1 slope, bearing pressures are

$$F_t = \frac{4\Sigma W + 0.15DS - 1.1094P}{(B + S)} + \frac{1.6641Ph - 6\Sigma Wa' - 6S\Sigma W + 0.45DBS}{(B + S)^2}$$

$$F_h = \frac{2.2188P - 2\Sigma W + 0.15DS}{(B + S)} + \frac{6\Sigma Wa' + 6S\Sigma W - 0.45DBS - 1.664Ph}{(B + S)^2}$$

Although these equations appear rather complicated, they can be set up in worksheet form, as shown in Appendix A, and solved without too much effort for values of S.

The equations for an increase in the heel length are unwieldy and it is much easier to go back to the basic equations and compute the soil pressures for the increased heel length.

The worksheets and resulting graphs for cases II, III, and IV are included in Appendixes A and B respectively. The actual derivation will not be presented because space does not permit and the individual designers may want to change the basic assumptions.

As stated previously, the assumptions may easily be changed for any conditions and similar curves constructed to facilitate future designs.

SUMMARY

It was found that a curve expressing bearing pressures, for increases or decreases in footing width, can be constructed for any particular loading condition or wall geometry. The relationships between changes in footing width and resulting bearing pressures can easily be derived and curves constructed. Although only a limited number of these curves are given, similar curves may be drawn for any particular design criteria. These curves are of particular value when used with a set of standards.

It was noted that in a great number of cases the sliding characteristics were of major concern. For these cases an increase in the heel length is more efficient than an increase in the toe length, but for sloping backfills a key is the best solution. A backfill on a steep slope will cause very high soil pressures and more sliding problems than flatter backslopes. For high soil pressures, increases in the toe length will be more effective in reducing soil pressures than increases in heel length.

ACKNOWLEDGMENTS

It is a pleasure to acknowledge the help received from Stanley Gordon and other members of the Bridge Design Section of the Washington, D. C., office. Without their assistance, these charts, and this paper, would not have been possible.

REFERENCES

1. U. S. Bureau of Public Roads. Typical Plans for Retaining Walls. U. S. Govt. Printing Office, Sept. 1967.
2. Terzaghi, Karl, and Peck, Ralph B. Soil Mechanics in Engineering Practice. Wiley and Sons, 1967.
3. Huntington, W. C. Earth Pressures and Retaining Walls. Wiley and Sons, 1957.

Appendix A

WORKSHEETS FOR CASES II, III, AND IV

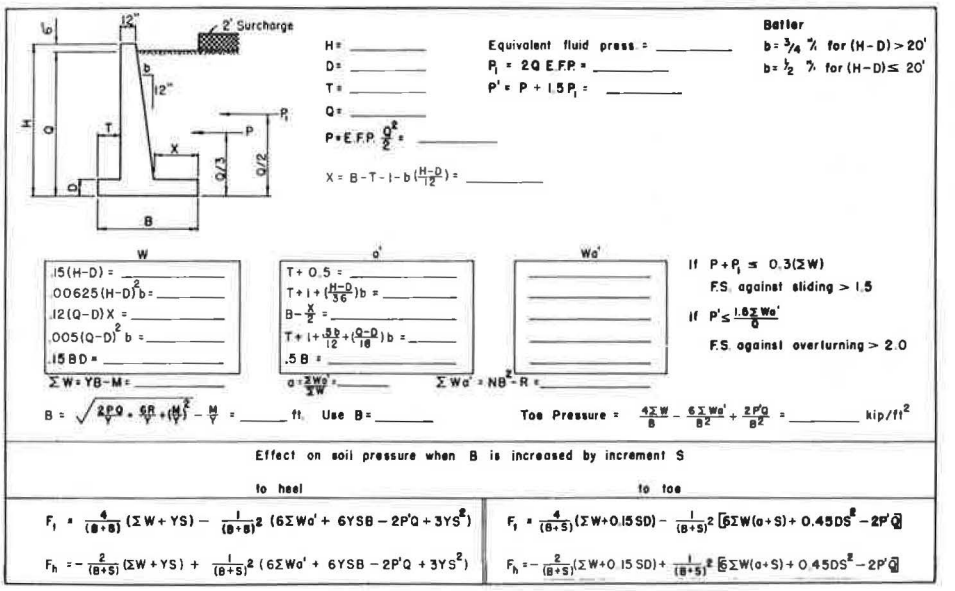

Figure A1. Solution for minimum width of footing for case II retaining walls.

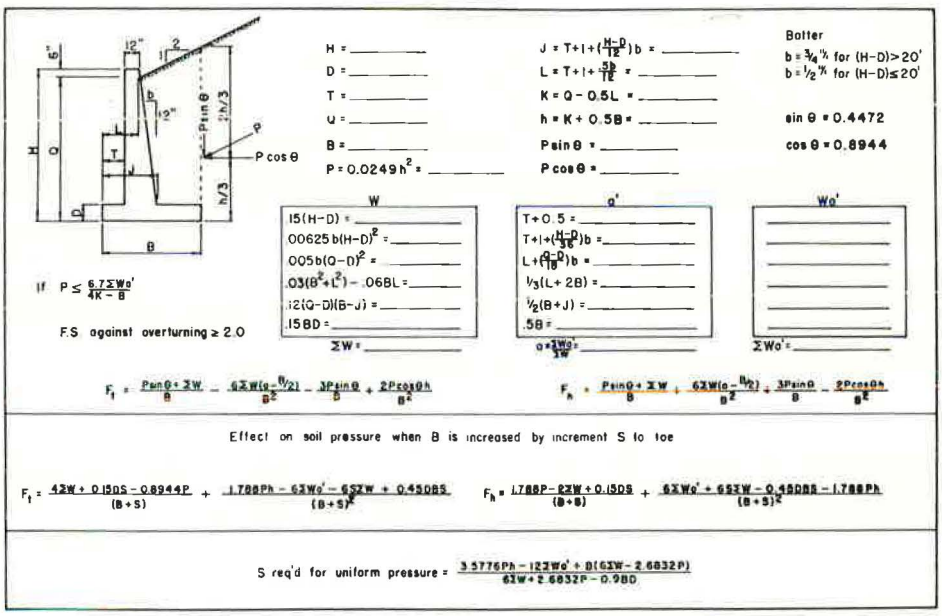

Figure A2. Solution for soil pressures for case III retaining walls.

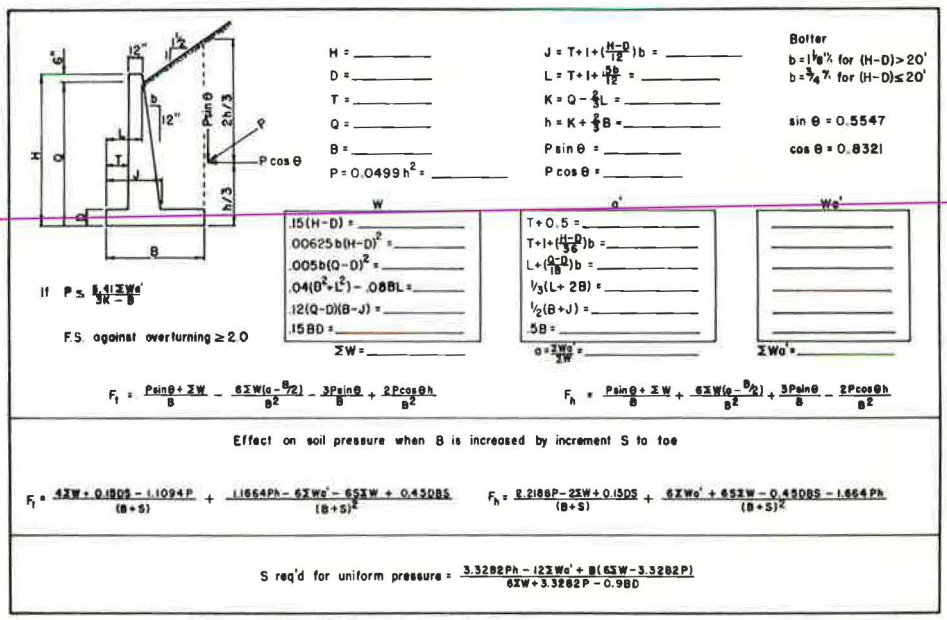

Figure A3. Solution for soil pressures for case IV retaining walls.

Appendix B

GRAPHS FOR CASES II, III, AND IV

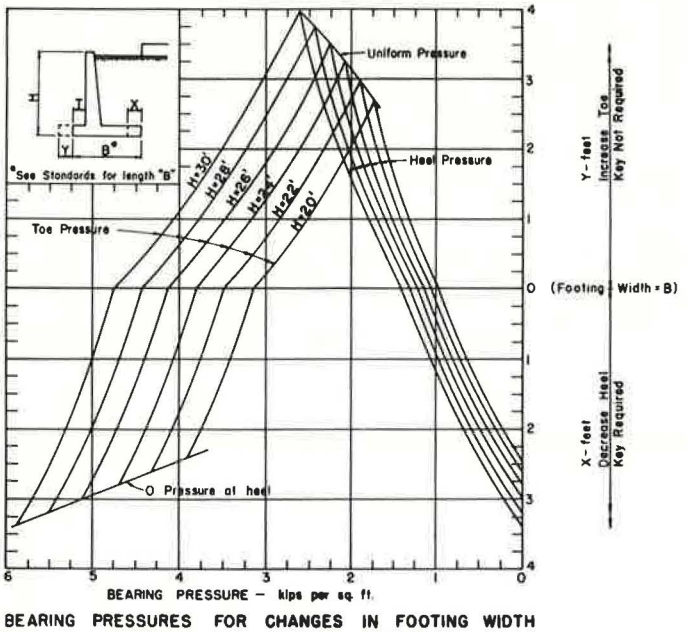

Figure B1. Case II.

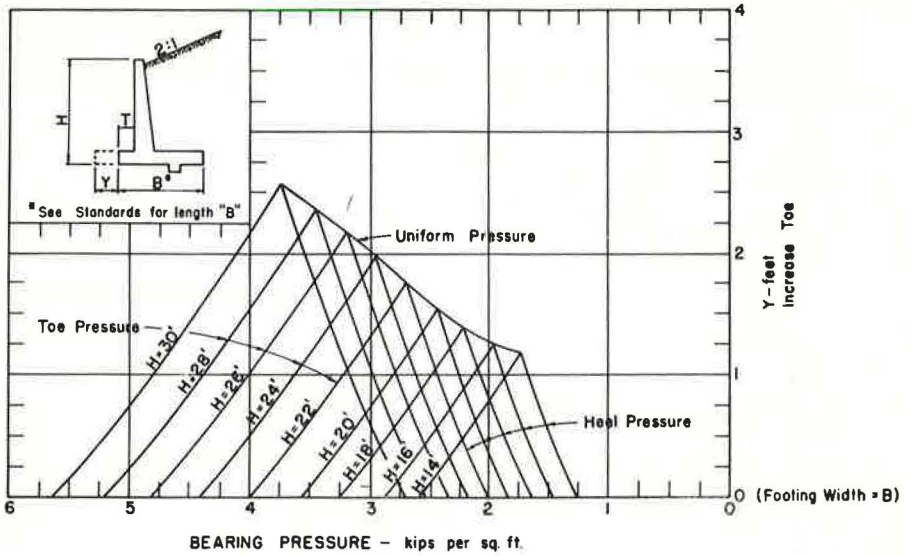

Figure B2. Case III.

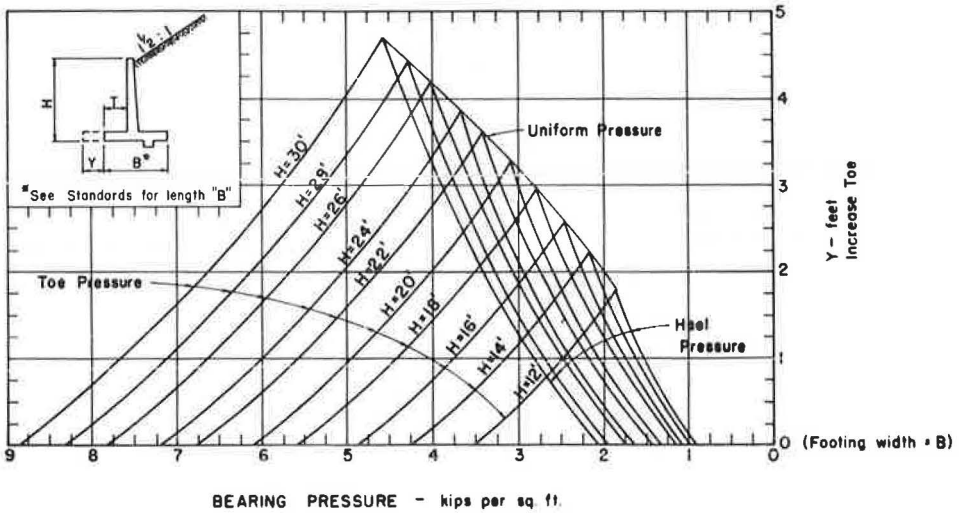

BEARING PRESSURES FOR INCREASES IN FOOTING WIDTH

Figure B3. Case IV.

Appendix C

NOTATION

B = footing width
D = depth of footing
F_h = soil pressure at heel
F_t = soil pressure at toe
H = total height of retaining wall
J = distance from toe of footing to intersection of inside face of wall and the footing
L = horizontal distance from edge of toe to point where backfill touches wall
P = soil force caused by backfill
P_1 = soil force caused by uniform surcharge
Q = height of backfill at face of wall
S = increase in footing length
T = distance from edge of toe to face of wall
W = weight of any section of wall or soil
ΣW = total vertical force
X = distance from back of footing to intersection of inside face of the wall and the footing
M, Y, N, R = constants for any particular wall geometry
a = distance from toe to centroid of resultant vertical forces
a' = distance from toe to centroid of any vertical force
b = batter of inside face of wall
h = vertical height from heel of footing to backfill surface
ϕ = angle of internal friction = 33 deg 41 min
γ = unit weight of soil = 120 pounds per cubic foot
ϵ = Rankine's constant
θ = angle backfill makes with horizontal

Metal Bridge Deck Form Specification Developed Cooperatively by Industry and Government

MARTIN DEUTERMAN, Bureau of Public Roads, Federal Highway Administration, U. S. Department of Transportation;
T. J. JONES, Wheeling Pittsburgh Corporation;
ROBERT E. LEE, Granco Steel Products Company;
F. H. LESSARD, Bethlehem Steel Corporation; and
R. W. SPANGLER, American Iron and Steel Institute

Investigations of bridge deck slabs formed with steel forms to remain in place, made in connection with the cooperative preparation of a specification by industry and government, are reported. Research and questionnaire survey results that were reviewed are also reported. It was found that so-called failures of steel forms were caused by the application of other steel sheet products as a forming material, design details that permit salt-laden moisture to attack the metal, specification error, construction abuse, and lack of proper placement and consolidation of the concrete. The resulting specification is included.

•WITH THE EXCEPTION of dwellings, the bridge is probably the oldest and most fundamental structure affecting the welfare of man. Throughout the world bridges of every size, shape, and character exist; some still in use are centuries old, and some are as modern and unique as tomorrow. Bridge engineers are continually producing modern designs for aesthetic and utilitarian purposes. Research is projecting this ageless, fundamental structure into the space age alongside the space vehicle, miniature circuitry, and nuclear engineering.

This paper is a review of one facet of this continuing research, namely, the forming of the bridge deck, on which considerable effort has been spent over at least the past 15 years.

HISTORY OF USE OF STEEL IN BRIDGES

One of the accomplishments during these years has been the introduction of steel remain-in-place bridge forms. Few products affecting the highway construction market have been the subject of so much controversy. Because this controversy creates a barrier to acceptance of the product and because specifications for the product and its use became so divergent in character, the U. S. Bureau of Public Roads and the industry began conversations aimed at resolving the objections and preparing a nationally acceptable specification. We are pleased to report that an acceptable specification for steel remain-in-place bridge forms has been developed cooperatively by the Bureau of Public Roads and the industry.

Removable timber forms have been the standard or conventional method of forming bridge deck slabs, but a review of the historical development since the early years of this century reveals that various types of steel sheeting have also been used to form bridge deck slabs. In fact, shortly after sophisticated methods of concrete placement

Paper sponsored by Committee on Construction Practices—Structures and presented at the 49th Annual Meeting.

Figure 1.

were developed, and with concrete and steel structures beginning to appear across the country around the turn of the century, contractors and bridge builders began seeking ways and means of economically using steel. Corrugated sheets of various thicknesses and with varying amounts of galvanizing, originally designed for use as siding, roofing, and other purposes, have been both applied and misapplied as bridge deck forms.

One of the earliest steel forms consisted of corrugated grave vault sections employed as a jack arch form spanning between the bottom flanges of the stringers. Figure 1 shows the construction of a bridge using the grave vault sections. It is undated, but a spokesman for the Baltimore and Ohio Railroad dates a car pictured in the same literature as existing before 1910. This construction is a remote ancestor in the chain of evolutionary development, but it is not a remain-in-place steel bridge form per se.

Figure 2, a photograph taken in 1969, shows one of these installations that we are told is rather typical. We are told this was installed in 1913, about 57 years ago. It is still serviceable and amazingly intact despite its age. The next step in the long process of product evolution was the use of corrugated barn siding to form the slab. The most talked-about installation of this type is a bridge over the Pecos River on Highway 90 near Del Rio, Texas—one that is frequently cited in the criticism of steel bridge forms.

The need facing the contractor for a new and safer means of forming bridge decks is graphically shown in Figure 3. The distance from bridge deck to canyon floor is 275 ft. This great height prompted the contractor to use barn siding as forming, supported by wood cross members that were removed when the concrete was set. Initially, the barn siding was chemically bonded to the slab quite adequately. However, over the years, the bond between the deck and the coating deteriorated under flexing caused by continuous traffic and aided by severe temperature changes.

As can be seen in Figure 4, the result has been the falling away of some of the unsupported middle sheets and the precarious hanging of others, virtually by a thread. Again, this is not a steel remain-in-place bridge form installation. And it is reports of these so-called failures resulting from such applications that continue to circulate and that are today often wrongly associated with the deep-corrugated galvanized steel forms specifically engineered for forming bridge decks. Understandably, many bridge engineers have confused this application with the present system and denied approval on the premise that steel bridge forms as presently designed have fallen out of the structure.

Other elementary, unorthodox applications have been found in numerous structures around the country. Although indicative of misapplication of steel sheeting, they are

Figure 2.

Figure 3.

still illustrative of contractors' efforts to use steel as a forming material. In these instances there was no effort made to design a steel forming system specifically for the bridge decks. The attempt was merely to substitute existing steel products, which were designed for other purposes, as a forming material without consideration of suitable permanent attachments between the steel sheet and the supporting stringers and a slab.

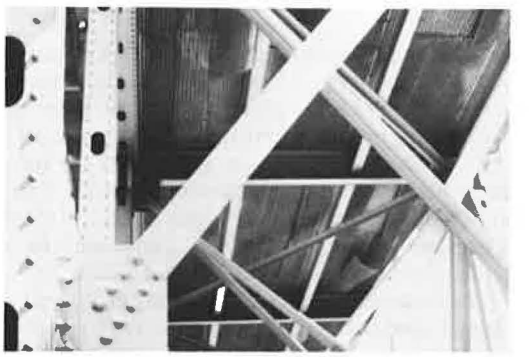

Figure 4.

In the middle 1950's, industry entered into an active research program and developed a steel forming system for bridge decks. This forming system has been used in a majority of the states. This steel forming system has been developed to meet design requirements of the various states, and to maintain the structural integrity of the slab required by bridge design departments. Design of the system has evolved to accommodate haunched slabs, lateral support, composite design, nonwelding in tension flange areas, changing of slab elevations, converging or diverging stringers, and other structural and aesthetic requirements set forth by bridge designers.

RESEARCH AND DEVELOPMENT OF THE SYSTEM

Design of the steel forming system for bridge decks has been engineered to allow the design strength of the deck slab to remain essentially unchanged from those designed to be formed by conventional methods. Actually, the basic element in the system is the deep-corrugated galvanized steel form. The custom-fabricated form has variable-width corrugations that can be provided in widths to accommodate spacing of the bottom main reinforcement when required. Of course, this remain-in-place sheet replaces the removable form. The gage of the base metal varies with load span, keeping deflection to a specified minimum.

A comparison of steel forms and removable forms is shown in Figure 5. The steel system becomes an integral part of the bridge slab where the support angles are securely fastened to the stringers and the deck panels rest on and are mechanically fastened to the supports. Design of the support allows vertical adjustment for camber and variable slab elevations. Recent development of the closed end or tapered form has eliminated the need for special end closures while increasing the efficiency of installation.

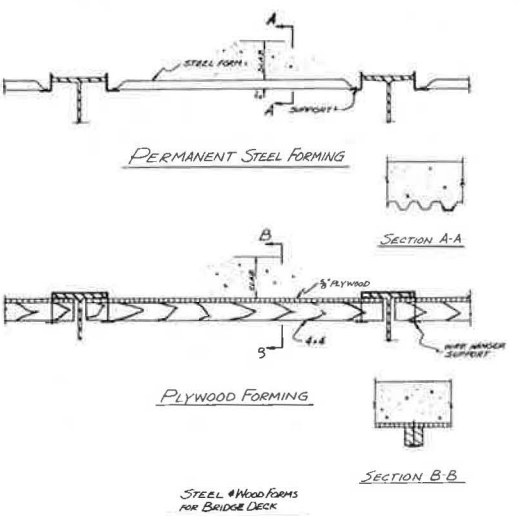

Figure 5.

Steel forms are installed from the top side of the structure and are properly attached to the stringers to provide a safe working platform, thus minimizing the need for safety nets. This is especially desirable over rivers, highways, and railroads, over electric power lines, and over great heights. Scaffolding and form stripping for the most part are eliminated and a fire hazard is avoided. The form work is completed when it is erected, and closer scheduling of other work is possible because the work can proceed on several structures simultaneously.

THE BURDICK REPORT

In 1966 a survey was conducted by Burdick (1) of the Connecticut Road Builders Association sponsored by the American Iron and Steel Institute. Burdick sent questionnaires to and received replies from those groups given in Table 1.

The purpose of Burdick's survey was to determine, among other things, the familiarity of the three groups with steel forms. Of the state highway and toll authorities who replied, 90 percent were familiar with steel forms and 53 percent used them. Of the consulting engineers who replied, 100 percent were familiar with steel forms and 73 percent used them. Of the contractors who replied, 100 percent were familiar with steel forms and 90 percent used them.

The acceptability rating of steel forms varied among the three groups. The state highway and toll road authorities who replied were 62 percent satisfied and 38 percent dissatisfied with steel forms. The consulting engineers who replied were 56 percent satisfied and 44 percent dissatisfied with steel forms. Of the contractors who replied, 61 percent rated the steel forms as being superior to other forms, 37 percent rated them as being equivalent to other forms, and 2 percent rated them as being inferior to other forms. The performance rating by those who replied is given in Table 2.

Burdick's report stated the following:

> The response to the questionnaire was sufficient to provide a fair and comprehensive expression of the attitude of owners, engineers, and contractors toward the use of permanent steel bridge forms. The great majority are familiar with the forms, and have used them and believe that they contribute to construction safety and speed in construction. The majority are satisfied with their performance and the resulting bridge deck and believe they are more economical than temporary forming. . . .
>
> It is to be expected that the acceptance of any new product, material, method or technique is predicated on increased knowledge of the application, testing, and refinement. This requires both usage and time. Eventually a pattern and a uniformity emerge. The use of permanent steel bridge forms has followed this sequence.
>
> It is apparent from this survey that steel forms have been used widely in many construction jurisdictions and a great deal of experience has been gained. It is also apparent that this experience has not been shared and that questions raised and satisfactorily resolved in one jurisdiction have not been so resolved in another. There appears to be a lack of uniform administrative policy in the use of the forms and a lack of uniformity in both design requirements and construction procedure and inspection.

The survey results and Burdick's study of the many remarks accompanying the replies encouraged industry to intensify its efforts to improve steel forms. To date, research has followed three distinct avenues: unsolicited research, joint government and industry investigation, and industrial research and development.

UNSOLICITED RESEARCH

Robert M. Barnoff of the Pennsylvania State University has made a significant contribution to the continuing development of this system and its performance. He is responsible for two studies that have established that steel forms contribute to the stiffness and durability of deck slabs.

TABLE 1

BURDICK REPORT—QUESTIONNAIRE SURVEY

Category	Canvassed	Replies From	Percent Replied
State highway and toll road authorities	69	58	84
Contractors	127	51	40
Consulting engineers	154	40	26
Total	350	149	43

TABLE 2

BURDICK REPORT—PERFORMANCE RATING OF STEEL FORMS

Category	Superior Safety (percent)	Greater Speed (percent)	Reduced Cost (percent)
State highway and toll road authorities	70	82	41
Consulting engineers	79	86	69
Contractors	87	94	69

It is interesting how Barnoff, in his research efforts, originally encountered this situation. The report (2) states that the behavior observed on two parallel, identical, continuous girder bridges located on Interstate 81 near Scranton, Pennsylvania, in conjunction with a research project, showed considerable difference in performance. One bridge constructed with steel forms was essentially free of cracking, while the bridge constructed with removable forms contained closely spaced, deep transverse cracks.

Physical tests and computational analyses were conducted and Barnoff's conclusions were as follows:

1. Corrugated forms, as designed and attached to the steel beam in this test, act as shear connectors and cause a significant amount of composite action between a concrete slab and a steel beam.
2. These forms cause significantly more composite action when the slab and beam are subject to positive moment stresses than if they were subject to negative moment stresses.
3. This composite action remains present after one million cycles of repeated loading with no apparent deterioration of the slab and beam.
4. After failure of the steel beam, a significant amount of the composite action is lost but the specimen still retains about half of the theoretical composite action.

The significance of Barnoff's study is not the recommendation for reappraisal of design concepts; however, it is an assurance that steel forms contribute a plus factor to the structure. Figures 6, 7, 8, and 9 show several views of the bridge studied.

Results of this unsolicited research prompted further study and a second investigation was conducted and reported by Barnoff (3). In this instance he conducted a series of push-out tests for various form applications. The outcome of this investigation determined that push-out test data could be correlated with full-scale test data, and, depending on design of haunch support, a significant added shear transfer was realized when steel forms were used.

JOINT GOVERNMENT AND INDUSTRY INVESTIGATION

No less significant than the unsolicited research is the joint investigation conducted by the U. S. Bureau of Public Roads and the American Iron and Steel Institute. This was the investigation of the performance of bridges having concrete decks constructed on remain-in-place steel forms conducted in conjunction with the development of a specification.

Burdick in his previously cited report (1) states that there were in excess of 1,500 structures using remain-in-place bridge forms as of 1966. Some dozen structures were reported to have had so-called failures of the form system. Before the specification was developed, it was decided to investigate these structures and ascertain whether parameters could be developed that would make future specifications more meaningful. The Pecos River bridge, described earlier, was one of those investigated.

Figure 6.

Figure 7.

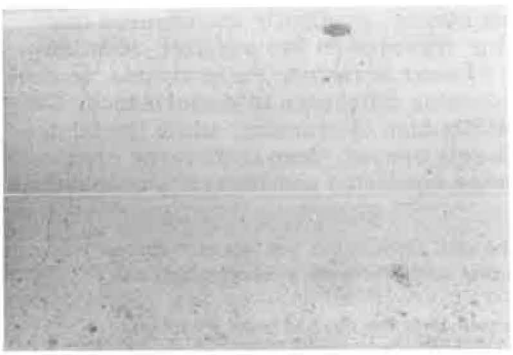

Figure 8.

Figure 9.

There remained several others that were thoroughly investigated both by industry and BPR. The following are representative cases:

1. Structure A—The problem was honeycombing in the flutes. It was found that an aggregate larger than the clearance required between the reinforcing bars and the form was used. This prevented proper consolidation of the concrete and resulted in voids. This could have occurred regardless of the type of form employed.
2. Structure B—The problem occurred when a truck poked a wheel through the spongy and crumbling concrete in the deck slab. It was found that inadequate cement in the concrete caused failure of the deck slab. Reports that metal forms were weak and had fallen during construction are attributable to clip attachments to stringers and form spline connections that are no longer used by the industry.
3. Structure C—The problem was rusting of forms. It was found that the longitudinal construction joint in the median allowed passage of salt-laden moisture, which attacked forms and created a line of rust. Calcium chloride, used as a retarder in concrete, contributed to deterioration.
4. Structure D—The problem was rusting of forms. It was found that design details and the longitudinal construction joint location provided a path for salt-laden moisture to infiltrate the deck slab and attack the metal form, thus causing a line of rust.
5. Structure E—The problem was form distortions. It was found that construction abuse and dropping loads of concrete from excessive height caused buckling of the forms. Forms were also incorrectly installed upside down, as indicated by the white tags (Fig. 10) that state "this side up".

Figure 10.

Figure 11.

6. Structure F—The problem was a salt atmosphere. It was found that these forms, installed in 1958, have shown excellent durability (Fig. 11) despite being occasionally submerged when a storm occurs at high tide.

7. Structure G—The problem was the presence of honeycomb and voids (Fig. 12) in the bottom of the concrete slab and inadequate cover for reinforcement, discovered when a slab cast on steel remain-in-place forms was removed for correction in grade. It was found that the reinforcement was not securely supported and fastened during placement and the concrete was not properly vibrated during placement.

8. Structure H—The problem was revealed in cores (Fig. 13) taken from a concrete slab cast on steel remain-in-place forms that showed honeycomb and voids in the bottom of slab. It was found that the concrete was not properly vibrated during placement.

Figure 12.

The contractor, of course, has the prime responsibility for adequate cover of reinforcement and for sound concrete around the reinforcement to the bottom of the form flutes and in the flutes at construction joints.

As a result of these investigations, a manual is being prepared that will provide guidance on appropriate design and construction details. It is planned that the manual will advise against the use of longitudinal joints located parallel to and between stringers, and will note that the metal form panels are subject to attack from salt-laden moisture penetrating these joints. Where undesirable longitudinal joints cannot be avoided, clips should be installed to anchor the steel forms to the first concrete pour in order to prevent breaking the existing bond during the second concrete pour and creating voids that would entrap moisture. Transverse construction joints present a similar problem. This can be solved by locating the joint in a bottom flute and providing weep holes through the metal forms plus assuring adequate compaction of the concrete to eliminate voids.

The manual will be submitted to the Bureau of Public Roads for a review and a check that details are accurate and are or are not in conformity with requirements of the Bureau and of the American Association of State Highway Officials for bridge construction.

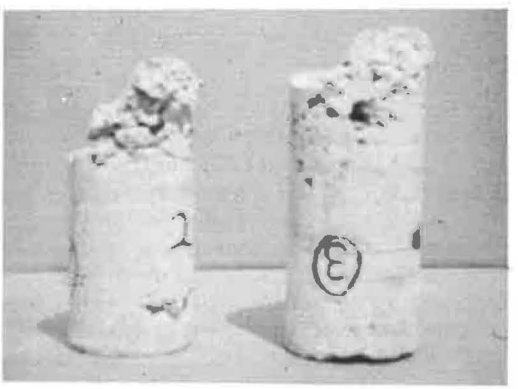

Figure 13.

INDUSTRIAL RESEARCH AND DEVELOPMENT

Research is constantly being conducted by manufacturers to improve the performance of the system. Some of the latest efforts are summarized in the following sections.

Closed End Flutes

Until recently, a special profile closure was generally provided to prevent passage of concrete through the flutes of the form resting on the support angles. Following

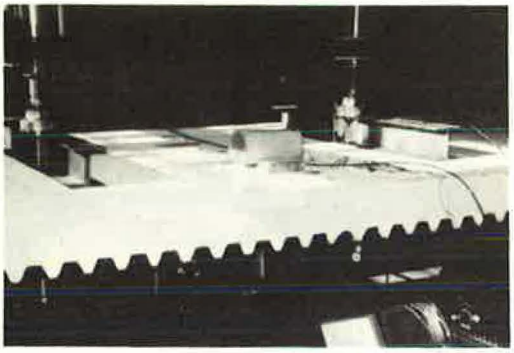

Figure 14.

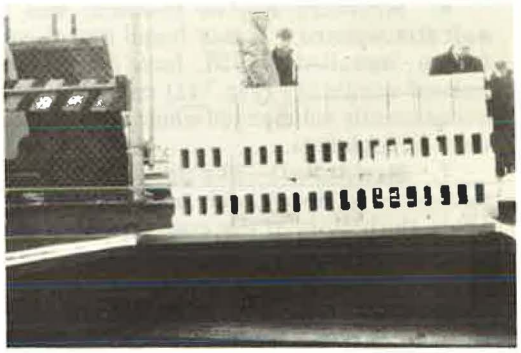

Figure 15.

extensive investigation, the industry produced a folded or tapered end finish to the flutes of the form, thereby eliminating the need for profile closures. This new feature minimizes the number of component parts and further simplifies the system. Tests of the system using closed ends have shown this scheme to be equal to or stronger than the conventional steel form sheet using profile closures.

Inspection

Obviously, one of the major points of contention is the inability of the inspector to visually check the bottom of the finished slab. The presently recommended method of post-construction inspection is to tap the underside of the form with a hammer in search of voids and to remove a specified number of form panels. Some states inspect by using a 22-caliber rifle fired at the points to be inspected for honeycomb. The impact or penetration identifies the presence of a void. These schemes are recognized by the industry and the Bureau of Public Roads as being unsatisfactory but the best available at the present time. Research is presently being directed at other methods of inspection, such as electronic, sonic, and nuclear means, for practical application to bridge decks.

Load Testing

Tests have been conducted on the performance of the entire system as well as individual component parts. As can be imagined, load-testing of the system and its parts is a continuing industry effort. Figure 14 shows a typical laboratory test (4) and Figure 15 shows a field load test.

With each change or development in this system, exhaustive tests and much investigative effort have been spent, with each manufacturer independently conducting research and testing on his product.

SUMMARY

Conversations between the Bureau of Public Roads and industry have led to the publication of a specification acceptable to both parties and recommended to all users of metal remain-in-place forms. A copy of the specification is included in the Appendix. It represents a truly constructive joint effort that has provided a standard for the industry and all users. Of course, this specification does not represent the only means of forming a bridge deck slab. The choice remains the prerogative of the bridge engineer as to whether he prefers removable forms or metal remain-in-place forms.

During the past 15 years, the American Iron and Steel Institute estimates that there have been 48,000,000 sq ft of remain-in-place steel bridge forms used in some 2,500 bridges located in 37 states. These have provided the Bureau of Public Roads and the industry with extensive experience in design, fabrication, and construction of this product.

REFERENCES

1. Burdick, E. B. A Survey on the Use and Performance of Permanent Steel Bridge Forms. American Iron and Steel Institute, Oct. 14, 1966, 21 pp.
2. Barnoff, R. M., Larson, T. D., and Love, J. S., Jr. Composite Action From Corrugated Bridge Deck Forms. Pennsylvania State Univ., March 1967, 43 pp.
3. Barnoff, R. M., and Jones, D. R. Push-Out Tests for Composite Action of Stay-in-Place Bridge Deck Forms. Pennsylvania State Univ., May 1969, 41 pp.
4. Pittsburgh Testing Laboratory. Pilot Test 60N22 Bridge Form. Wheeling-Pittsburgh Steel Corp. Jan. 9, 1969, 13 pp.

Appendix

ATTACHMENT TO CM 32-40
DATED 9-19-69

Typical Special Provisions for Fabricated Metal Forms, to Remain in Place, for Concrete Floor Slabs of Bridges for Federal-aid Projects

---

General

Fabricated metal forms, to remain in place, for concrete floor slabs of bridges shall be used only when shown on the contract plans, except that such forms may be used in unusual or extraordinary cases when approved by the engineer in a change order agreed to after award of the contract. The design and material of the forms, in the judgment of the engineer, shall be such as to give an expected maintenance free service life equal to the service life of the concrete slab. The pay quantity of concrete in the floor slabs shall be computed from the dimensions shown on the plans with no allowance for form deflection.

Materials

Typical metal forms, to remain in place, for concrete floor slabs may be of zinc-coated (galvanized) steel sheet conforming to ASTM Specification A-446 with coating class of 2.00* and shall otherwise meet all requirements relevant to steel forms to remain in place and placing concrete of the contract specifications and as specified herein.

*NOTE: Coating class 1.50 should be used instead of coating class 2.00 until April 1, 1970. Only coating class 1.50 is presently stocked by manufacturers.

Design

The metal forms, to remain in place, shall be designed on the basis of dead load of the form, reinforcement and the plastic concrete plus 50 pounds per square foot for construction loads. Unit working stresses shall be in accordance with the standard specifications for construction loads and the unit stress in the steel sheet shall be not more than 0.725 of the specified minimum yield strength of the material furnished but

not to exceed 36,000 pounds per square inch. Maximum deflection under weight of plastic concrete, reinforcement and form shall not exceed 1/180 of the form span or 1/2-inch, whichever is less. Maximum deflection under 60 pounds per square foot of live load shall not exceed 1/360 of the form span or 1/4-inch, whichever is less. The form span for design and deflection shall be the clear distance between the flanges of the supporting beams less two inches, measured parallel to the form flutes.

Physical design properties shall be computed in accordance with requirements of American Iron and Steel Institute Specification for the Design of Cold-Formed Steel Structural Members, latest published edition.

All reinforcement shall have a minimum concrete cover of 1-inch. Bars in the bottom layer of the main reinforcement shall be approximately centered over the valleys of the forms when necessary to achieve the minimum 1-inch concrete cover. The distance from the top of the slab to the bottom layer of main slab reinforcement shall be not less than that shown on the plans. Provision shall be made for positive lateral support by the concrete slab of steel beam or girder top flanges in compression except where shear connectors are provided.

Metal forms to remain in place should not be used in panels where longitudinal slab construction joints are located between stringers.

Construction

All forms shall be installed in accordance with detailed fabrication plans submitted to the engineer for approval. The fabrication plans shall clearly indicate locations where the forms are supported by steel beam flanges subject to tensile stresses.

Form sheets shall not be permitted to rest directly on the top of the stringer or floor beam flanges. Sheets shall be securely fastened to form supports and shall have a minimum bearing length of 1-inch at each end. Form supports shall be placed in direct contact with the flange of stringer or floor beam. All attachments shall be made by welds, bolts, clips, or other approved means. However, welding of form supports to flanges of steels other than ASTM A 36, A 441, A 588 and A 572 of a weldable grade and to those portions of a flange subject to tensile stresses shall not be permitted. Welding and welds shall be in accordance with the provisions of AWS D2.0 pertaining to fillet welds, except that 1/8-inch fillet welds will be permitted.

Any exposed form metal where the galvanized coating has been damaged shall be thoroughly cleaned and wire brushed, then painted with two coats of zinc oxide-zinc dust primer, Federal Specification TT-P-641d, Type II, no color added, to the satisfaction of the engineer.

Transverse construction joints shall be located at the bottom of a flute and 1/4-inch weep holes shall be provided in the field at not less than 12 inches on center along the line of the joint.

Placing of Concrete

Concrete shall be placed in accordance with the contract specifications. Particular emphasis should be placed on proper vibration of the concrete

to avoid honeycomb and voids especially at construction joints, expansion joints and valleys and ends of form sheets. Pouring sequences, procedures and mixes shall be approved by the engineer. Calcium chloride or any other admixture containing chloride salts shall not be used in the concrete placed on metal forms, to remain in place.

Inspection

The contractor's method of construction should be carefully observed during all phases of the construction of the bridge deck slab. These methods include installation of the metal forms, to remain in place; composition of concrete items; mixing procedures and particularly the concrete placement and vibration; location and fastening of the reinforcement; and finishing of the bridge deck.

The contractor shall remove at least one section of the forms at a location and time selected by the engineer for each concrete pour on each span in the contract. This should be done as soon after placing the concrete as practicable in order to provide visual evidence that the concrete mix and the contractor's procedures are obtaining the desired results. An additional section shall be removed each time the concrete mix or the contractor's procedures are changed.

After the deck concrete has been in place for a period of two days, the concrete shall be tested for soundness and bonding of the forms by sounding with a hammer as directed by the engineer at least 50 percent of the area of at least 25 percent of the individual form panels, the individual form panels to be selected by the engineer on a random basis. If areas of doubtful soundness are disclosed by this procedure, the contractor will be required to remove the forms from such areas for visual inspection.

At locations where sections of the forms are removed, the contractor will not be required to replace the forms but the adjacent metal forms and supports shall be repaired to present a neat appearance and assure their satisfactory retention. As soon as the form is removed, the concrete surfaces will be examined for cavities, honeycombing and other defects. If irregularities are found, and in the opinion of the engineer these irregularities do not justify rejection of the work, the concrete shall be given a Class 1, Ordinary Surface Finish in accordance with the contract specifications and shall be repaired as the engineer may direct. If the concrete where the form is removed is unsatisfactory, additional forms, as necessary, shall be removed to inspect and repair the slab, and the contractor's methods of construction shall be modified as required to obtain satisfactory concrete in the slabs.

The amount of sounding and form removal may be moderated, at the engineer's discretion, after a substantial amount of slab has been constructed and inspected, if the contractor's methods of construction and the results of the inspections as outlined above indicate that sound concrete is being obtained throughout the slabs.

The contractor shall provide all facilities as are reasonably required for the safe and convenient conduct of the engineer's inspection procedures.